BRNO UNIVERSITY OF TECHNOLOGY

VYSOKÉ UČENÍ TECHNICKÉ V BRNĚ

FACULTY OF CHEMISTRY

FAKULTA CHEMICKÁ

INSTITUTE OF PHYSICAL AND APPLIED CHEMISTRY

ÚSTAV FYZIKÁLNÍ A SPOTŘEBNÍ CHEMIE

DEVELOPMENT OF LIGHT EMITTING ELECTROLUMINESCENT DEVICE BY MEANS OF MATERIAL PRINTING

DEVELOPMENT OF LIGHT EMITTING ELECTROLUMINESCENT DEVICE BY MEANS OF MATERIAL PRINTING

DOCTORAL THESIS
DIZERTAČNÍ PRÁCE

AUTHOR
AUTOR PRÁCE

Ing. Michal Hrabal

SUPERVISOR
ŠKOLITEL

doc. Mgr. Martin Vala, Ph.D.

BRNO 2019

VYSOKÉ UČENÍ TECHNICKÉ V BRNĚ
FAKULTA CHEMICKÁ

Zadání dizertační práce

Ústav:	Ústav fyzikální a spotřební chemie
Student:	**Ing. Michal Hrabal**
Studijní program:	Fyzikální chemie
Studijní obor:	Fyzikální chemie
Vedoucí práce:	**doc. Mgr. Martin Vala, Ph.D.**
Akademický rok:	2018/19

Název dizertační práce:

Development of Light Emitting Electroluminescent Device by Means of Material Printing

Zadání dizertační práce:

Cílem této práce je vývoj světelného zdroje založeného na technologii tlustostěnného elektroluminiscenčního panelu napájeného střídavým elektrickým proudem pomocí materiálového tisku. Výzkum bude prováděn zejména za účelem odstranění vybraných současných nedostatků této technologie. Konkrétně se bude jednat o studium možností využití organických fluoroforů pro cílenou změnu luminiscenčního záření a studium klíčových faktorů ovlivňujících dlouhodobou stabilitu takového elektroluminiscenčního prvku.

Termín odevzdání dizertační práce: 15.3.2019

Ing. Michal Hrabal student(ka)	doc. Mgr. Martin Vala, Ph.D. vedoucí práce	prof. Ing. Miloslav Pekař, CSc. vedoucí ústavu

prof. Ing. Martin Weiter, Ph.D.
děkan

V Brně dne 1.9.2018

ABSTRACT

The topic of this thesis is development of a printed alternating current powder-based phosphor electroluminescent (ACPEL) light source. It is the only present technology suitable for fabrication of large area, flexible and patterned light sources by the means of material printing and so it represents a promising alternative to some traditional light sources. Emphasis is placed on introduction and investigation of some red brick wall problems associated with this technology. These are a limited hue of colors of emitted electroluminescent light and an operation lifetime of panels exposed to environment.

The first part of this thesis is focused on identification of suitable deposition techniques and their operation conditions leading to reproducible preparation of panels followed by determination of appropriate physical parameters suitable to characterize large area light sources. Therefore relevant coating and printing techniques are introduced along with their practical advantages and disadvantages with respect to preparation of the ACPEL panels.

A photometric quantity luminance L_V together with electric energy consumption P was evaluated to determine driving conditions for a suitable application of ACPEL panels. The maximum luminance $L_V = 133\ \mathrm{cd \cdot m^{-2}}$ was achieved on a blue panel driven by $U_{pp} = 500$ V and $f = 1000$ Hz. Achieved values of power consumption per unit area are (7 ± 3) mW make the light sources based on this technology interesting for practical applications.

The effect of driving conditions on stability of panels together with means to improve a long term stability of ACPEL panels is important topic this thesis deals with. Parameters L_{50} and L_{75} were established from the values of spectral irradiance. It was found that increasing the frequency has a negative effect on the long term stability of panels. A panel driven by 3 times higher frequency with the same voltage showed almost 3 times less values of L_{50} and L_{75} with the same type of lamination while a panel encapsulated by glass showed almost 7 times higher stability than the laminated panel. Optimal stability conditions were achieved when the driving frequency was set between 400 Hz and 800 Hz with robust encapsulation between two glass panels.

Limited hue of colors of light emitted by ACPEL panels is one of the known problems this thesis addresses. This work investigates a promising method, an addition of a color conversion material (CCM) with suitable spectral characteristics. A derivative of diketopyrrolopyrrole (DPP) was found to be a suitable novel CCM for blue phosphor. Using this CCM a 7-times increase of spectral irradiance of a blue panel at 580 nm was easily achieved.

An ease of fabrication, very low power consumption and long life time of the developed ACPEL panels together with developed possibility to modify a hue of emitted light, make them potentially ideal light sources for low-light background illumination for example in automotive industry, safety signs in public buildings, indoor decorative illumination or “branding”etc.

KEYWORDS

Printed electronics, Material printing, Alternating-current Powder-based electroluminescence, Electroluminescent panel, Screen-printing, Phosphor Large area light source, Luminance

ABSTRAKT

Cílem této práce je vývoj světelného zdroje založeného na technologii tlustostěnného elektroluminiscenčního panelu napájeného střídavým napětím (ACPEL). V současné době se jedná se o jedinou technologii založenou na metodách materiálového tisku vhodnou pro přípravu velkoplošných, flexibilních a vzorovaných zdrojů světla. Důraz je v této práci kladen na představení, prozkoumání a odstranění typických problémů, které jsou spojovány s touto technologií. Tyto problémy jsou omezený odstín barvy emitovaného světla a dlouhodobá stabilita elektroluminiscenčního prvku, který je vystaven vlivům prostředí.

Rešeršní část dizertační práce je zaměřena na představení a identifikaci depozičních technik, vhodných pro reprodukovatelnou přípravu ACPEL panelů. Dalším cílem je identifikace fyzikálních parametrů, vhodných pro charakterizaci velkoplošných zdrojů světla.

Praktickým cílem práce je nalezení vhodné metodologie pro popis a charakterizaci panelů, jakožto plošných světelných zdrojů. Fotometrická veličina jas L_V a spotřeba elektrické energie P byly vyhodnoceny jako vhodné parametry, určující aplikaci ACPEL panelů. Na modrém panelu bylo dosaženo maximální hodnoty jasu $L_V = 133\ \mathrm{cd \cdot m^{-2}}$ při napětí $U_{PP} = 500$ V a frekvenci $f = 1000$ Hz. Hodnoty spotřeby elektrické energie, vztažené na jednotkovou plochu panelů zkoumaných v této práci, jsou (7±3) mW. Tyto dosažené hodnoty dělají ze světelných zdrojů založených na ACPEL technologii zajímavé kandidáty pro různé aplikace.

Vliv rostoucí amplitudy a frekvence budícího napětí na dlouhodobou stabilitu panelů je důležitým cílem této práce. Pro popis stability byly zavedeny parametry L_{50} and L_{75}. Bylo zjištěno, že rostoucí frekvence budícího napětí zkracuje životnost panelů. Laminovaný panel napájený napětím s přibližně trojnásobně vyšší frekvencí vykazoval přibližně třetinové hodnoty parametrů L_{50} a L_{75}. Nejvyšších hodnot stabilitních parametrů dosahoval panel enkapsulován mezi skleněné pláty – přibližně sedminásobnou hodnotu oproti laminovanému panelu s trojnásobnou frekvencí. Optimální stability panelů lze dosáhnout při nastavení frekvence v rozmezí 400–800 Hz a zapouzdřením mezi sklo.

Úzká paleta odstínů barev emitovaného světla je jeden z typických problémů, který dále zkoumán v dizertační práci. Tato práce zkoumá nadějnou metodu, přídavek vhodného materiálu pro konverzi barvy (CCM). Nový derivát diketopyrrolopyrrolu (DPP), absorbující v modré oblasti, byl přidán k modrému fosforu a byl pozorován sedminásobný nárůst hodnot absolutního spektrálního ozáření v oblasti vlnových délek odpovídajících maximální emisi CCM materiálu.

Jednoduchost přípravy vyvinutých zdrojů světla spolu s velmi nízkou spotřebou a vysokou dobou života dělají z ACPEL panelů zajímavé kandidáty pro podsvícení prvků například v automobilovém průmyslu, pro dekorativní osvětlení, pro „branding“ – zvýraznění reklamních značek.

KLÍČOVÁ SLOVA

Tištěná elektronika, Materiálový tisk, Prášková elektroluminiscence, Elektroluminiscenční panel, Sítotisk, Fosfor, Velkoplošný světelný zdroj, Jas

HRABAL, M. *Development of light emitting electroluminescent device by means of material printing.* Brno: Vysoké učení technické v Brně, Fakulta chemická, 2019. 84 s. Vedoucí dizertační práce: doc. Mgr. Martin Vala, Ph.D.

PROHLÁŠENÍ

Prohlašuji, že jsem dizertační práci vypracoval samostatně a že všechny použité literární zdroje jsem správně a úplně citoval. Dizertační práci je z hlediska obsahu majetkem Fakulty chemické VUT v Brně a může být využita ke komerčním účelům jen se souhlasem vedoucího práce a děkana FCH VUT.

DECLARATION

I declare that the dissertation thesis has been worked out by myself and that all the quotations from the used literary sources are accurate and complete. The content of the dissertation thesis is the property of the Faculty of Chemistry of Brno University of Technology and all commercial uses are allowed only if approved by both the supervisor and the dean of the Faculty of Chemistry, BUT.

Ing. Michal Hrabal

……

PODĚKOVÁNÍ

Rád bych poděkoval vedoucímu dizertační práce Martinu Valovi za čas, který věnoval zkultivování finální podoby této práce. Velmi významně mi pomohli také pánové Petr Dzik a Ivaylo Zhivkov, kterým tímto děkuji za vše, co jsem se od nich naučil.

CONTENT

1 AIM OF DISSERTATION THESIS

The first goal of this dissertation thesis is to find a methodology of reproducible preparation of alternating current powder-based panels (ACPEL) and identification of typical problems connected with the procedure. Therefore the first step is an introduction of possible deposition techniques with respect to their suitability to print patterned and homogenous films from very viscous printing formulation. A need to identify parameters and operating conditions of the chosen printing technique leading to reproducible production of panels exhibiting the best optoelectronic properties results from the first aim.

In the view of the fact that electroluminescent panel is a large area light source, identification and implementation of suitable methodology for measurement and evaluation of relevant parameters describing the suitability of the light source for a specific application is the one of the main goals of this thesis. This work also deals with further determining of optimal optoelectronic performance under different driving conditions. An increase of both an amplitude and frequency of harmonic alternating voltage leads to a higher luminance but is one of the causes decreasing the lifetime of ACPEL panels. Lifetime has been a well-known limit speaking against their mass-production in the field of printed electronics.

Since a narrow palette of emitted light hues is a known deep throat of this technology, another aim of this dissertation thesis is to investigate possible ways leading to extending the color palette. The study and identification of the main factors decreasing the lifetime of panels, together with evaluation of stability parameters under different driving conditions lead to the most important goal of this thesis – a removal of well-known red brick wall problems preventing the ACPEL panels to find broader use in applications.

2 INTRODUCTION

Organic and printed electronics (sometimes also called emerging and many other names) is a novel type of electronics which is beyond the classical approach based on silicon. This new technology offers a way of producing thin film, light-weight, flexible and environmentally friendly products and also a production of printable electrical components that can be integrated into the classical microelectronic systems. Flexible OLED displays, electroluminescent panels, smart clothing, solar cells, printed batteries, supracapacitors, memory or label-protection tags are just few examples of promising application of such systems. These electrical devices are built by stacking of multiple thin layers (usually in the order of nanometers and microns) with specific properties atop each other. These materials are soluble in suitable organic solvents and therefore a mass-volume production of specific devices is achievable by various printing techniques. This is a key fact for deployment of printed electronic devices in various applications since their preparation is much more cost-effective then the inorganic devices prepared by traditional techniques. This technology leads to the development of brand new concepts such as wearable electronics, Internet of Things and smart labels.

Organic and printed electronics is based on the combination of new materials and cost-effective large area deposition techniques. These materials were at the beginning almost exclusively of organic origin, hence the name *organic electronics*. Diketopyrrolopyrrole (DPP), poly(3,4-ethylenedioxythiophene) polystyrene sulfonate (PEDOT:PSS), TIPS pentacene and poly[2-methoxy-5-(2-ethylhexyloxy)-1,4-phenylenevinylene] (MEH-PPV) are just few examples. The amount of organic materials exhibiting interesting properties such as electrical conductivity, magnetic properties and excellent durability and so on has been steeply rising for more than 40 years. The fact that Heeger, MacDiarmid and Shirakawa were awarded Nobel Prize in chemistry in the year 2000 for: "*The discovery and development of conductive polymers."* may serve as a convincing fact. Recently however more and more inorganic and hybrid materials started to be deployed because of the overall development of technology. Printable inorganic formulations of silicon, silver, ZnS, TiO_2, perovskites, carbon nanotubes etc. have been developed as well. Advantage of inorganic materials is their better stability which results in better processability during manufacturing. A list of some notable representatives can be seen in **Tab. 1**.

Tab. 1 *Various examples of materials suitable for organic and printed electronics.*

DPP	TIPS pentacene	PPV
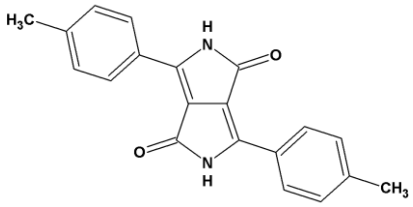	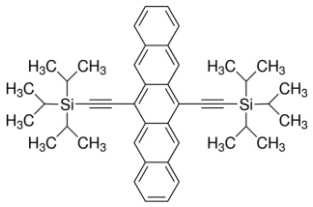	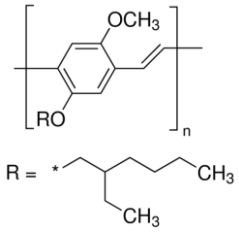
Organic photovoltaics (PVs)	PVs, OFET	OLED
P3HT	Perovskite (adapted from Ossila)	Carbon nanotubes (CNT – adapted from Ossila)
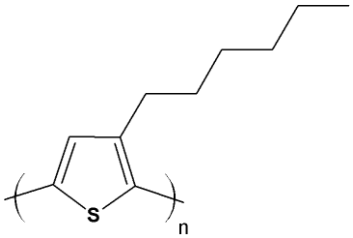	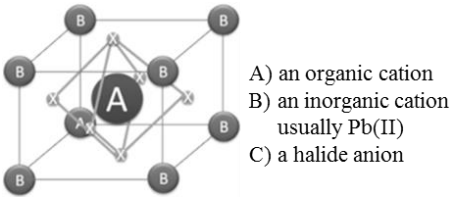	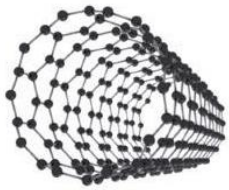
PVs, biosensors	PVs	Transparent conductive layers

As can be seen in **Tab. 1** all of the organic materials have a common trait that is a conjugated system of π-bonds that is responsible for specific properties of materials. These electrons can easily travel along such a delocalized system in a plane of the molecules.

The current leader in the field of development and commercialization of printed electronics is a Norwegian company Thin Film Electronics ASA. Memory labels, product protection and anti-theft tags that are all fully printed belong to their products. Konarka Technologies, Inc. was a pioneer in the field of printed electronics whose focus was aimed on a production of fully printed solar cells.

Organic and printed electronics has made a significant progress in entering a market in the last years. It could be said with confidence that it is an ever growing industry that has already started to generate significant profit. Sales of products that are fully based on organic and printed electronics or that include printed components are estimated to be 31.7 billion US$ in 2018 and 77.3 billion US$ in 2029. 26 billion US$ falls to a mature technology OLED displays while OLED lighting technology represents 50 million US$. [1].

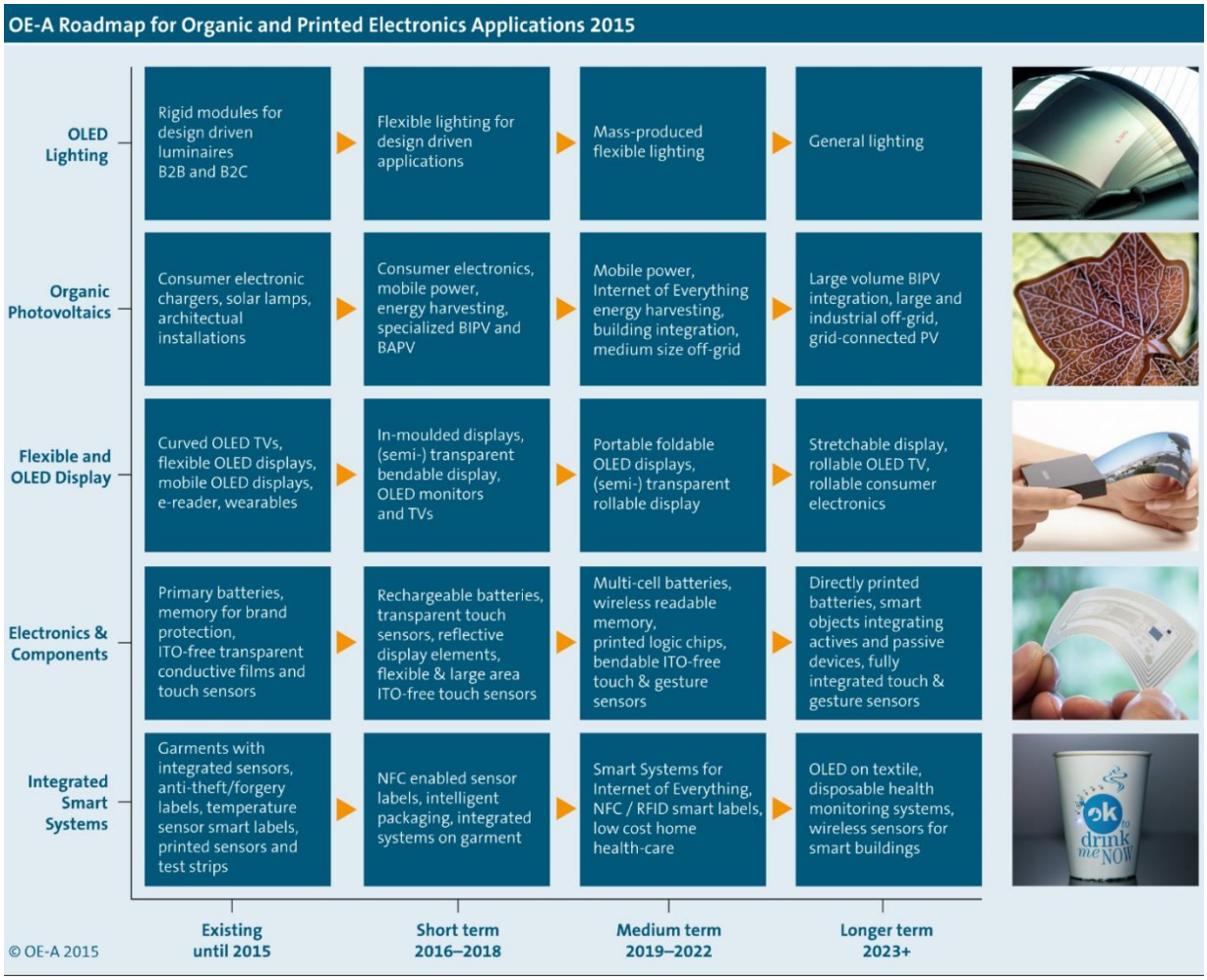

Fig. 1 *OE-A roadmap for organic and printed electronics application, with the forecast for the market entry [2].*

A roadmap shown as a **Fig. 1** has been brought together by experts from the Organic and Printed Electronics Association (OE-A) which is a group of more than 215 members from 31 countries from Europe, Asia, Australia and North America. OE-A consists of material/equipment suppliers, research institutes and universities, producers and developers and end-users. OE-A is assigned to the German Engineering Federation (VDMA) which is one of the key industry associations in Europe. The whole field of printed electronics has been divided by the experts of OE-A into 5 subcategories: OLED lightning, organic photovoltaics, flexible and OLED displays, electronic components and integrated smart systems. The state of the art is described for all the categories and visions for further short and long term (2023+) development are introduced together with a list of key technology parameters and so called red brick walls for each of the five subcategories. These red brick problems represent technological problems and difficulties that need to be overcome in order to incorporate organic electronic devices into everyday life. Each subcategory will be rendered technologically useless without successful solving of the below mentioned problems. Some of these problems concerning the lighting industry are:

- Substrate sizes – the production cost decreases with larger deposited areas. This fact indicates that currently well-established evaporation techniques will have to clear a way for material printing techniques

- Development of new flexible substrates (improvement of a bending radius) – at the moment only glass substrates are being deployed which are difficult to process by means of material printing

- Development of barrier films – environmental stability of OLED panels is poor and without proper barrier films a lifetime is unacceptably low

For instance memory tags for brand protection are currently being developed and introduced in the field of electronic components. In a long term fully printed batteries and other either active or passive components will be standardized. The field of organic photovoltaics in long term counts with standard solar cells with efficiency around 12–15 % and a full building-integration. It is quite clear from the road map which fields of the intelligent electronics are in the main focus of scientists, developers and manufacturers all around the world.

The above mentioned road map shows that display and lightning technology are both very important areas. While OE-A predictions are focused mainly on OLED technology, it is still far from solving all its problems. Mainly poor environment stability is problem for displays because of the fact that contact with molecules of water destroy the display permanently. Another problem is that criteria for processing conditions are difficult to meet because the deposition needs to be conducted under highly controlled atmosphere. Also the lifetime of OLED displays is not as high as lifetime of other, more traditional devices (such as LED and LCD). All these factors make the OLED displays and lighting sources very expensive at present.

The aim of this work is focused on study and development of light sources based on an alternative technology – powder-based electroluminescence (ACPEL). **Chapter 3** briefly introduces a phenomenon of light generation by ACPEL panel. The panel consists of an active film – phosphor (ZnS with various dopants) separated from the electrodes by a dielectric film. This type of devices is interesting from multiple points of view. There is no need of new exotic, extremely complicated and expensive molecules. Panels can be fabricated with basic equipment accessible to many manufacturers and relatively large well patterned panels can be produced in short time. The overall concept is very easy and cost-effective in contrast to some of the devices mentioned above. The typical luminance of electroluminescent panel is usually in the range of 100–200 $cd \cdot m^{-2}$ while average modern TV (either OLED or LCD) ranges between 500–1000 $cd \cdot m^{-2}$. ACPEL panel is not as effective as other devices but for some applications (back light, interior decoration etc.) it could represent serious alternative to the above mentioned technology.

Material printing techniques represent an optimal tool for cheap, easy and large-scale preparation of electroluminescent panels and will therefore be presented in more details in **Chapter 4**.

3 FULLY PRINTED POWDER-BASED ELECTROLUMINESCENCE DEVICE

Electroluminescence (EL) is a conversion of electrical energy to optical by the electronic conversion process. It is nowadays considered as a process of non-thermal (which excludes incandescence – generation of light by heating) generation of light in materials by application of high intensity electric field. The material can be both organic and inorganic. The electroluminescence in inorganic materials is divided into two distinctive branches: injection EL and high-field EL. The latter is further divided into thin-film EL (TFACEL) and powder-based phosphor EL (ACPEL) which is topical for this thesis. A summary of EL types with respect to the devices that operate on the mentioned principles of electroluminescence is depicted in **Fig. 2**.

A schematic of typical powder-based electroluminescence panel and all the films forming it (upper image) with a photo of fully printed device in off-mode (bottom left) and on-mode (bottom right) are presented as a **Fig. 3.**

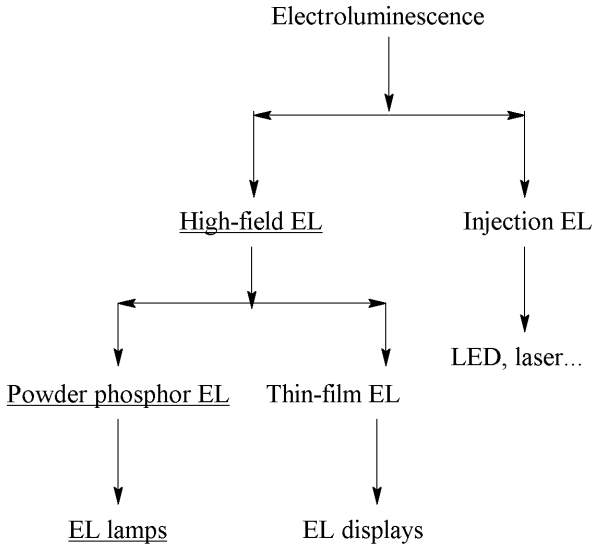

Fig. 2 *Various categories of EL types with typical devices. Underlining notes the type which is topical for this thesis.*

The effect of alternating-current electroluminescence (ACEL) in ZnS was first observed by Georges Destriau in 1936 [3]. The lighting devices based on ACEL were at first considered as very promising new sources of light. This first generation of devices didn't show sufficient light output and also the life-time of original materials was very limited. All these factors ensured that ACEL light sources didn't become commercially interesting at late thirties. It took almost 20 years to form basic concepts and first theoretical background of electroluminescence [4, 5]. A search for better performing device led to discovery of new types of electroluminescence-based devices. Namely DC (direct-current) thin film electroluminescence, DC powder luminescence, AC thin film electroluminescence (ACTFEL) with sputtered or evaporated phosphor layer. A comprehensive review with specific advantages/disadvantages of various approaches was given here [6].

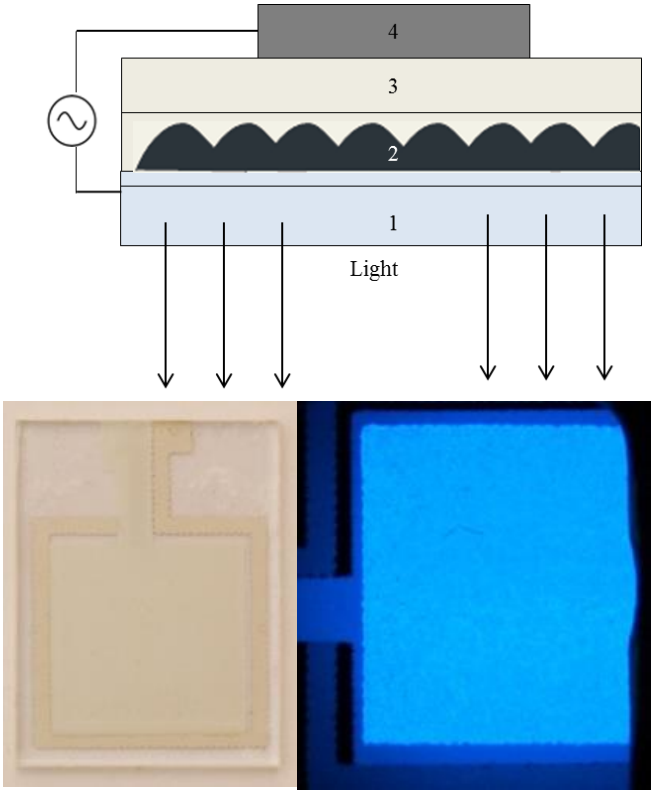

Fig. 3 *Schematics of ACPEL. 1 – PET/glass substrate with ITO electrode/ 2 – phosphor/ 3 – double layer of dielectrics/4 top metal electrode (on the left). Printed (in the middle) and emitting panel (on the right) under 250* V_{pp} *and 4 kHz can be seen on the right.*

The ACPEL based light-emitting devices show promising potential for industry since the preparation can be done by material printing on various substrates including flexible foils [7, 8]. Material printing is a well-established simple method for deposition of large area patterned devices bringing economical advantage compared to the classical evaporation or sputtering deposition, typical for ACTFEL. A disadvantage of ACPEL is a very low efficiency and radiance output compared to other types of lightning sources (LED, fluorescent tubes…). It could be commercially utilized as a source of background lightning or as a lamp in rooms with ambient illumination. On the other hand it bears the benefits from the material printing.

Pioneering work in the field of electroluminescence has been conducted by Fischer who first clarified the process of generation of electroluminescence in doped ZnS phosphor devices. He later presented improved models that remain valid until today [9]. A comprehensive review on ACPEL was published by [6] where the process of generation of electroluminescence is described in depth from a physical point of view. Smet [10] introduced extensive overview of differently doped phosphors with respect to the emitted light color. Winscom et al 2015 [11] introduced a review on ACPEL devices (materials, mechanism of operation and life time of devices), comparison of ACPEL and other plane light sources and introduction to different approaches of utilizing color conversion materials (CCM) for tuning of emitted light color. And finally the operation of EL devices, especially the study of micro-regions both on the surface and in the bulk of phosphor grains, where the electroluminescence is generated, was introduced by Harris [12].

3.1 Mechanism of light emission in the powder-based EL device

All the phosphor materials are based on zinc sulfide (ZnS) doped with various metal or transition element cations (Cu^{2+}, Mn^{2+} Al^{3+}, etc.). A study was conducted by Fischer (9) where a ZnS:Cu, Cl grain was observed under optical microscope and light-emitting region in a form of needle-like precipitate of $Cu_{2-x}S$ inside the bulk of a grain. Fischer proposed a model that these $Cu_{2-x}S$ needles are formed on structural defects that occur thanks to the phase transition of ZnS from hexagonal wurtzite which is formed by preparation of zinc blend under high temperature (>1000 °C) to cubic form by subsequent cooling of a zinc powder. The precipitate $Cu_{2-x}S$ is a known p-type semiconductor with high conductivity. Microscopic hetero-junctions are formed between ZnS and the copper-based precipitates which are shown in **Fig. 4**.

The total thickness of phosphor and dielectric layers is usually around 50 μm. When this structure is sandwiched between bottom and rear electrode and relatively high voltage (in the order of hundreds of volts) is applied on the electrodes the electric field with large intensity **E**, usually in the order of $10^6 – 10^7 V \cdot m^{-1}$, is generated. The intensity of homogenous electric field with respect to distance of electrodes follows **Eq. 1**

$$E = \frac{U}{d} \tag{1}$$

Where E is the magnitude of intensity of electric field ($V \cdot m^{-1}$), U is voltage (V) and d is the distance between electrodes (m).

The electric field focused on the ZnS grains E_L is responsible for the high efficiency of luminescence. When the ZnS grains with relative permittivity ε_{r1} are surrounded by the binder with relative permittivity ε_{r2} the intensity of the local field, influencing directly the particles can be calculated by the **Eq. 2**

$$E_L = \frac{U}{d}\left[\frac{3\varepsilon_{r2}}{2\varepsilon_{r2} + \varepsilon_{r1} - \varphi_V(\varepsilon_{r2} - \varepsilon_{r1})}\right] \tag{2}$$

The parameter φ_V represents volume fraction of ZnS grain in the formulation.

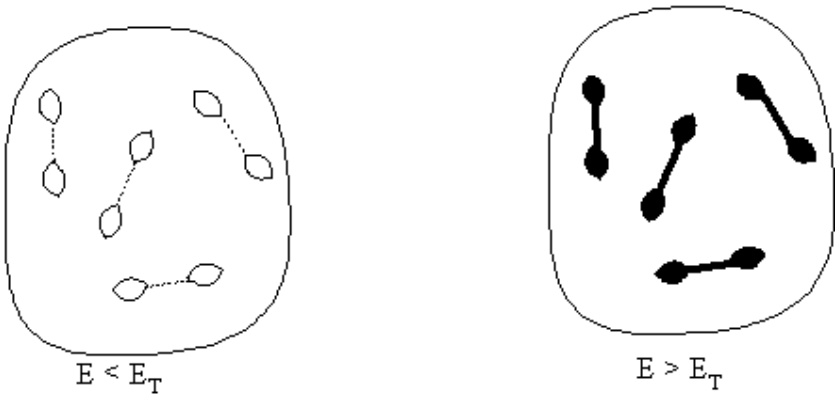

Fig. 4 *Schematic view of typical ZnS particle with light-emitting regions with the needle-like shapes. When the applied electric field has higher intensity than the threshold intensity the impurities start to glow. Adapted from [9].*

Moreover a very strong electric field is further "concentrated" on the sharp tips of $Cu_{2-x}S$ needles reaching the intensity of local electric field up to 10^8 $V \cdot m^{-1}$ since the radius of tips is typically in the order of hundreds of nanometers. Such strong local electric field induces tunneling of electrons and holes from $Cu_{2-x}S$ conductive needles into the phosphor lattice. Here electrons are trapped by shallow traps at Cl while holes are captured by Cu acceptor sites in the lattice. Trapped charge carriers are forced to move in opposite direction with the reversion of polarity of electric field. Electrons radiatively recombine with holes upon the contact and the light is emitted by the grain. This process established by Fischer is called bipolar field emission model and is schematically shown in **Fig. 5** [13]. When applying insufficient voltage on the electrodes the intensity of electric field (E) is less than threshold intensity (E_T) and the luminescence does not occur because electrons and holes don't have enough energy to tunnel from the conductor to the bulk of the crystal. On the other hand when the applied voltage exceeds some critical value, the intensity of field is higher than the threshold intensity E_T and the above mentioned process of generation of light takes place.

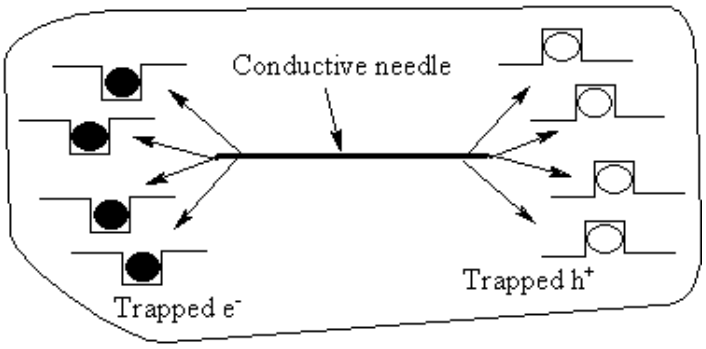

Fig. 5 *Schema of bipolar field emission model proposed by Fischer. Adapted from [9].*

4 SOLUTION-BASED DEPOSITION OF THIN FILM LAYERS

As was mentioned before the printed electronics is based on a stack of thin films fulfilling a specific role. Thin films are produced by the deposition of an active material on a substrate (polymer foil, paper, textile etc.) by some contact or contactless printing method. Printed material can be of organic, inorganic or hybrid nature. One of the advantages of printed electronics is the ability to prepare a large amount of devices in a relatively short time. One of the prerequisites for this is the ability of an active material to be soluble in an organic solvent without a loss of a needed property and then deposited under atmospheric conditions. This is in contrast to traditional deposition techniques such as microlithography or physical vapor deposition techniques where the deposition needs specific conditions with limited amount of prepared devices.

There exists a great variety of techniques that are suitable for preparation of thin films from solution but each printing technique has its typical shortcomings. It is needed to deeply consider which technique is to be used according to the desired outcome. First of all, many methods require large amounts of material and a lot of waste is being produced. Secondly, to achieve a good reproducibility is challenging at very least and the third problem is that many of these techniques are suited only for small scale laboratory applications but cannot be transferred to large scale production. Spin coating can be named as a typical example of such a problem. A lot of printing processes have been optimized for a preparation of large volume of devices and they will be introduced briefly in this chapter.

All these methods can be basically divided in two categories – (*i*) coating and (*ii*) printing processes. Coating can be described as a process of forming a film on a substrate without creating a complex pattern whereas printing involves creation of a patterned layer. It could be said that the thickness of a layer prepared by coating is the only parameter that is of concern [2].Techniques can also be divided according to whether the substrate does or does not come in direct contact with the deposition unit. Then we talk about contact methods and contactless methods respectively.

Material printing techniques differ from techniques deployed in classical graphical printing. The main difference is that careful formulation of inks – an active material, suitable solvent and additives – must be taken into consideration. Additives adjust crucial physical-chemical properties such as wetting, dynamic viscosity, and adhesion of layers atop each other etc. The printed layer still needs to perform its specific role.

4.1 Coating techniques

As was mentioned before coated films include no pattern in contrast to printed films. The thin film can be prepared by spraying, casting, smearing or painting over the surface. Techniques such as spin coating, doctor blade coating, spray coating, slot-die coating, curtain coating or knife-over-edge coating can be categorized as coating techniques [14].

4.1.1 Casting

Casting is definitely the simplest technique for preparation of layers. This procedure involves just a transport of ink on a substrate followed by drying of a solvent. The only real advantage of this technique is that no special equipment is needed. It is possible to prepare thick films with a good quality as well. The lack of control of film thickness, picture framing at the edges and sometimes even a precipitation of the ink during a drying are significant drawbacks for the use of

casting. Another problem could be a control of surface tension of substrate and the fluid. The process of a drying is inhomogeneous when a surface tension of the ink dominates over the surface tension of a substrate.

4.1.2 Spin coating

There can be no doubt that the spin coating is practically the most wide spread method for deposition of thin layers from the solution. It is used in microelectronics for application of polymeric photoresist on silicon wafers during preparation of transistors. It is also involved in some steps for manufacturing of CDs and DVDs. This technique has been subject of many studies, for instance Norrman et al [15]. Typical spin coating operation involves placement of substrate on the vacuum pad and application of solution on top. The pad with the substrate rotates with specific speed (up to thousands of rotations per minute) which is the key parameter of this process. Fast evaporation of a solvent and subsequent forming of a layer occurs as can be seen in **Fig. 6**. When the rotation is started the abundant material is ejected away thanks to the high angular speed and only the preferable thin film remains on the substrate. Resulting properties of layers (thickness, homogeneity, topology…) show excellent repeatability when using the same solvent and concentration of an active material.

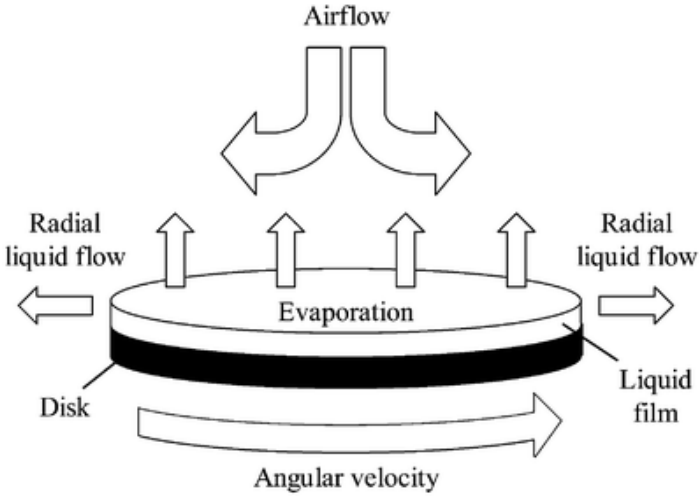

Fig. 6 *A typical spin coating process [15].*

The thickness and morphology of resulting layers depend strongly on rotational speed, viscoelastic properties of the ink, volatility, molecular weight and so on but are not very dependent on the amount of solution placed on the rotating disc or the spinning time. The thickness of the layer can be roughly estimated from the empirical **Eq. 3**

$$d = k_{spin} \cdot \omega^{\alpha} \tag{3}$$

Where ω is rotational speed (rot·min^{-1}) and k_{spin} and α are empirical constants that take into account the physical properties of solvent, active material and substrate. Constant α typically attains the value around − 0.5. More detailed information can be found at [15]. It is also possible to start the rotation and apply the solution on the rotating substrate. This second approach is preferable when the solution is based on volatile solvent which would start to evaporate too quickly to form a homogenous layer. Relatively large area (substrates up to 550 mm in diameter) could be coated at once with very good homogeneity of the targeted layer [16].

Spin coating has found a special place for application in many fields of printed and organic electronics probably due to the fact that formation of thin film with relatively fixed thickness, morphology and topography of the surface can be easily achieved. Thanks to its simplicity it is usually a starting point for development of systems based on thin films.

Few examples of using spin coating in polymer solar cells is the preparation of layer P3HT-PCBM with 1,2-dichlorobenzene [17, 18]. Carbon nanotubes (CNT) and metal oxides (MOX) gas sensors prepared by various deposition techniques were subject of this research [19].

Although the lab scale application of spin coating is extensive the mass production of various components is probably not going to be fully achieved. At this point it is dubious whether spin coating will gain more popularity in the industry of printed electronics.

4.1.3 Blade coating

A sharp blade is placed at a defined position (10–500 μm) over the substrate and a coating solution is placed in front of the blade. The blade is then drawn with a certain linear speed (usually several cm s^{-1}) across the substrate forming the wet thin layer of declared height. This process can be seen in **Fig. 7**.

In theory the thickness of wet layer should be roughly half of the distance between the substrate and the blade [14]. But this can vary significantly due to various physical phenomena such as surface energy of the substrate, surface tension and viscosity of the solution. Forming of the meniscus between the blade and solution is another important criterion.

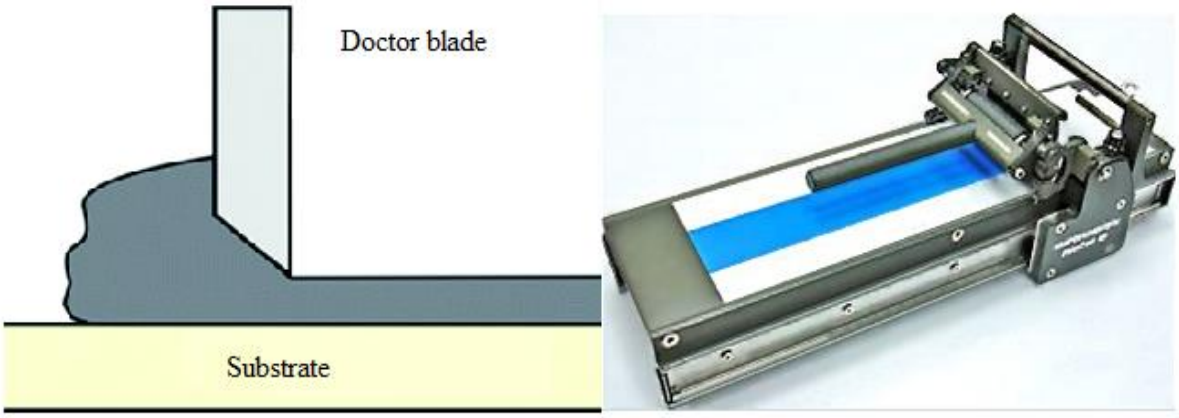

Fig. 7 *Illustration of blade coating technique on the left side and image of blade coater on the right side of the image [20].*

The thickness of a dry layer can be predicted by an empirical **Eq. 4**

$$d = \frac{1}{2}\left(g\frac{c}{\rho}\right) \tag{4}$$

Where g is the gap distance, c is the concentration of the solid material in solution ($g \cdot cm^{-3}$) and ρ is the density of the solution ($g \cdot cm^{-3}$). Blade coating is very simple technique that is not based on extremely expensive machinery with good ability to produce homogeneous layers. This fact makes the blade coating very popular and commonly deployed technique in both the laboratory and large scale production.

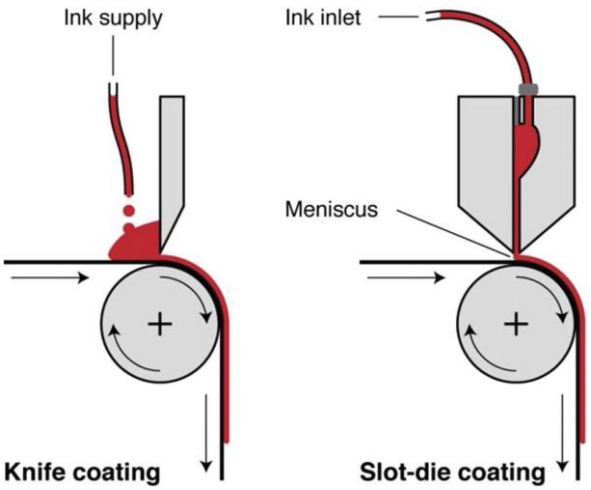

Fig. 8 *Basic principle of a rotary knife over edge and rotary slot-die coating method [21].*

It is usually stated that blade coating is a parsimonious technique compared to other coating techniques (such as spin coating) with almost no loss of the functional material. But a lot of material needs to be wasted in a process of finding the optimal properties of the coated solution. Also this method is not well suited for creation of prototypical devices. In the end the amount of material that is wasted by this method can be easily compared to spin coating or the other methods.

Advantage of this process compared to spin coating (which is much more used in laboratory practice) is that it is easily possible to convert blade coating into R2R method where the flexible substrate is placed on a cylinder as can be seen in **Fig. 8**. In the last two decades blade coating has experienced increasing interest in fabrication of small scale lab devices. One of the studies where blade coating was used as a technique of deposition was conducted by *Mens et al.* Polymer solar cells based on a mixture of MDMOPPV and $PC_{60}BM$ were manufactured and the crystallinity of the active material was determined by the solid state NMR. Crystallinity of layers deposited by this technique was higher compared to the spin coated layers [22]. Jong *et al* used this technique for preparation of perovskite solar cells (SCs) with 9.5 % power conversion efficiency (PCE) [23]. Pierre *et al* used blade coating for deposition of organic thin film transistors (OTFTs) aiming to study physical-chemical parameters leading to reproducible deposition of printed electronics [24]. The use of R2R in printed electronics is to this date limited except for fully printed ZnO layer on the ITO [25].

4.1.4 Slot-die coating

Slot-die coating is a contactless large area deposition technique suitable for preparation of thin films with excellent uniformity. This method is well suited for manufacturing of multilayer polymer solar cells [25], secondary batteries and electrodes for printed electronics [26]. This technique represents a unique combination of 3 key properties.

- Premetered – coating thickness is predetermined by the feeding pump, coating speed and width of the mask and does not depend on any extra adjustments of the head

- Contact free – substrate is in contact only with the coating liquid which gives the advantage of avoiding scratches on the substrate

- Fully sealed – coating system is fully closed and solvents don't evaporate so that the concentration of ink is kept constant

Fig. 9 *Open slot-die head. From left to right the ink distribution chamber, feed slot, lip and internal mask (shim) can be seen [27].*

It is quite a simple technique where the ink is fed into the printing head with very well defined shape. The real challenge is the printing head that is usually of very complicated design. It consists of an ink distribution chamber, feed slot and up and downstream lip as shown in the **Fig. 9**. The internal mask (shim) is a critical part which is responsible for the resolution and the dimension of the slots. Both the shim and the whole printing head are made of stainless steel and the typical width of the printing mask ranges 10–100 μm. It needs to be noted that masks thinner than 20 μm are difficult to handle and the masks wider than 60 μm might require a more viscous ink for the correct deposition [26]. Theoretically very broad range of dynamic viscosities ranging from less than 1 mPa·s up to several thousand Pa·s can be used. When the dynamic viscosity of an ink is relatively low (<20 mPa·s) the ideal width of the mask is roughly 25–50 μm. R2R type of slot-die coating is widely studied for high viscous inks at high speed deposition (> 11 mm·min^{-1}) [28].

The thickness of a wet film can be roughly estimated by the empirical **Eq. 5**

$$d = \frac{\dot{V}}{v_c \cdot w} \cdot \frac{c}{\rho} \tag{5}$$

Where $\dot{V}$ is the flow rate (cm^3·min^{-1}), v_c is the coating (or web) speed (cm·min^{-1}), w the coating width (cm), c is the concentration of the solids in the ink (g cm^{-3}) and ρ is the density of the active dried material in the final film (g·cm^{-3}).

A complex research was done by Krebs in 2009 [29] when a polymer solar cell based on the active material P3HT was prepared almost fully from the solution by slot die coating. Bottom electrode based on nanoparticle silver was deposited on polyethyleneternaphthalate (PEN) substrate. An electron transporting layer of nanoparticle ZnO followed by an active layer of P3HT:PCBM and a hole transporting layer PEDOT:PSS were all deposited by slot-die coating and only the top electrode was screen-printed. No ITO layer was involved which is a significant economic advantage but the overall performance was paltry 0.3 %.

Similar research was conducted by Krebs [25] when ITO was introduced by screen-printing and the other layers were either slot die coated or deposited via knife-over-edge or screen-printed. Top silver electrode was slot-die coated. The length of each individual stripe was 25 cm and the width was 0.9 cm. An active area for each individual stripe was 15 cm^2. Performance was ten times higher compared to the fully screen-printed devices. The processing speed for all the layers was in the range 40–50 $m \cdot h^{-1}$.

Slot-die coating was also used for production of polymer based light emitting diodes (OLEDs) [30] or more process-tolerant light-emitting cells (LEC) [31].

A research topical to this work was conducted by Bellingham et al [32] where an electroluminescent fiber was fabricated using the R2R slot-die technique. The authors conclude that the slot-die coating leads to a faster deposition of functional layers and in general is more suitable than dip-coating technique.

4.2 Printing techniques

Printing techniques are typically contact methods (with one exception of digital inkjet printing) that allow a certain pattern to be deposited on the substrate. Various printing techniques give a wide variety of achievable thickness and resolution of layers and speeds of deposition.

4.2.1 Screen-printing

Screen-printing is a two dimensional technique (2D) which means that complex well defined patterns can be fully printed by this technique. The pattern is defined by open slots in an otherwise closed screen. The closed slots are usually filled with almost insoluble photo emulsion. The ink is deposited on top of a screen and a so called squeegee is drawn over the entire area. The ink is mechanically forced through the open image and deposited on a substrate. The mesh itself is placed in a snap-off distance above the substrate. Theory on this subject is described exhaustively for example here [33].

From the technological point of view the printed electronics market is segmented into several main areas: flexography, gravure-printing, screen-printing, and inkjet-printing. The screen-printing technology accounts for the largest share in the global printed electronics market at the moment. The extensive use of screen-printing technology is evident in numerous industries such as printed electronics, circuit board printing, thick film technology, displays, and product labels.

Screen-printing is currently the most well established printing technique in the field of printed electronics. The most notable advantages of screen-printing are its simplicity and cost-effective manufacturing of both large areas and small specific patterns with high resolution. Last but not least is the ability to convert screen-printing to fully R2R mode where the mesh is cylindrical and the squeegee is placed inside the rotating screen. The screen rotates with the same velocity as a substrate and a full printing is conducted in each cycle by the stationary squeegee. It is possible to obtain much higher printing velocities by the rotary screen-printing (up to 180 $m \cdot min^{-1}$) [34] than by the flat bed screen-printing (0-35 $m \cdot min^{-1}$) [21]. Logical disadvantages of this process are high initial waste of material since it requires long time to adjust all the moving parts and a high price of the rotary screens in hand to hand with reduced possibility of cleaning the screens. A basic scheme of both the bed and rotary screen-printing can be seen in **Fig. 10**.

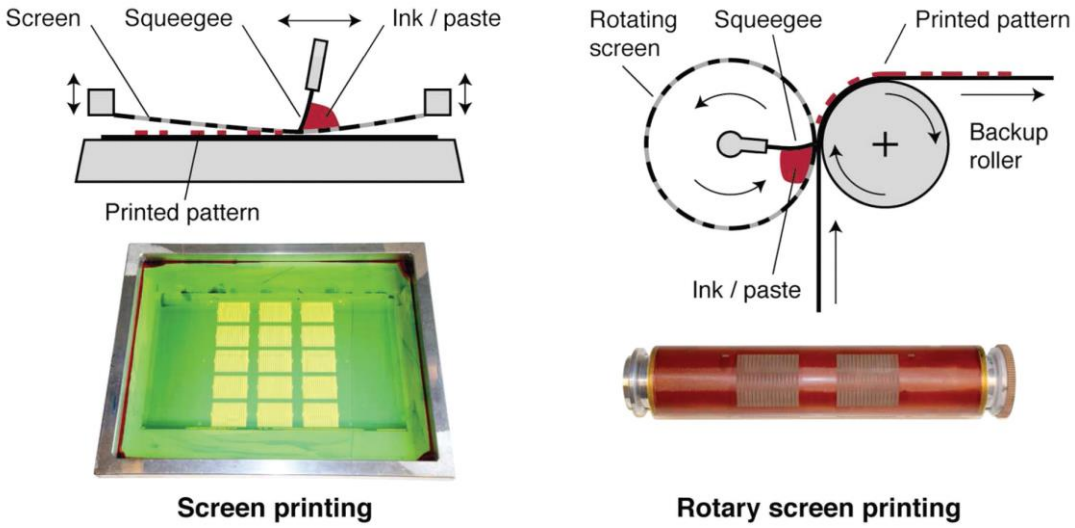

Fig. 10 *A scheme of flat bed screen-printing on a left side and a rotary screen-printing on a right side [21].*

Typically inks (pastes) with much higher viscosity compared to the other methods are used (usually several tens or hundreds of Pa·s). A paste must be highly viscous so that it doesn't pour through the open slots by itself. The resulting thickness of a dry layer depends on several factors such as the theoretical paste volume of the screen, V_{screen}, which is the volume between the threads of the screen and the thickness of emulsion, concentration of the solid in a ink, density and an empirical parameter called pick-out ratio k_p, which depends on factors like ink rheology, snap-off distance and snap-off angle, printing speed and squeegee force. A thickness of a wet layer is empirically given by **Eq. 6**:

$$d = V_{screen} \cdot k_p \cdot \frac{c}{\rho} \tag{6}$$

Where c is the concentration ($g \cdot cm^{-3}$), ρ is the density of material in the dry film ($g \cdot cm^{-3}$) and V_{screen} is the paste volume of the screen ($cm^3 \cdot m^{-2}$).

Screen-printing in the field of organic and printed electronics was applied for instance by Bao et al for preparation of fully printed organic field-effect transistor (OTFT) based on polymer P3HT with similar characteristics as devices prepared by spin coating or casting [35]. A hole-transport layer in OLED was screen-printed by Pardo et al [36]. Another example is printing of PEDOT:PSS as either conductive layer or as an active layer forming organic electrochemical transistors (OECTs) by various authors [37, 38]. Bendoni et al (2015) [39] conducted a research where terpineol-based TiO_2 screen-printing inks where thoroughly investigated as a very promising material for printing of photo anode layers.

Very demanding requirements for the ink such as low volatility and high viscosity and the resulting thickness of the layer are somewhat limiting factors for the use in the field of organic photovoltaics (OPV). Polymer MEHPPV suits these demands best up to this date and it appears to be the top candidate from the polymer based materials as can be seen from this US patent [40]. Commercially available PEDOT:PSS and silver inks exist and are usually used for preparation of electrode system, conducting lines or semiconducting layers. A good example is rotary screen-

printing of electron transport layer of PEDOT:PSS|ZnO described here [41]. A study was conducted on this topic to evaluate the influence of various silver paste solvents on the OPV characteristics.

It is worth noting that thanks to unique properties of this technique, such as easy and cheap operating, basic principle and a possibility to produce patterned layers is screen-printing the ideal printing technique for manufacturing of ACPEL devices. Several companies such as American GSI Technologies [42] and British Display Innovations [43] and Elumin8 [44] are large manufacturers of EL light sources for various application and use screen-printing for manufacturing exclusively.

According to IdTechEX report from 2017 ~ 98 % of products on the market are based on screen-printing. [45]. It can be concluded that screen-printing is the ideal technique for preparation of ACPEL light sources and therefore this technique was deployed for their preparation.

4.2.2 Gravure-printing

Gravure-printing is a classical high-volume printing method usually used in the graphic industry. This technique is based on an ink transfer from the gravure cylinder on a substrate. A pattern is etched mechanically or laser engraved on the gravure cylinder immersed in an ink tank. The printing ink is attached by a surface tension to the gravure cylinder and wiped by a doctor blade which is in contact with the form cylinder. Only the ink contained in engraved cells is transferred in a defined pattern on a substrate as can be seen in **Fig. 11**. The gravure cylinder itself is made of steel, a thin copper plate holds the predetermined pattern and the upmost layer is made from chromium and works as a wear resisting layer. A lot of theoretical work is focused on prediction of final film morphology and homogeneity. Computational simulations of the resulting layers as a function of the physical properties of the printing formulations were conducted by [46] and [47].

In the recent years gravure-printing gained popularity in the field of printed electronics due to multiple facts. It is a quick method with ability to achieve velocities higher than 15 $m \cdot s^{-1}$ and is perfectly R2R adjustable when polymer substrates are being used. Typical substrates are poly(ethylene 2,6-naphtalate) (PEN) or polyethylene terephthalate (PET). Significant disadvantage of this method is however the lack of possibility of changing the already engraved pattern. If a new pattern has to be introduced the cylinder must be reshaped or a new cylinder must be purchased and the operational price is thus significantly increased.

Thanks to the ability to print lines with resolution below 30 μm and the variability of materials that can be used the gravure-printing becomes an optimal method for printing thin layer transistors (TFT) or functional traces for organic electronics. Interesting work was done with polymer semiconductor poly[2,5-bis(3-tetradecylthiophen-2-yl)thieno[3,2-b]thiophene] (pBTTT) as an active film forming an organic field-effect transistor (OTFT). Silver source/drain (S/D) electrodes and busbarrs were inkjet-printed. The thickness of the dry pBTTT film was 50 nm [48]. Private company Thin Film Electronic ASA (TFE) is using rotogravure or bed gravure for mass production of memory labels consisting of a conductive grid layer and an active ferroelectric layers. R2R gravure-printing of OTFTs based on different active organic materials was subject of this research [49].

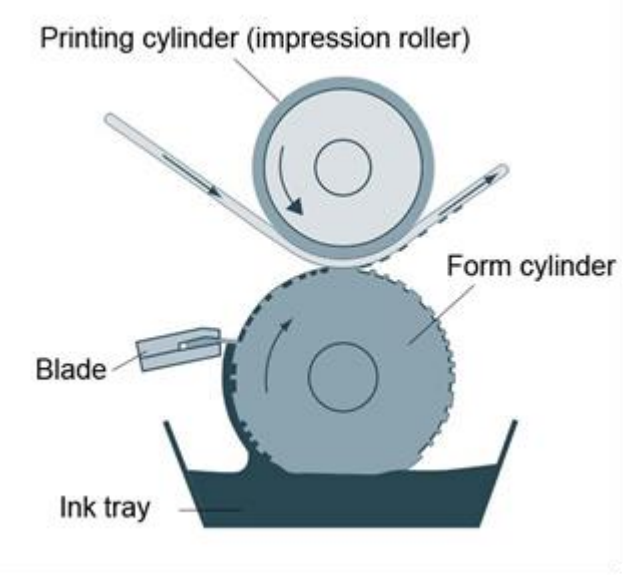

Fig. 11 *Basic principle of rotogravure-printing technique [50].*

Thanks to the ability to deposit very thin and homogenous layers (in the scale of ten of nanometers) the gravure print was used to prepare organic solar cells (OSCs) and organic light emitting diodes (OLEDs) with similar structure. The most typical active materials have been usually investigated: PEDOT:PSS and mixture P3HT:PCBM. The investigation involved solvent composition, morphology and wetting behavior of inks among other parameters. Small modules with total area 15.45 cm^2 on PET substrate with ITO were printed on R2R compatible gravure printer. The efficiency of these modules was 1.92 % but not all the layers were printed. Metallic electrodes were cathode evaporated [51]. Another work was exhibited again by Kopola et al where the active layer P3HT:PCBM and hole injection layer PEDOT:PSS were gravure-printed and an effect of printing parameters, ink composition and printability was examined. The obtained PCE from this work, 2.81 %, is the highest obtained value for the gravure printed OSCs [52].

In general this material printing method is too complicated and expensive for printing of ACPEL panels. Moreover the phosphor and dielectric films forming panels need to be thick in the order of tens of microns to ensure the proper behavior of the ACPEL light sources. This thickness is not compatible with the typical films formed by the gravure-printing method.

4.2.3 Flexography

Flexography is widely used technique especially in the industry of foil substrates. It is very quick printing method with speeds exceeding hundreds of meters per minute. Basic principles of this method can be seen in **Fig. 12**. It is based on an ink transfer from soft printing plate to a substrate which is located on an impression cylinder. The transfer is handled by the raised area of the cylinder in a shape of the pattern. It works in exactly opposite way than gravure-printing. Suitable material for the printing cylinder is a rubber or a photopolymer of various type and chemical behavior. The ink is transferred to the printing cylinder via a ceramic anilox cylinder which holds small engraved cavities on its surface. A doctor blade is attached above the cylinder and removes an abundant ink.

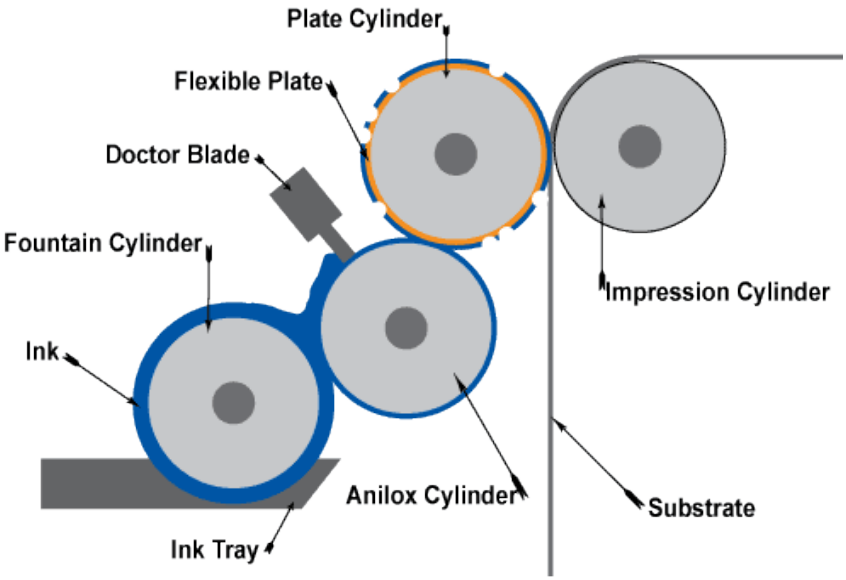

Fig. 12 *A simplified scheme of flexographic-printing [53].*

Demands on an ink rheology are similar to the gravure printing with values of a dynamic viscosity up to few hundred cPs. The other parameters that could be tuned in order to optimize the printing process are the printing speed, ink surface tension, nip force (the force of impact between printing and impression cylinders) and anilox cell geometry.

Flexography is not a broadly used technique in the field of organic and printed electronics. It was deployed for a printing of silver nanoparticles and PEDOT:PSS electrode. A paper based OSC has been published where transparent PEDOT:PSS acted as an anode layer on top of an active layer. This device exhibited a PCE around 1.3 % with an active surface 9 mm^2. Despite this research the main application of flexography in the OSCs field is still the deposition of silver based inks for the grid of front electrode – sometimes referred to as flextrodes. Variety of devices ranging from small lab-scale prototypes up to several meters long modules based on flextrodes with either honeycomb or slanted grid fingers structure were prepared and examined [54]. It was shown that fabrication speeds exceeding 20 $m \cdot min^{-1}$ is achievable.

Some other examples of use of flexography in the field of organic and printed electronics are printing of electrodes, dielectric layers for OTFTs, paper-thin loudspeakers and various electroluminescent layers [55–57]. This technique is quite similar to a gravure-printing and therefore can be said that its suitability for manufacturing of ACPEL panels is as limited as that of a gravure-printing.

4.2.4 Inkjet-printing

Inkjet printing has been a very well-known technology for at least 30 years and it found many interesting applications beyond the conventional printing [58]. This technique is based on a generation of multitude of small droplets by a printing head with typical volume in the range of picoliters (pL). These droplets are then transferred in a form of predetermined image on a substrate. A lot of interdisciplinary research had to be done in order to make this technique reliable. Good knowledge of fluid mechanics, electrostatics, optics, ink chemistry and other scientific fields needed to be exercised.

Inkjet-printing can be divided into two distinct categories: continuous inkjet (CIJ) and drop-on-demand technique (DOD). Only the DOD will be mentioned in this work since the CIJ doesn't meet requirements for the field of printed electronics [34]. Among the biggest advantages of this method is its versatility and the fact that no hardware master is needed (compared to other techniques) since the image is in a digital form with excellent resolution [14]. On the other hand DOD inkjet suffers also from several disadvantages. Printing speed is limited by the amount of nozzles and also a wide variety of physical-chemical properties of both the ink and the substrate need to be taken into consideration. Fine droplets with good cohesion with the substrate have to be formed to ensure that a sharp pattern with no stains or coffee ring defects is deposited. The formulations of inks based on clever materials suitable for application in the field of material printing have their limits.

Majority of modern DOD printing heads use piezoelectricaly actuated transducers that eject droplets on demand when external voltage is applied. This voltage waveform induces a pressure pulse that is propagated through the ink in a chamber situated just behind the printing nozzles. Once the pressure pulse exceeds the threshold at the nozzle the droplet is ejected. All this is controlled by computer via the specific digital pattern created by software. The ink itself is contained within the chamber through surface tension and static pressure that further help to stabilize the meniscus at the nozzle [59]. Simplified process can be seen in **Fig. 13**.

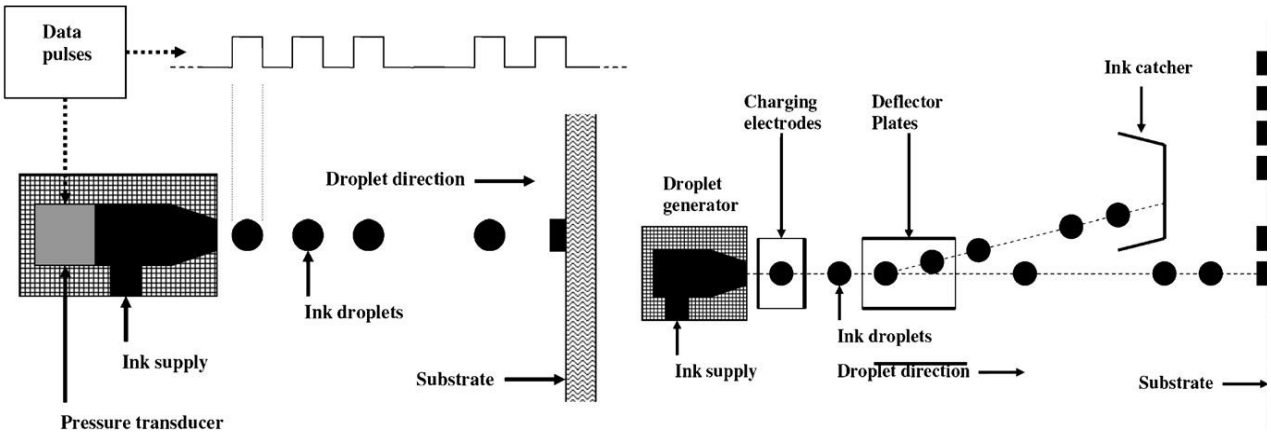

***Fig. 13** Difference between DOD (on the left) and continuous inkjet [14].*

Thickness of a dry inkjet-printed layer, **Eq. 7** is given by number of droplets deposited per area, volume of droplets and the concentration of solid phase in an ink.

$$d = N_{\mathrm{D}} \cdot V_{\mathrm{D}} \cdot \frac{c}{\rho} \tag{7}$$

Where N_{D} is the number of droplets deposited per area in cm^{-2}, c is the concentration ($\mathrm{g \cdot cm}^{-3}$), ρ is the density of material in the dry film ($\mathrm{g \cdot cm}^{-3}$) and V_{D} is the volume of droplets in cm^3.

A lot of very different parameters affect a quality of ink-jet printed layer. Key physical-chemical properties such as viscosity of ink (dynamic viscosity in range approximately 4–30 cP), surface energy of the substrate, surface tension of the ink for forming droplet or stream of droplets (typically > 35 $\mathrm{mN \cdot m}^{-1}$), suitable mixture of solvents (sometimes 5 – 8 different volatile solvents) and printing parameters such as a drop distance, printing head volume and printing velocity govern a quality of the printed film. A lot of adjustment and optimization is

required in order to meet satisfying resolution, pattern definition and homogeneity of the printed films [58–60]. Because of these limitations it is currently hard to determine the future of the ink-jet printing and its potential to be used for mass production of printed electronics [14].

As was said earlier when the voltage waveform is applied a droplet is shot from the nozzle with relatively high initial velocity. At this moment the droplet is still connected with the ink in the nozzle by a stretching ligament. At some point the ligament is broken and a surface tension of the liquid forces a droplet to take spherical shape. If the ligament was long enough it can even form satellite droplets that negatively affect the resolution of layer.

Both the viscosity and the surface tension are dominant forces that control behavior of droplets and streams of an ink. It is useful to describe the behavior of forming droplets and films by specific dimensionless numbers. Reynolds number given by **Eq. 8**, Re describes the ratio between inertial and viscous forces in a fluid.

$$\mathrm{Re} = D \cdot v \cdot \frac{\rho}{\eta} \tag{8}$$

Where D is a characteristic length – jet length of droplet diameter (m), v is velocity ($\mathrm{m \cdot s^{-1}}$), ρ is density and η is dynamic viscosity (Pa·s).

Another dimensionless number, given by **Eq. 9**, taking into account kinetic energy and surface energy is Weber number, We.

$$\mathrm{We} = D \cdot v^2 \cdot \frac{\rho}{\sigma} \tag{9}$$

Where σ is surface tension ($\mathrm{mN \cdot m^{-1}}$)

Important number is Ohnesorge number, Oh expressed by **Eq. 10**, which describes a ratio of the viscous and surface forces.

$$\mathrm{Oh} = \frac{\mathrm{We}^{0,5}}{\mathrm{Re}} \tag{10}$$

Theoretically valuable research was conducted by Martin et al [58] where a window of printing conditions was determined for CIJ and DOD in respect with the values of dimensionless criteria. This window can be seen in **Fig. 14**. Jang et al determined a range of another dimensionless parameter a Z-number ($\mathrm{Z = Oh^{-1}}$) for the inkjet-printing. This interval seems to be $\leq \mathrm{Z} \leq 14$.[61].

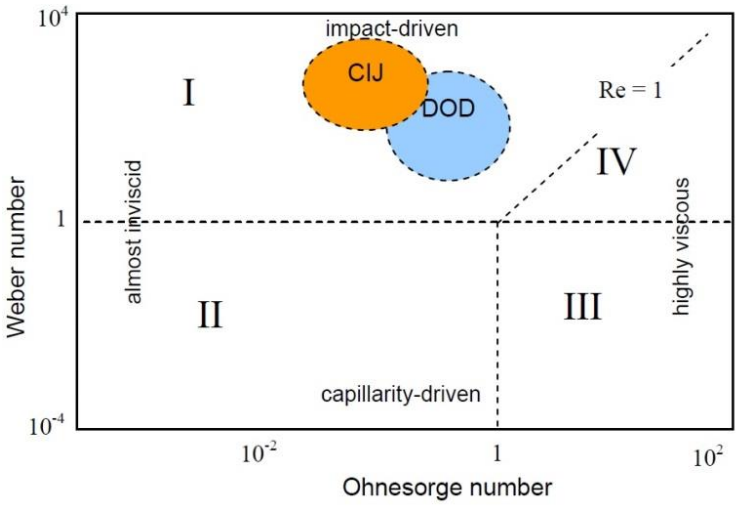

Fig. 14 *Schematic diagram showing four regimes of behavior of liquid drop based on the values of* We *and* Oh *[61].*

It can be said that the recent years have seen increasing interest in using inkjet for fabrication of printed electronic devices in a lab scale. Both the active layers and PEDOT:PSS were printed in the form of homogenous layers and silver nanoparticles were printed in the form of grid as a current collecting electrode. Reported inkjet printed solar cells with the highest achieved PCE 3.7 % so far are based on the active layer of PFDTBTP:PCBM [62]. In this study a lot of different mixtures of solvents were used (such as anisole/tetraline, p-xylene/tetraline etc.). This research proves how complex is the problematic of finding optimal printing conditions. Otherwise a lot of work has been done with the standard polymer P3HT. Interesting discovery was made on the use of additives which influence the morphology and optoelectronic properties of the active layer. The best result was achieved with 1,8 octanedithiol which lead to an efficiency of 3.71 % [63]. A comprehensive research on fully ink-jet printed TFTs was given here [64] with aim to find causes of defects that are formed during printing.

Even though inkjet printing has seen its rise in the field of organic and printed electronics there has been virtually no report on up-scaling this technique for a high volume application up to this moment. This technique is virtually useless for printing of phosphor layers forming the ACPEL panels because of the grain sizes. Inkjet-printing of either dielectric or electrode layer could be processed after immense optimization of printing formulations.

4.3 Recapitulation of relevant deposition/printing techniques.

Some relevant deposition and printing techniques were introduced in **Chapter 4** with short description of properties of deposition formulations, physical-chemical properties of materials and the properties of printed films from the point of view of the desired application. Both advantages and disadvantages of each technique were summarized in order to choose the most suitable technique for printing of an electroluminescent panel.

It is notable that preparation of fully printed electronic devices is extremely demanding and the results so far are not very convincing. Slot-die coating is well suited for application where no pattern is needed but homogeneity and well defined layer thickness is demanded. For instance various planarization layers and blocking layers for charge carriers in organic and printed electronics were successfully deposited by this technique.

Gravure-printing and flexography are in general similar methods and could be used for similar applications. Gravure-printing is the most suitable technique in cases where thickness of layers is of a special concern and needs to be less than 100 nm. Together with flexography this technique finds application for development of printed OTFTs [49] and also good results in the field of organic photovoltaics were achieved by printing of an active layer P3HT:PCBM [52].

Screen-printing is a technique that gives well defined pattern on one hand but puts severe demands on the physical-chemical properties of the ink on the other hand. This method finds application among many others for deposition of electrodes for devices not based on ITO. Deposition of an active layer of MDMO-PPV:PCBM [65] by screen-printing with increased PCE was published. Important advantage is the fact that it can be modified for R2R print. It is the most promising technique for mass-printing of devices based on the organic and printed electronics currently. Screen-printing found also its application in the field of printed biosensors where electrode grid with semiconducting PEDOT:PSS was printed by this technique [66]. Screen-printing is also a key deposition technique for manufacturing of printed, powder-based electroluminescence panels. This is supported by the fact that screen-printed large area EL panels have already found their place in the industry [44, 1].

Inkjet printing is the most versatile method since it needs only a digital master for printing. So far inkjet-printing has been mainly used in the field of photovoltaics [63]. At the moment the best results in OSCs were obtained by the inkjet printing technique but it does not necessary mean that the technique is the best suitable. Inkjet-printing is not R2R compatible and therefore it goes slightly against the idea of mass-volume high-speed manufacture of devices.

Some techniques are very simple to operate and very appealing from the economical point of view but their inability to produce a fully patterned layer is their shortcoming and **Chapter 4.1** of this thesis deals with them briefly while some other techniques enable preparation of precisely patterned layers but at significantly higher costs. Some techniques produce relatively very thick layers (from tens of micrometers up to millimeters) while layers prepared by for instance gravure-printing and flexography can be up to several nanometers thick. The truth is that up to this day the screen-printing method is still by far the most wide-spread technique in the field of organic electronics.

As can be seen a lot of different coating and printing techniques can be applied for the manufacturing of printed electronic devices. **Tab. 2** summarizes results and typical examples of application of several key printing and deposition techniques.

Tab. 2 *A summary of printing techniques in various applications.*

Material	**Type of layer**	**Additional information**
Slot-die coating		
P3HT:PCBM	Active layer for SC	Fully printed OSC (PCE = 0.3%) [25]
NP ZnO	Electron transport layer	

PEDOT:PSS	Hole transport layer	
Organic polymer	ITO-free polymer anode	[30]
-	Planarization layer	R2R deposition for memory tags (Thin Film Electronics)
Screen-printing		
MDMO-PPV:PCBM	Active layer	Only the active layer (PCE = 4.2 %)[65]
P3MHOCT:PCBM:ZnO	Active layer for SC	All layers printed by the mean of screen-printing
Terpineol-basead TiO_2	Photoanode layer	Promising new material [39]
High conductivePEDOT:PSS	Electrodes	ITO-free OPV devices
PEDOT:PSS	Gate and semiconductor layer	[66]
-	System of protective layers	Rotary screen-printing for memory tags(Thin Film Electronics)
Material	**Type of layer**	**Note**
Gravure-printing		
pBTTT	Active semiconductor layer	-
Ag	Electrode system	OTFTs (Thin Film Electronics)
-	Planarization and dielectric layers	Development of OTFTs (Thin Film Electronics)
P3HT:PCBM	Active layer for SC	Complex study of several factors, The best PCE so far (2.81 %) [52]
PEDOT:PSS	Hole transport layer	

Ferropolymer	Active memory layer	Large scale fully R2R preparation (TFE)
Material	**Type of layer**	**Note**
Flexography		
Ag NP	Electrode layer	
PEDOT:PSS	Electrode/hole mobility layer	
-	Dielectric layers	OTFT
Inkjet printing		
Ag NP	Current collecting grid	Various applications
PFDTBTP:PCBM	Active layer for SC	Best PCE (3.7 %) with addition of 1,8 octanedithiol [63]

From the review of the deposition and printing techniques provided by this thesis the screen-printing is the optimal technique for printing of all the layers the ACPEL display consists of. It is a simple and well established technique widely spread in many different areas and highly viscous printing formulations can be printed in a wide range of patterns and sizes.

Coating techniques in general are not very suitable because of their inability to produce a patterned layer. Gravure-printing and flexography could be used for mass-production of metal top electrodes. Otherwise both these techniques require much optimization and are impractically expensive for printing of ACPEL panels. Demands on physical-chemical properties of inks for inkjet-printing are not compatible with paste formulations for ACPEL.

5 METHODS OF FILM CHARACTERIZATION

In general a layer is an object whose one dimension (thickness) is significantly smaller than the other two dimensions. When the thickness is small enough, usually in the order of nanometers, the material starts to exhibit so called quantum dimension phenomena which are unparalleled to the bulk objects. The two surfaces of a thin layer are so close to each other that physical properties of these layers start to show much different behavior than bulk layer from the same material. This is valid for the mechanical, thermal, optical and magnetic and electrical properties just to name few. Optical phenomena especially thin-layer interference in the form of interference colors on their surfaces are most easily distinguishable and can sometimes be seen by a naked eye as is shown in **Fig. 15**.

We typically talk about thin layer when the thickness of a material film ranges from 0.1 nm which are monoatomic layers up to approximately 1 μm. From the point of this definition the films prepared by a screen-printing should not be classified as thin layers. But films with thickness in the order of units and tens of microns, as is typical for screen-printed films, are still too thin to be classified as bulk layers and this work will continue to deal with them as thin layers. In the 20th century thin film coatings experienced tremendous rise and helped develop some modern day areas of technology and science. Multilayer metal and insulating films in microelectronics, semiconducting films in optoelectronics and stacks of dielectric films for optical coating, ceramic layers and many others can be taken as a short list of examples.

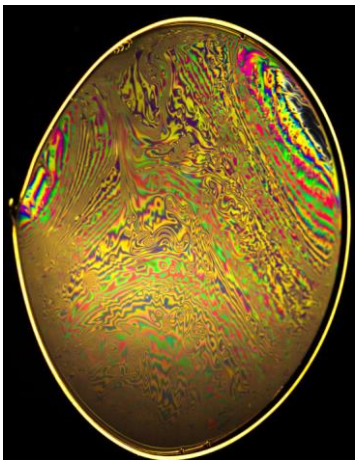

Fig. 15 *Interference color patterns on a thin layer [67].*

Because of such a broad use of thin films and their overall impact on the modern technology a need for development of techniques leading to their characterization has risen. The layers can be characterized from a multiple points of view. A comprehensive background on conducting measurement and interpretation of the data can be found here [68].

All the methods can be divided, according to the physical principle of measurement, into 3 main areas: (*i*) mechanical, (*ii*) optical and (*iii*) electrical. Mechanical methods are based on contact profilometry, quartz crystal microbalance and frequency of damped oscillations of crystal oscillator. Optical methods involve methods such as interference on the thin layer, determination of interference colors, interference microscopy and ellipsometry. Electrical methods are based on measurement of either electrical resistance or capacity of samples connected in an electrical circuit.

ACPEL panels presented in this work are large area sources of light that consist of multiple stacked films. Thickness *h* and homogeneity – represented by parameters roughness (*Ra*) and waviness (*Wa*) – of the layers dramatically influence performance of panels. Unit of all the above mentioned parameters is meter (m). For instance if the dielectric layer is not homogenous and pinholes are present, top and bottom electrodes are connected and the panel is short-circuited. There exist a wide variety of different techniques for determination of quality of films. Some of these methods in general can be used only for the deposited films while other techniques can be used for measurement of the growth of thin layer in time. Some methods are destructive while some are not. It is important to realize that the thin layer can be smooth and continuous or rough or even non-continuous and only an average value (the so called weight-thickness) of its thickness can be determined. The layers forming ACPEL panels in this work were characterized by mechanical profilometry.

Mechanical profilometry is a technique vaguely similar to AFM. A diamond stylus slides over a surface for a specified distance a thickness is determined from deflection of the arm holding the tip. If an artificial step is created either by a mechanical scratching or by a deposition through a mask its thickness can be easily measured. In the modern instruments the height position of the stylus creates an analogue signal that is converted into a digital signal. Diamond stylus with cone angle either 45° or 60° is standardly used and the stylus impact force typically ranges from 0.1–50 mg, allowing step heights from 50 Å (5 nm) to 800 μm to be measured. Vertical magnification from several thousand up to approximately 1 million can be achieved. It is possible to measure layers which thickness is in a scale of ångströms and uncertainty of ± 1 nm can be obtained when measuring 100 nm thin layers [69]. Both the calibration and leveling is computer controlled.

Several factors limit the accuracy of mechanical profilometry. For instance penetration of stylus through a very soft layer occurs when an impact force is too high. This is typical for In, Sn films [69] or some organic films. An excessive roughness of a film generates noise which decreases the accuracy and resolution of the measurement. Machinery also needs to be stabilized in order to minimize shocks and vibrations of the surroundings. Resolution of these techniques is insufficient to show microscopic defects or exact surface topography down to individual atoms or molecules. It is also impossible to determine composition of surface.

5.1 High resolution surface imagining methods

There are various methods that can provide us information about the surface topography and composition of a film. Images taken by high resolution techniques among other confirmed theoretical predictions of ZnS crystals excitation and generation of light [70]. It is also possible to show cross-section images of panels to show a size of the ZnS clusters for optimization of a structure of the panel – mainly the overall thickness of dielectric film.

The atomic force microscopy (AFM) which is a special type of scanning probe microscopy (SPM) is commonly used technique similar to mechanical profilometry. A charged cantilever moves across the surface of a sample and interacts with it. A cantilever displaced by this interaction reflects a laser beam to different pixels of a charge-coupled device (CCD) photodiode matrix. Profile topography could be obtained from displacement of the laser beam.

Another widely used technique is scanning electron microscopy (SEM) which is a type of electron microscopy where a sample is scanned by a focused electron beam. Energetically rich electrons interact with the atoms forming a surface of the sample. As a result of these interactions reflected, scattered, secondary emitted electrons or X-ray beams are analyzed by suitable detectors. These processes reveal information about the surface topology but also about the composition of layers very close to a surface. **Fig. 16** represents an image from scanning electron microscope (SEM) showing the cross-section of the ACPEL panel with all distinguishable layers.

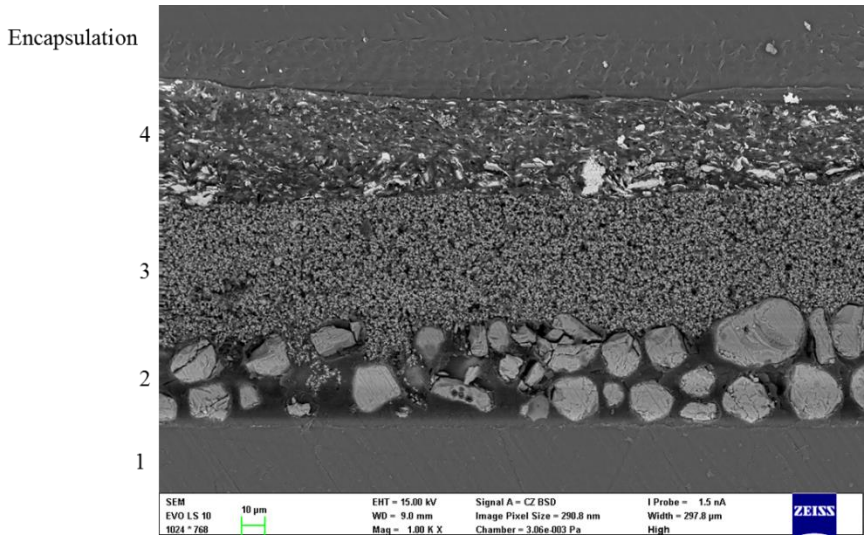

Fig. 16 *A SEM image showing cross-section of fully printed ACPEL device with labeled layers: 1 – ITO substrate; 2 – phosphor; 3 – double dielectric layer; 4 – top metal electrode.*

Both these methods have their advantages and disadvantages. Whereas AFM gives a 3D profile the SEM provides only 2D images. There is no need to specially treat samples for the AFM. But for SEM an expensive vacuum system has to be used for preliminary treatment of the sample (deposition of conductive layer) and during the scanning of the probe. Higher resolution can be obtained by AFM but SEM gives significantly quicker, nearly real-time measurement with in-depth information about the composition of the films.

All these methods provide a complex characterization of films including their thickness and surface homogeneity. A logical disadvantage of these high resolution techniques is their astronomic acquisition price. For many applications is it enough to have pieces of information just about the thickness and surface.

6 PHYSICAL PROPERTIES AND HUMAN PERCEPTION OF LIGHT

Printed electroluminescent panels are an extended source of light. It is therefore appropriate to introduce light from various angles of view. A basic physical background together with relevant parameters characterizing both the emitted light and a quality of a light source will be a topic of this chapter.

Light provides us a powerful tool to perceive a reality around us. It is thanks to absorption and emission of all objects around us that we are able to see them. It is possible to determine the composition of stars on the other side of galaxy or watch the processes that occur in living cells through the study of optical phenomena.

There are 3 distinct ways how to perceive light: geometric, wave and quantum optics. The most modern and comprehensive theory of light is called quantum electrodynamics (QED). The geometric optics presents light as a ray, according to the wave-mechanical concept is light a wave of an electric and magnetic field propagating by the speed of light ($c \sim 3 \cdot 10^8\ m \cdot s^{-1}$) in the vacuum. Quantum model introduces light as a set of particles called photons. All three concepts have their merits and limitations.

6.1 Geometric optics

Geometric optics is the oldest and most intuitive way to describe light. The propagation of light is described as a ray taking the shortest path between two points under certain circumstances

a) particles propagate in a straight line while travelling in a homogenous medium

b) trajectory of ray is curved by traversing two media with different optical density (refractive indices n_1 and n_2)

c) rays can be reflected under certain angle depending on the angle of impact

Fig. 17 shows an illustrative schema of the above mentioned phenomena.

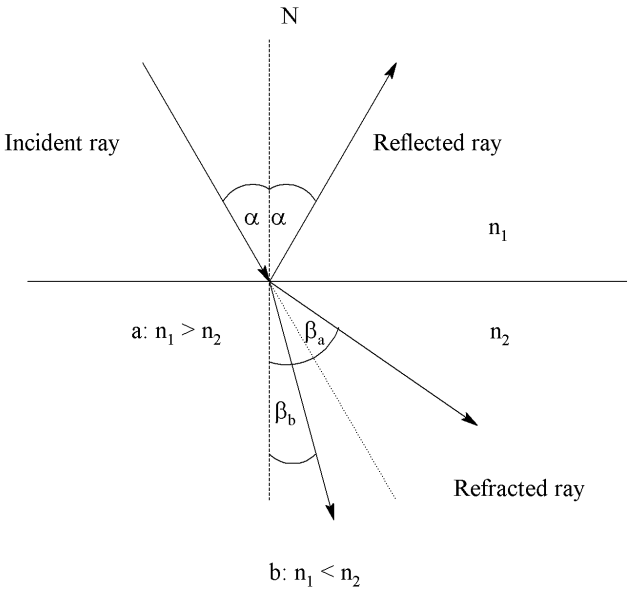

Fig. 17 *Illustration of light beam refraction according to Snell's law.*

The point b) represents a Snell's law (**Eq. 11)** describing the angle under which the trajectory of a ray is changed upon entering a medium with different optical density

$$n_1 \sin\alpha = n_2 \sin\beta = v_1 \sin\alpha = v_2 \sin\beta \tag{11}$$

n_1 and n_2 are the refractive indices, α and β are angles of incident and refracted light and v_1 a v_2 are group phase velocities of light in different media ($m \cdot s^{-1}$)

It is worth noting that not all the rays undergo refraction but some portion of the incident light is reflected under the same angle to the surface normal as the incident light. This concept of optics is particularly useful for solving problems concerning optical imagining, construction of lenses, collimators and mirrors and basic dispersion systems based on the light traversing optical prism. Knowledge of a refractive index of a layer is also crucial for construction of optical fibers collecting a light on one spot and delivering it to a detector. Because of slightly different values of the refractive indices of light with different wavelengths – colors ($n_{RED} < n_{VIOLET}$) the white light is dispersed into rainbow of colors as can be seen in **Fig. 18,** which was first noted by Isaac Newton. Focusing and collimating lenses constructed on the equations originating from this concept of light are used in the state of the art spectrometers of today. Geometrical principles also rule setups for various light measurements.

Contribution of geometric optics for description of light and imagining methods is vast but its clear disadvantage is its inability to describe some phenomena such as photoelectric effect, color of light or radiation of a black body to name very few.

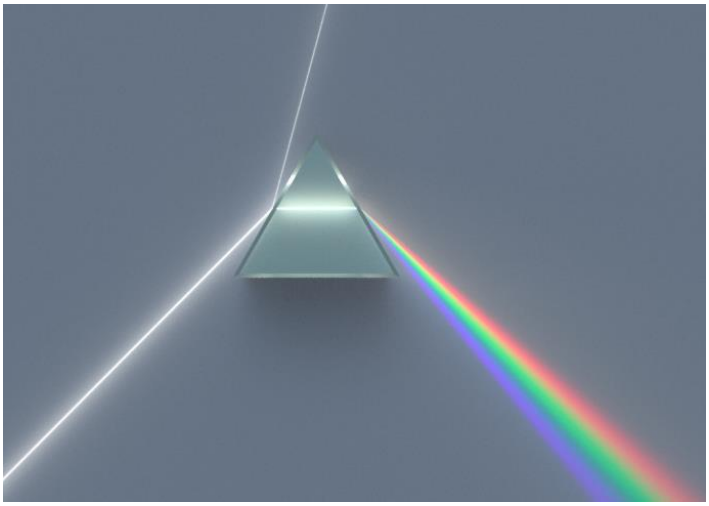

Fig. 18 *A dispersion of light beam on an optical prism.*

6.2 Wave and quantum models of light

The wave model describes light as a wave of electromagnetic radiation propagating in a space by a finite velocity. Vectors of electric intensity **E** and magnetic induction **B** are perpendicular to each other and to the direction of propagation as can be seen in **Fig. 19**. Electrical and magnetic field were considered as two distinct areas which have nothing in common but thanks to the heroic effort of James Clerk Maxwell a series of equations (known as Maxwell equations) were derived

unifying both fields of classical physics into the electromagnetic theory. On the other hand the quantum model describes light as a particle called photon.

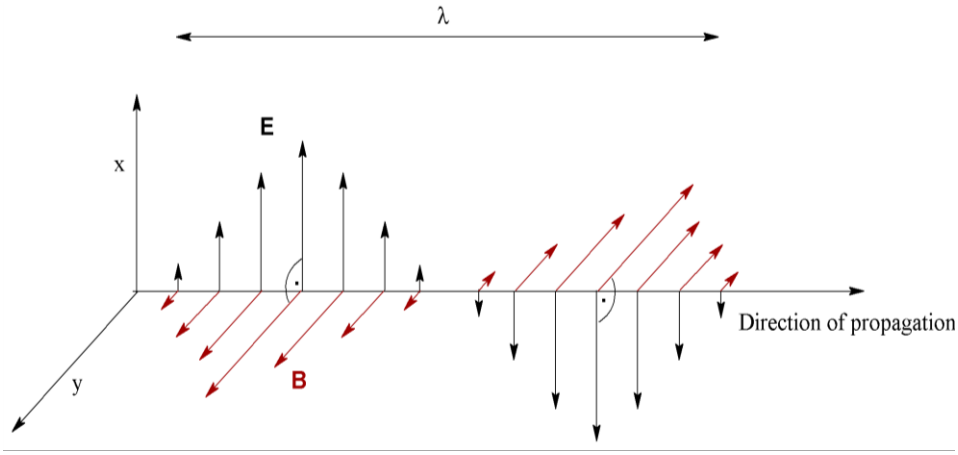

Fig. 19 *Propagation of an electromagnetic wave in space.*

Important parameter of the light is its wavelength λ (m) describing the distance of two points oscillating with the same phase. The wavelength of light carries information about the energy contained in the light quantum/wave. Both wave and quantum model appear to contradict each other but experiments – such as diffraction on a thin double layer or a slit – prove the wave nature of light while other experiments – such as Compton scattering – at the same time prove the particle nature of a light. This phenomenon is called wave-particular duality.

Wavelength of a wave/oscillating particle carries information about the energy of radiation. **Eq. 12**.

$$E = \mathrm{h}\nu = \mathrm{h}\frac{\mathrm{c}}{\lambda} \tag{12}$$

Where h is Planck constant ($\mathrm{h} = 6.626 \cdot 10^{-34}$ J·s), ν is frequency of oscillation of a particle (Hz), c is speed of light in vacuum ($\mathrm{c} \sim 3 \cdot 10^{8}$ m s^{-1}) and λ is wavelength (m).

Visible light is only very small fraction of radiation in the range of wavelengths approximately 380–760 nm. **Fig. 20** depicts the visible region as a fraction of the full band of wavelengths. **Eq. 12** shows that the energy of blue photon is higher than energy of the red one.

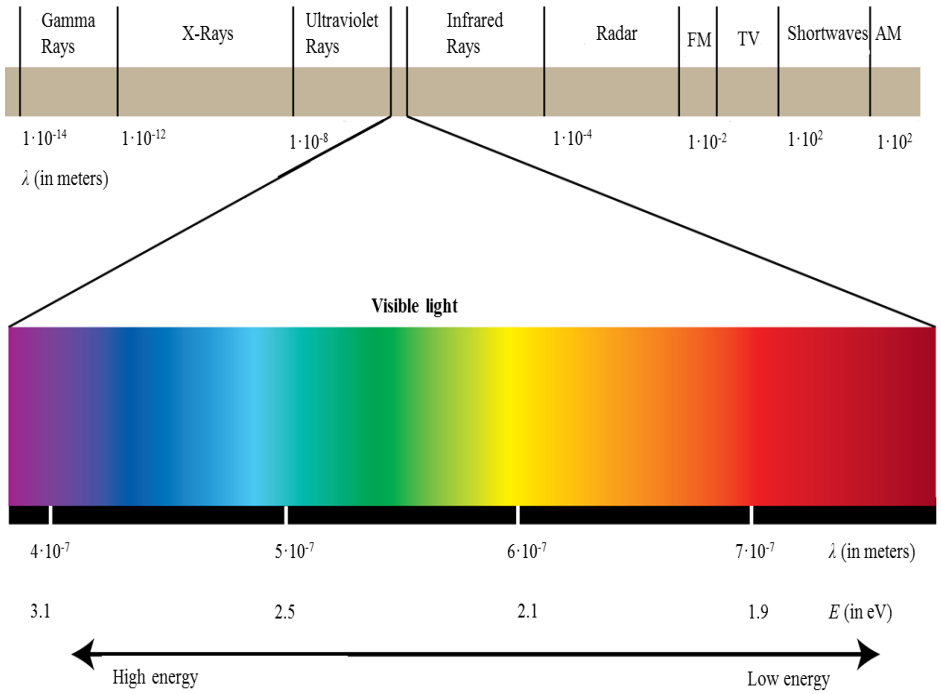

Fig. 20 *Visible light as a part of other types of radiation with their typical wavelengths and corresponding energies of a photon in electronvolts.*

The achievements of both concepts are manifold. Diffraction (bending) of light occurs when light is traversing through a slit with a diameter comparable to the wavelength of light. As a result a diffraction patterns appear in the region of a geometrical shadow in specific areas where the light waves are constructively superposed. Such a phenomenon cannot be explained by the classical geometric optics. Various optical systems, such as monochromators that are based on diffraction gratings, are integral part of modern analytical spectrometers and their function is based on explanation and analysis of this phenomenon. The quantum approach toward light gave rise to many research fields (such as spectroscopy) and technological advance.

6.3 Human perception of light

The light emitted by a panel must be appropriately described from the point of view of how intensely it will be processed by an observer. There are two distinct ways how to characterize the emitted light. Radiometry is a part of physics dealing with detection and characterization of electromagnetic radiation in the region from UV–IR. The physical properties of light are characterized by radiometric quantities such as: the number of incident photons, optical power (also known as radiant flux), irradiance, radiant intensity and many others. Radiometric quantities are defined in terms of the fundamental units of energy, time and length. This approach however bears little relevance for description of light as perceived by human eye. For instance both ultraviolet and infrared radiations cause no luminous response by the eye no matter how much power they contain. A new set of units was defined that take into account a response of the standard observer toward the optical signal. These units are called photometric quantities. **Tab. 3** shows some basic radiometric quantities and their photometric counterparts.

Tab. 3 *Basic radiometric and photometric quantities. The indices "v" denotes "visible" and "e" "radiative" for distinction of radiometric and photometric quantities.*

Meaning	Radiometric	Photometric
Energy received/emitted per unit time	Radiant flux, Φ_e	Luminous flux Φ_v
Flux per solid angle	Radiant intensity I_e	Luminous intensity I_v
Flux received by a surface unit area	Irradiance E_e	Illuminance E_v
Irradiance per 1 nanometer of radiation	Spectral irradiance $E_{e,\lambda}$	Spectral illuminance $E_{v,\lambda}$
Flux emitted per solid angle per projected area	Radiance L_e	Luminance L_v

Tab. 4 shows comparison of photometric and radiometric units. It is worth noting that the unit lumen is a photometric analog of unit watt.

Tab. 4 *Some basic radiometric and photometric quantities their units.*

Quantity	Radiometric	Photometric
Flux	watt (W)	lumen (lm) = cd·sr
Intensity	$W \cdot sr^{-1}$	candela (cd)
Irradiance/Illuminance	$W \cdot m^{-2}$	lux (lx) = $lm \cdot m^{-2}$
Spectral irradiance/Spectral illuminance	$W \cdot m^{-2} \cdot nm^{-1}$	$lm \cdot m^{-2} \cdot nm^{-1}$
Radiance/Luminance	$W \cdot m^{-2} \cdot sr^{-1}$	$lm \cdot m^{-2} \cdot sr^{-1} = cd \cdot m^{-2}$

Detection of light by human is mediated by the detectors called the eyes. The inside of human eye is covered by photo sensitive layer called retina. A retina is formed by two types of photosensitive cells – cones mediating colorful vision and more sensitive rods mediating a vision in dark. There exist 3 types of cones sensitive in red, green and blue region. Human eye with its internal structure can be seen in **Fig. 21**. When the luminance of light source is too low the more sensitive rods are activated and the eye works in the scotopic white – black vision regime and vice versa when the luminance is high, the colorful photopic vision regime mediated by cones is activated. A bridge between these two regimes is mesopic regime when both rods and cells are active. **Fig. 22** shows typical values of the luminance for all three types of regimes.

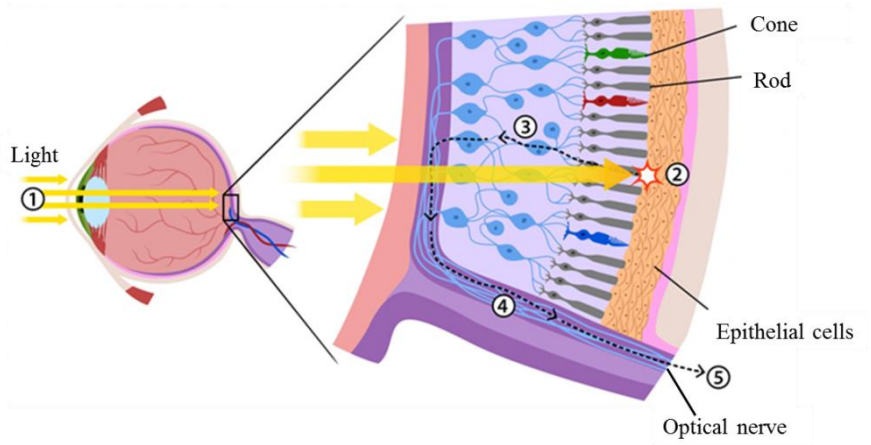

Fig. 21 *Cross-section of human eye. Point 1) represents light transmission through optical lens 2) light incident on a photoactive cell points and 3 – 5) transfer of the generated electrical impulse to the brain. Adapted from [71].*

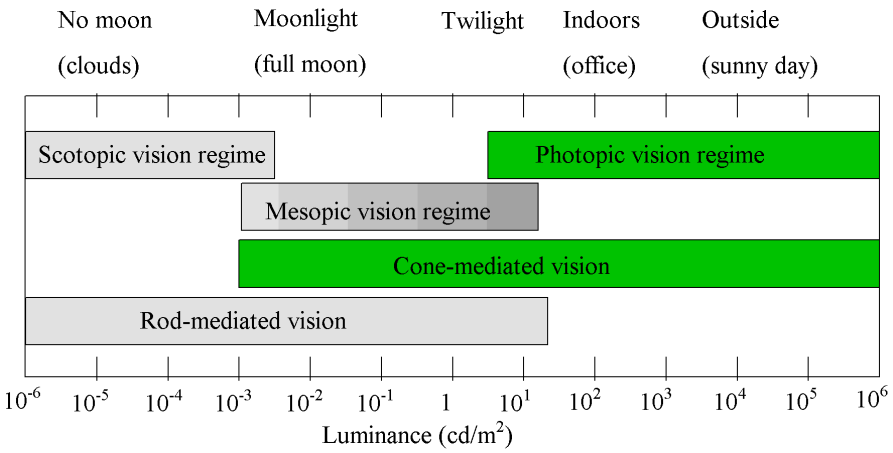

Fig. 22 *Vision regimes under different values of luminance. Adapted from Osram Sylvania 2000.*

The bridge between radiometry and photometry is a photopic spectral luminous efficiency curve $V(\lambda)$ that was defined as a standard by CIE in 1931 for 2-degree field of vision. Human eye contains three different types of cones that are sensitive in blue, green and red region so three different color matching functions $\bar{x}(\lambda)$, $\bar{y}(\lambda)$ and $\bar{z}(\lambda)$ respectively (shown in **Fig. 23**) were defined to model optical response of cones. These three functions are called the standard observer. It was stated by definition that $V(\lambda)$ is identical with $\bar{y}(\lambda)$ curve. The **Eq. 13** shows the transition from spectral radiant flux $\Phi_e(\lambda)$ to luminous flux Φ_v. The constant standing before the integral is taken from definition of basic SI unit candela.

$$\Phi_v = 683{,}02\ \mathrm{lm/W} \int_{390}^{830} \Phi_e(\lambda) \cdot \bar{y}(\lambda) \mathrm{d}\lambda \tag{13}$$

The photopic function can be fitted by function given as **Eq. 14**

$$V(\lambda) = 1.019 \cdot \exp\left(-285.4 \cdot [\lambda - 0.559]^2\right) \tag{14}$$

where λ is wavelength in micrometers.

It is very illustrative to characterize color by its coordinates in a color space. One of the most basic and most used is RGB color space. Each color is represented by its *x* and *y* coordinate inside the chromaticity diagram with its characteristic horseshoe like shape. This color space will be used later in this thesis to estimate the photometric quantities and to modify a spectral profile of the emitted light. The values of *x* and y can be calculated from the trichromatic values *X*, *Y* and *Z* by **Eq. 15**.

$$\begin{aligned} x &= \frac{X}{X+Y+Z} \\ y &= \frac{Y}{X+Y+Z} \end{aligned} \tag{15}$$

The trichromatic values are dependent on the spectral luminance $L_{v,\lambda}$ (cd·m^{-2}·nm^{-1}) of the source multiplied by respective color matching function – shown as **Eq. 16**

$$X = \int_{\lambda} L_{v,\lambda}(\lambda) \cdot \bar{x}(\lambda) \mathrm{d}\lambda$$
$$Y = \int_{\lambda} L_{v,\lambda}(\lambda) \cdot \bar{y}(\lambda) \mathrm{d}\lambda \qquad (16)$$
$$Z = \int_{\lambda} L_{v,\lambda}(\lambda) \cdot \bar{z}(\lambda) \mathrm{d}\lambda$$

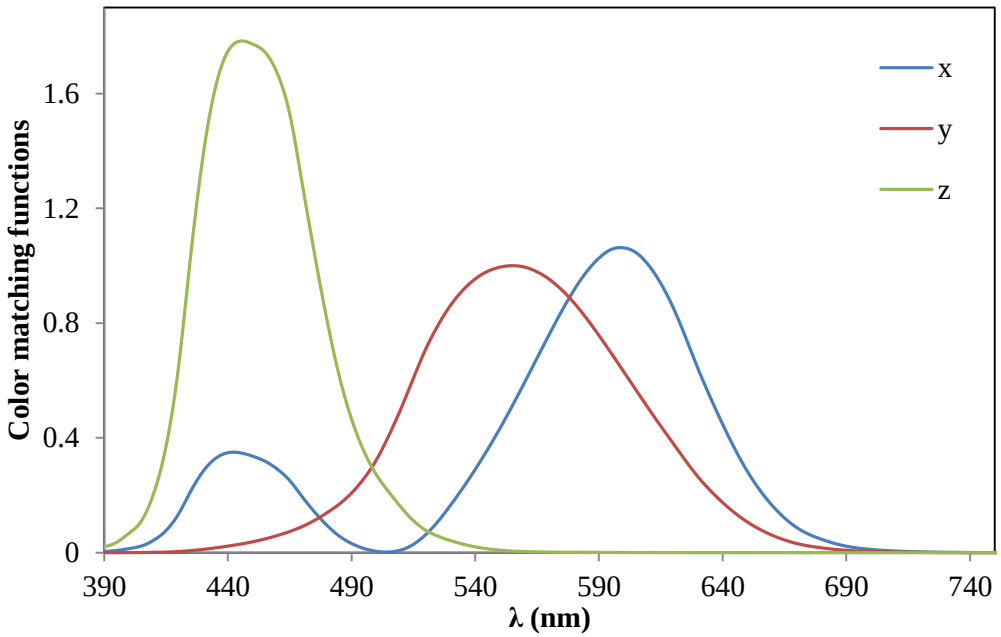

Fig. 23 *CIE-1931 2-degree field of vision color matching functions.*

7 PROCESSING CONDITIONS AND OPTOELECTRONIC PROPERTIES OF FULLY PRINTED PANEL

This chapter is focused on optimization of processing conditions leading to reproducible preparation of fully printed light emitting panels and their optoelectronic characterization. **Chapters 7.1–7.3** deal with optimization of a printing process of films forming the panel and its impact on their specific physical properties. **Chapter 7.4** is focused on photometric characterization of panels as sources of light and on estimation of their electrical power consumption. **Chapter 7.5** deals with a stability of the shining panels, description of specific factors decreasing its lifetime and encapsulation of the printed source of light. Estimation of specific time constants L_{50} and L_{75} is the aim of this chapter. The stability of printed electroluminescent devices is one of the red brick problems for this technology. The topic of **Chapter 7.6** is a modification of color of emitted light. A limited portfolio of colors emitted by printed ACPEL panels is also one of deep throats preventing this technology to achieve its full potential.

The complete panel consists of flexible substrate with fully transparent electrode (ITO), active phosphor film, dielectric film and top metal electrode. With the exception of transparent electrode all the films are prepared by screen-printing technique. All the printing formulations are commercially available and were purchased from GWENT GROUP Advanced Material System. The fully printed panel based on these pastes serves as a reference panel for determining of optimal printing parameters, operating conditions such as driving voltage and frequency, stability and power consumption. These parameters serve for further optimization of the optoelectronic properties and further improvement of performance of the commercially successful panels. All the layers as fulfill very different roles and different parameters need to be evaluated in order to ensure the optimal behavior of the whole device.

7.1 Dielectric film

The thick layer of dielectrics is incorporated in the panel as a tool for separation of rear and top electrode. The applied voltage is usually in the order of hundreds of volts to achieve an electric field intensive enough to generate light. Therefore several key physical properties are required of the materials to be used as dielectrics. The first critical parameter is the dielectric strength of an insulating material ($V \cdot m^{-1}$) which defines the maximum intensity of electric field that can be applied on the electrical insulator. If this value is exceeded the dielectrics exhibits a breakdown and consequently a short-circuit occurs. The second important parameter is the relative permittivity of material, ε_r (-). This property is specific to a given material and is defined as a ratio of the Coulomb force between the two charges in vacuum and in given material. Relative permittivity also governs the induction of displacement current I_D flowing through the material and exciting electrons and holes in the of $Cu_{2-x}S$ needles.

Typical material with long tradition of use in this type of devices is barium titanate ($BaTiO_3$) with ε_r in the order of several thousand units. Dielectric properties of $BaTiO_3$ are not constant and show very strong dependency on temperature of preparation, size of grains and morphology of final layer. An extensive study concerning the properties of $BaTiO_3$ material based on the size of the particles and temperature of preparation was conducted among others by [72]. They showed that with the increasing size of crystals the value of relative permittivity decreases. They propose

that the optimal size of grains from the permittivity point of view is 0.7–1 μm. A size of crystals used in this work was estimated by dynamic light scattering to be around 0.9–1.0 micrometers. Other important properties when considering the use of $BaTiO_3$ as a dielectric material in ACPEL based devices is the fact, that it can be easily incorporated into polymer binders and printable formulation can be prepared. The printed layer of dielectric is white upon deposition which is usually preferable since some colorful layer would meddle with the light emitted from the phosphor itself.

As was said earlier the printing formulations show extremely high dynamic viscosity η, in the order of Pa·s. For comparison this value is 1000 times higher than that of distilled water. Screen-printing is an optimal method for preparation of highly patterned (if needed) and relatively thick films of both dielectric and phosphor materials. All these above mentioned facts make $BaTiO_3$ based printable formulations as an optimal material for this type of devices.

Dielectric layer was printed with RokuPrint SD05 screen-printing machine through the polyester stencil with fiber density of 61 threads per centimeter. Both homogeneity and thickness of a dielectric film play critical role for the performance of the device. Too thin and inhomogeneous layers can lead to breaking through the dielectric layer and destroying the panel. Homogenous layer with minimal roughness and waviness is vital in order to ensure the homogeneity of applied electric field which in turn leads to the high homogeneity of emitted light.

Several panels were printed under different printing conditions and characterized by mechanical profilometer in order to find the optimal printing conditions to ensure reproducible preparation of the printed layer. Conditions and characterization of the printed dielectric layers is depicted in **Tab. 5**.

Tab. 5 *Printing conditions and relevant parameters describing a quality of the layer surface. All layers were printed as double layer to ensure the desirable thickness.*

Sample	printing speed ($m \cdot s^{-1}$)	pre printing	on-off ratio (mm)	*h* (μm)	*Ra* (μm)	*Wa* (μm)
1	0.2	x	1	11.12 ± 0.15	0.78 ± 0.07	0.34 ± 0.10
2	0.2	x	1.5	11.70 ± 0.01	0.90 ± 0.09	0.24 ± 0.06
3	0.2	yes	1.5	19.10 ± 0.30	0.67 ± 0.10	0.48 ± 0.09
4	2.0	x	1.5	11.30 ± 0.80	2.37 ± 0.27	1.20 ± 0.30
5	0.2	wet print	1.5	9.50 ± 0.20	0.52 ± 0.02	0.22 ± 0.04

Parameters describing the quality of printed layer thickness *h*, roughness *Ra* and waviness of profile *Wa* (all in microns) were used as a mean to evaluate optimal printing conditions. A parameter on-off ratio is a distance between the mesh and the substrate and wet print means that the first layer was not dried and a second layer was immediately printed atop. Dielectric layer printed by this method showed good roughness and waviness but the overall thickness is too low. Higher printing speed (sample 4) influences negatively homogeneity of printed layer represented here by surface parameters roughness and waviness. It was concluded from the data that low printing speed is better suited for deposition of dielectric layer because of the high dynamic viscosity and density of the printing formulation.

Very important factor is the so called “pre-printing” which means that the paste was mechanically pressed into the mesh before printing on the substrate. The double layer achieved by this process is almost twice as thick making the panel more stable towards higher applied voltage while not affecting negatively roughness and waviness of the deposited layer. The key factor improving the surface quality is a thorough mixing of printing formulation (in the order of hours) before printing. A comparison of layers printed under different conditions – thus exhibiting different performance – can be seen in **Fig. 24**.

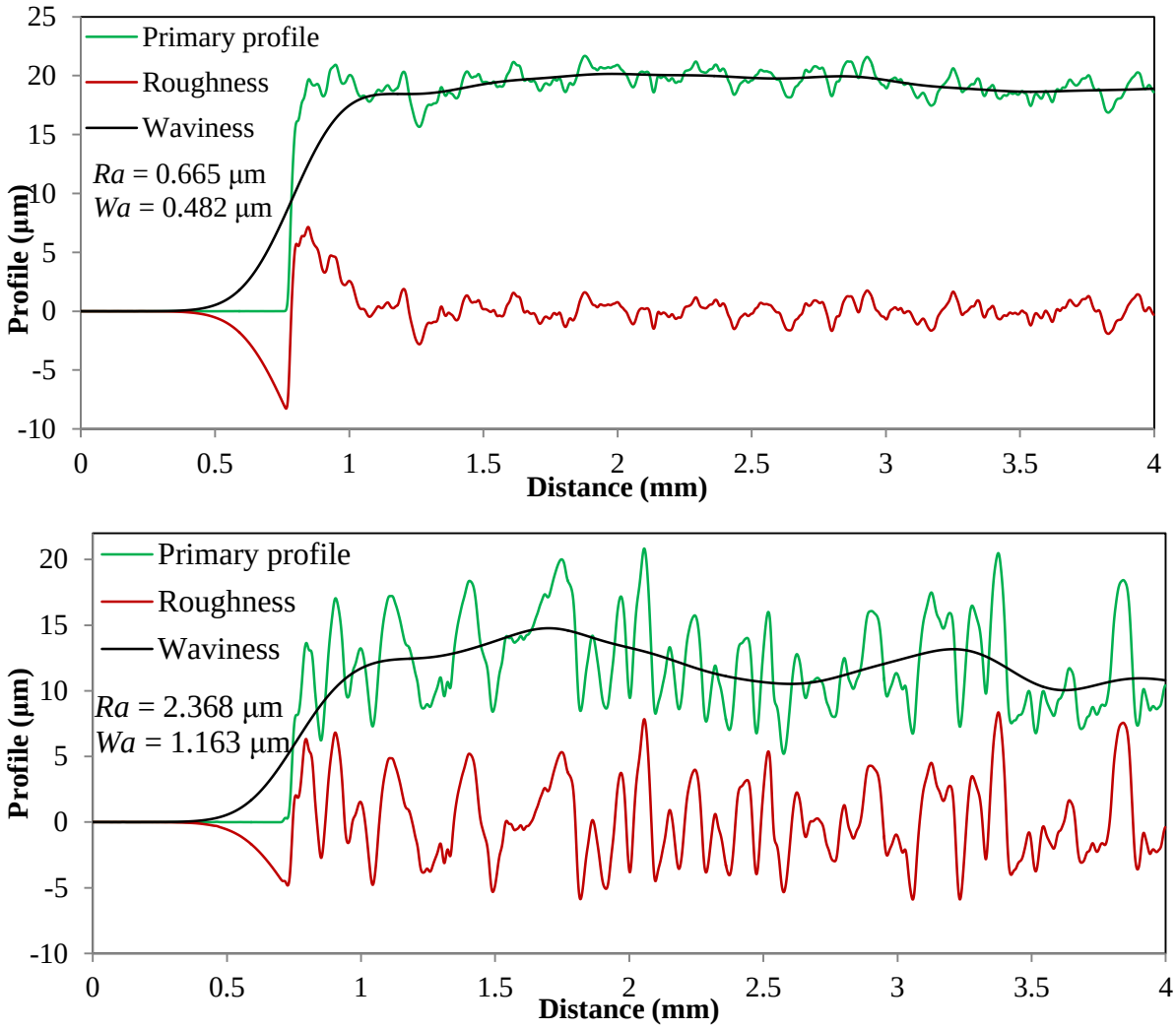

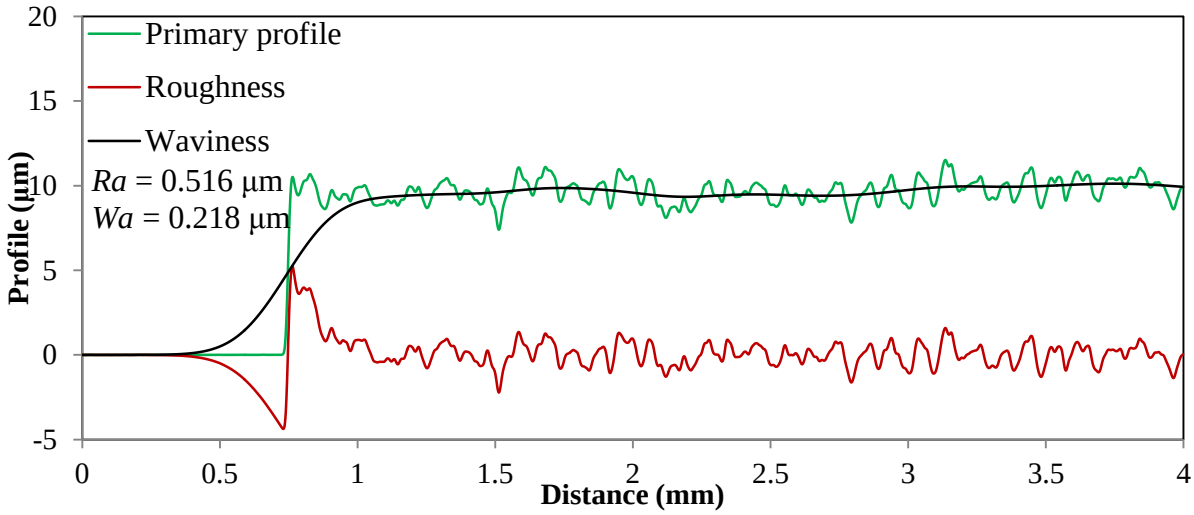

Fig. 24 *A comparison of profiles of samples 3 (top); 4 (middle) and 5 (bottom) made by mechanical profilometer. Specific conditions are the same as in* **Tab. 5**.

It can be concluded that both extensive homogenization in order of several hours and minimal printing speed are beneficial for printing of dielectric layer with such a high dynamic viscosity. **Fig. 24** shows that sample 5 – where the second layer of dielectric was printed directly on the still wet first layer, shows the best roughness and waviness. On the other hand this layer shows significantly lower thickness and therefore will be more susceptible to a breakthrough by a high intensity electric field.

A test was conducted to determine how the total thickness of a dielectric film influences the optical performance of the prepared panel. Four samples (A–D) with increasing amount of dielectric layers and one phosphor layer were prepared and their spectral irradiance was measured. Minimal driving voltage (U_{MIN}) is the lowest voltage at which the panel starts to emit light. Exact values where calculated from quadratic dependencies of the maximum of absolute spectral irradiance ($E_{\lambda,max}$) on the driving voltage shown in **Fig. 25**. The specifics are given in **Tab. 6**.

Tab. 6 *Samples with different thickness of dielectric film and respective minimal driving voltages. 1 layer of dielectric is approximately 12 microns.*

Sample	Amount of dielectric layers	U_{MIN} (V)
A	1	76
B	2	107
C	3	99
D	4	97

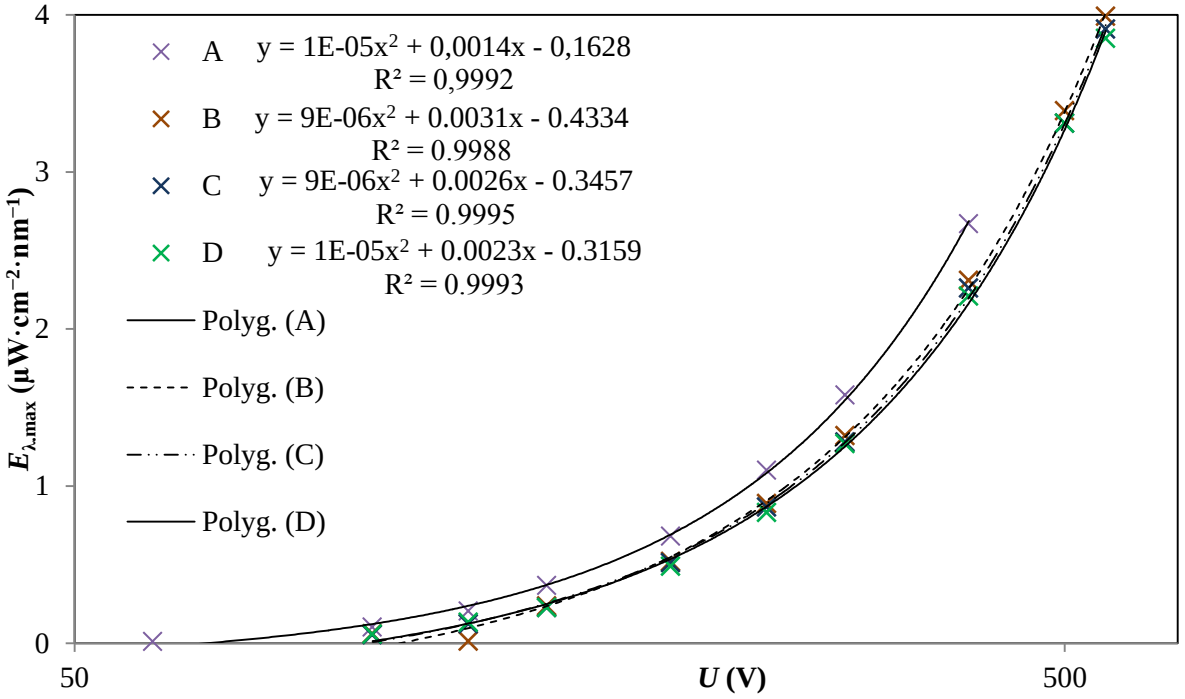

Fig. 25 *Quadratic dependencies of maximal spectral irradiance on the driving voltage with constant driving frequency.*

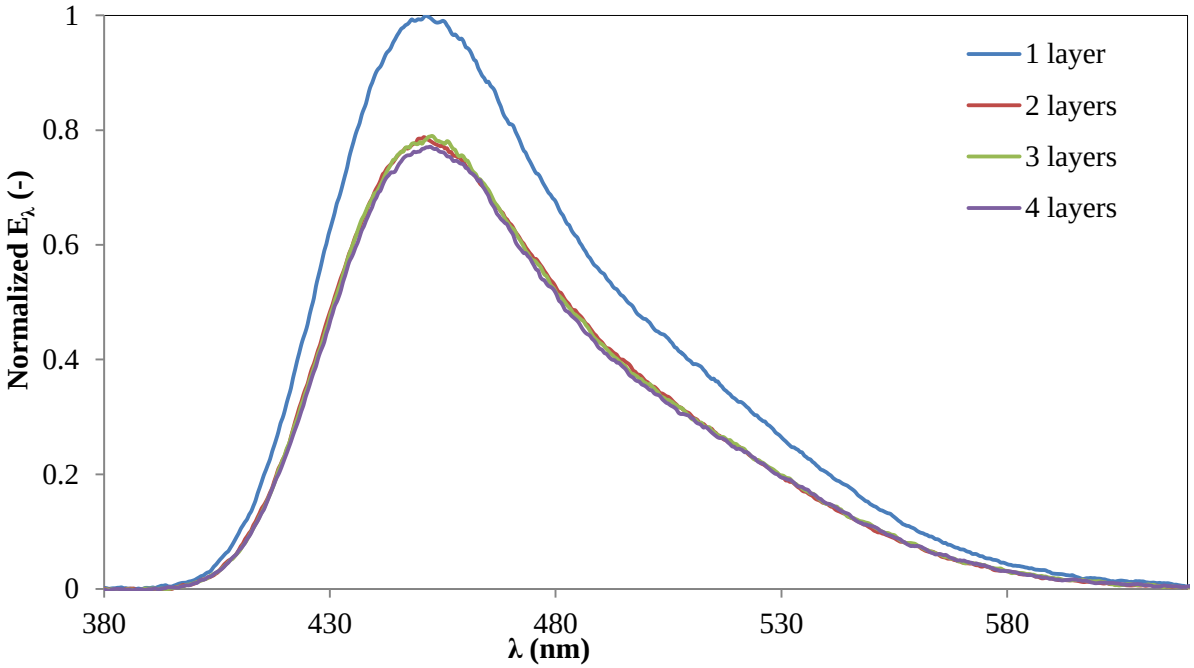

Fig. 26 Normalized spectral irradiance of samples with varying thickness of the dielectric layer.

Normalized spectral irradiance of panels A–D was plotted as a **Fig. 26** for better visualization of optical performance of the sample with the thinnest dielectric film.

It was shown that finding of optimal printing conditions is a necessary step in order to prepare a device with best performance. Intensive homogenization of printing formulation with preprinting and setting low printing speed influence positively the quality of the resulting layer as was proved by mechanical profilometry. **Fig. 25** and **Fig. 26** show that the total thickness of the dielectric layer doesn't seem to influence the spectral characteristic of the device negatively. The thinnest dielectric film (sample A) shows lower minimal driving voltage and better optical performance than thicker layers (samples B–D) but at the cost of increased susceptibility of the device toward higher electric field intensity. Other devices with dielectric film thickness increasing from approximately 25–50 microns show practically the same performance. On the other hand from the commercial point of view the reduction of thickness of the dielectric layer is desirable for reduction of the driving voltage which goes in hand to hand with reduction of cost of the full device.

7.2 Electrode film

In general not many materials are relevant in order to prepare flexible powder-based panel so the goal of this chapter is a study of various conductive materials and their effect on the optoelectronic properties of the panel as a light source. A serious limit is the fact that the bottom electrode needs to be transparent while still having high electrical conductivity. Indium-tin oxide (ITO) used as a conductive transparent electrode is the most typical material at the moment but its most prominent shortcoming is limited source of indium and the resulting high price. Possible alternatives can be Al-doped zinc oxide (AZO) [73] or Sb-doped stannous oxide (ATO) [74] but these materials are still far away from a successful commercial application. Various conductive polymers such as well-known PEDOT:PSS could be a real deal while they are easily printable,

commercially available, show sufficient conductivity with relatively neutral inherent color [75]. Multitude of various reviews dealing with novel polymer or small molecule materials can be found. Novel conductive materials based on graphene and graphene-oxide have already entered the field of organic electronics and their rise in the near future is expected. First working transparent electrodes based on graphene-oxide have already found its application in organic photovoltaics [76].

On the other hand the top electrode doesn't need to be transparent and can be fabricated from a wide range of conductive materials such as cured carbon or various metals. It is crucial for use in the field of organic flexible electronics that particles of the conductive material can be incorporated into an organic binder so that the printing formulation can be created. Various printable formulations are commercially available with a wide range of conductive materials from carbon based pastes through aluminum up to platinum based curable pastes. The in this thesis study was conducted on 3 different materials, silver paste, carbon paste and PEDOT:PSS. Silver and carbon pastes were obtained from Gwent group and water based PEDOT:PSS solution was obtained from Clevios.

No special treatment or time consuming optimization was needed in the process of printing of above mentioned pastes. Thanks to their extremely high dynamic viscosity and density and overall similar character as the dielectric paste, similar printing conditions were set for deposition of the top electrode. One layer of both the silver and carbon electrodes have thickness around 10 microns while the PEDOT:PSS electrode consisted of 3 layers with total thickness less than 1 micron.

The most important property of an electrode layer is the conductance G (siemens $S = \Omega^{-1}$), which represents the ability to conduct electric current. Conductance – **Eq. 17** is a property given by the geometry of the conductor and is the inverse value of the electric resistance.

$$G = \frac{1}{R} = \sigma \frac{A}{l} \tag{17}$$

A is the area (m^2), l is the length of conductor (m) and σ is conductivity ($S \cdot m^{-1}$) – inherent ability of a given material to conduct electric current. Conductivity is the inverse value of electrical resistivity ρ (Ω m) **Eq. 18**. In other words the higher the resistivity of a conductor the worse is its property to conduct electric current.

$$\sigma = \frac{1}{\rho} \tag{18}$$

Both the conductance and resistance of layers is affected by geometry of the sample. More general approach is to determine a sheet resistance R_s given by **Eq. 19** (also known as surface or sheet resistance) with unit ohm per square ($\Omega \cdot sq^{-1}$). It is a common electrical property used to characterize thin films of conducting and semiconducting materials. It is a measure of the lateral resistance through a thin square of material, i.e. the resistance between opposite sides of a square. The key advantage of the sheet resistance R_s over resistance R is that it is independent on the size of the square – enabling an easy comparison between different samples.

$$R_s = \frac{\rho}{h} \tag{19}$$

Where R_s is the sheet resistance, ρ is electrical resistivity and h is thickness of the layer (m). Another advantage is that it can be measured directly using a four-point probe technique. The measurement consists of four conductive needles placed on a thin surface with an electric current I (A) flowing through two outer probe pins and voltage U (V) is measured on the inner pins as can be seen in **Fig. 27**. When the probe spacing r is constant and the thickness of the film (in the case of silver and carbon electrodes in this work h ~ 12 μm and PEDOT:PSS less than 1 μm) is less than 40 % of the spacing than the sheet resistance is given by **Eq. 20**

$$R_s = \frac{\pi}{\ln 2}\frac{U}{I} \tag{20}$$

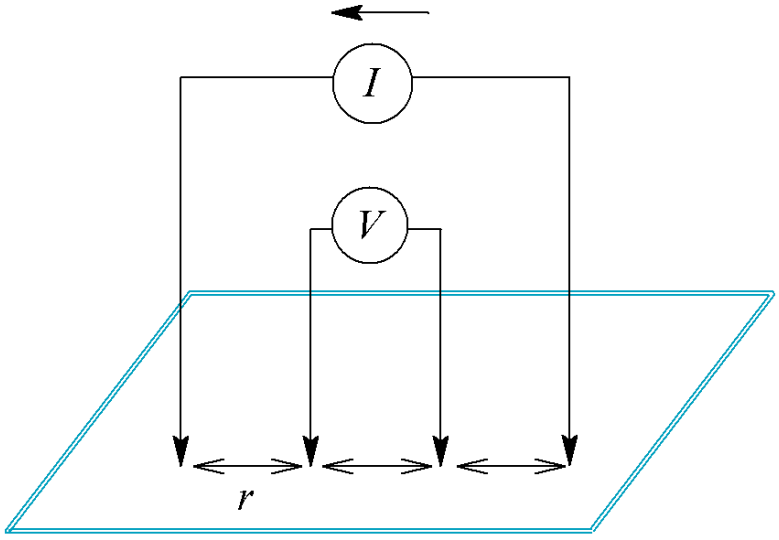

Fig. 27 *A schematic picture of four-probe technique.*

Tab. 7 shows the values of sheet resistance of three different electrode materials which were measured to determine which one is the best suited as a conductive top electrode.

Tab. 7 *Comparison of sheet resistances of silver, conductive polymer and carbon thin layers.*

R_{sAg} ($\Omega \cdot sq^{-1}$)	$R_{sPEDOT:PSS}$ ($\Omega \cdot sq^{-1}$)	R_{sC} ($\Omega \cdot sq^{-1}$)
0.07	240	240
0.09	249	263
0.06	240	435
0.12	240	272
0.05	249	254
0.05	254	349
0.08	281	231
0.10	258	285
0.10	294	240
0.08	254	236
0.07	267	263
0.08 ± 0.02	**257 ± 18**	**280 ± 60**

It is clear that the sheet resistance of thin layers of silver is in the order of 4 times lower than the sheet resistances of the other materials and thus electric conductivity of silver is much higher.

To evaluate the effect of the different sheet resistances on the optoelectronic properties of the panel, the panels with different top electrodes were printed and their absolute spectral irradiance was measured. **Fig. 28** shows normalized spectral irradiance of panels consisting of different top electrode. The panel with silver top electrode shows maximal irradiance due to its excellent electric conductivity. A panel with carbon electrode exhibits around 80 % of irradiance of that with silver electrode while both layers have approximately the same thickness (around 12 μm). The sample with PEDOT:PSS electrode exhibits only 50 % of irradiance of the sample with silver top electrode. While both carbon and PEDOT:PSS have very similar sheet resistance the thickness of PEDOT:PSS layer is significantly lower so the bulk conductivity of PEDOT:PSS is much less (**Eq. 19**) than the one compared to the carbon layer which leads to the decrease of light output of the emitted light.

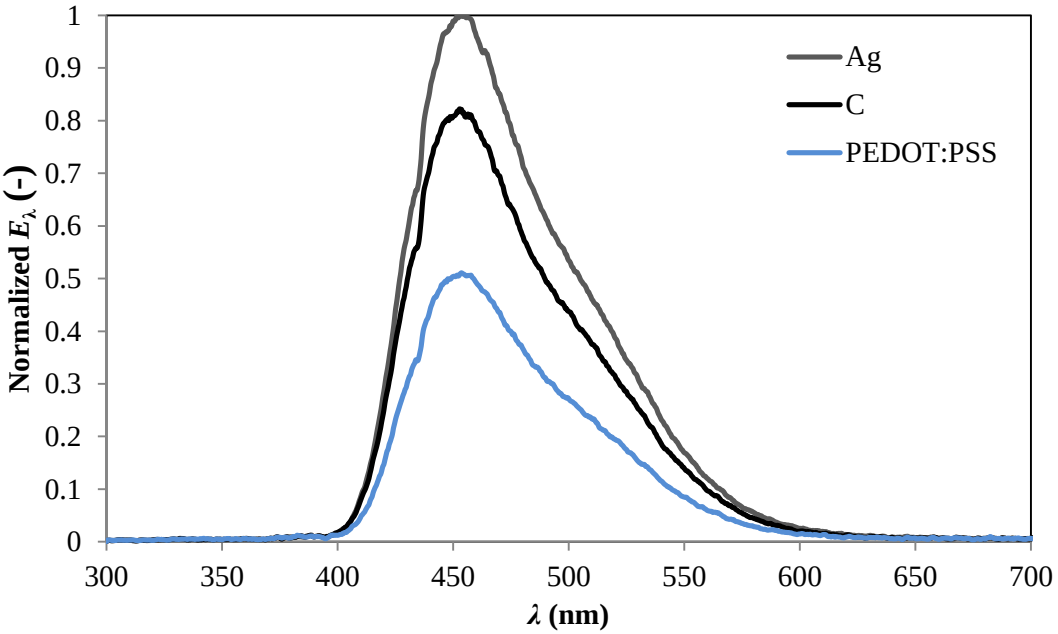

Fig. 28 *A relative comparison of normalized spectral irradiance of panels with different top electrode.*

7.2.1 Conclusion

Three different printing formulations of top electrode conductor – carbon paste, silver paste and PEDOT:PSS – were examined in order to find the most suitable material for preparation of a top electrode. Printing conditions were found to be very similar to the conditions under which dielectric layer was printed due to the overall similar physical-chemical character of the pastes. A four-probe technique was employed for measurement of sheet resistance of the conductive materials. It was shown in **Tab. 7** that the silver layer exhibits 4 orders of magnitude lower sheet resistance than the other two materials. According to **Fig. 28** the light output of panel with silver top electrode achieves almost 25 % and 50 % better performance than panels with carbon or PEDOT:PSS electrode, respectively. Therefore the printable silver printing formulation is the most suitable candidate of these three tested materials.

A promising advantage of the conductive PEDOT:PSS is its light transparency. When using printed PEDOT:PSS top electrode a panel emitting light in both directions could be manufactured. However it was shown that the conductivity of the polymer is not as high to generate light with sufficient irradiance. Another problem is the amount of the conductive layers stacked one on another to meet the required performance. Although few layers of PEDOT:PSS are highly transparent the stack of multiple layers show dark blue shade leading to decrease of light transparency and increase of a haze of the film. In the case of effective reduction of the dielectric layer (less than 1 micron) an ACPEL panel with a semitransparent PEDOT:PSS top electrode emitting light in both ways could be deployed. A suitable dielectrics printing formulation with reduced $BaTiO_3$ grain sizes (with median around 100 nm) was found and it was shown that dielectric films based on this formulation are transparent. Therefore there arises a need for the top electrode to be transparent as well. [77].

All the above discussed materials are candidates for the top electrode. As for the bottom electrode ITO remains to be excellent candidate for the bottom fully transparent electrode with a good conductivity even despite its economic disadvantage.

7.3 Phosphor film

Phosphor-based high intensity electroluminescence in solid materials was discovered in late 30's by Destriau [3] on the Cu-doped ZnS which is a semiconductor with band gap 3.6 eV. There are two structural modifications: cubic close-packed (3C) sphalerite and hexagonal close packed (2H) wurtzite with transition temperature around T_T = 1290 K. Both modifications show similar properties to emit light. Although zinc oxide was the first material discovered, it remains to be with slight modifications – different dopants – the most prominent representative of materials showing electroluminescence in solid phase up to this day. Devices that have found their way to commercial application are exclusively based on Cu doped ZnS. Very comprehensive work concerning physical properties of phosphors and preparation of doped ZnS is described in *Phosphor handbook* from Yen and Shionoya [78]. The aim of this chapter is optimization of printing conditions of a phosphor paste leading to reproducible preparation of phosphor film under optimal conditions and estimation of optimal thickness of phosphor film on the optoelectronic properties of the panel.

The first step in preparation of various phosphor materials is the creation of pure ZnS by precipitation method and chemical purification of the product from the transition elements. The phosphor is then obtained in the form of a sintered cake that must be milled into smaller pieces. Strong milling however decreases the efficiency of the luminescence probably due to introducing new non-radiative centers by the destruction of the ZnS crystals. Therefore milling conditions must be mild. The solution of desired dopant is then added to the dispersion of raw ZnS in water. The mixture is then dried under low temperature and the resulting fine powder is annealed under the temperature slightly higher than T_T and cooled under controlled atmosphere and conditions. This step is critical since the dimension of ZnS crystals and amount of structural defects play vital role for the resulting electroluminescence properties. It was shown that perfect and pure ZnS crystals show electroluminescence as well but at much higher voltage and with a decreased brightness. A very fine powder of ZnS crystals is then added into a polymer binder in order to prepare a printing formulation with specific physical-chemical properties [78].

Blue, orange, green and white emitting phosphor commercial printing formulations were obtained from GWENT GROUP Advanced Material System with a typical dynamic viscosity η in the order of few Pa·s with the solid content around 80 %. Deposition of the active layer was realized through the polyester mesh with fiber thickness 66 fibers per cm and the lowest achievable printing speed. Printing parameters were set very similarly to the printing parameters of the phosphor layer because of their overall physical-chemical similarity. Coverage of the substrate by the phosphor was clearly insufficient as can be seen in **Fig. 29**. The key parameter drastically improving the quality of a printed layer was the pre-printing. Because of the high density of the printing formulation and the size of phosphor grains the paste needed to be forced into the mesh and only then printed.

Figures *a* and *b* represent a picture taken by optical microscopy of phosphor layer with and without preprinting respectively. The difference of coverage of the phosphor is plainly visible by a naked eye. Figures *c* and *d* show the analysis by mechanical profilometer of the printed layers. The

substrate is fully covered by the phosphor grains and the layer is compact when the phosphor paste was preprinted. The roughness and waviness of layer is not optimal but it is given by the size of phosphor grains and cannot be averted with this printing formulation. The layer represented by figures *b* and *d* show presence of holes reaching to the substrate and cannot be considered as a compact layer. Individual grains are visible and are almost entirely separated from each other.

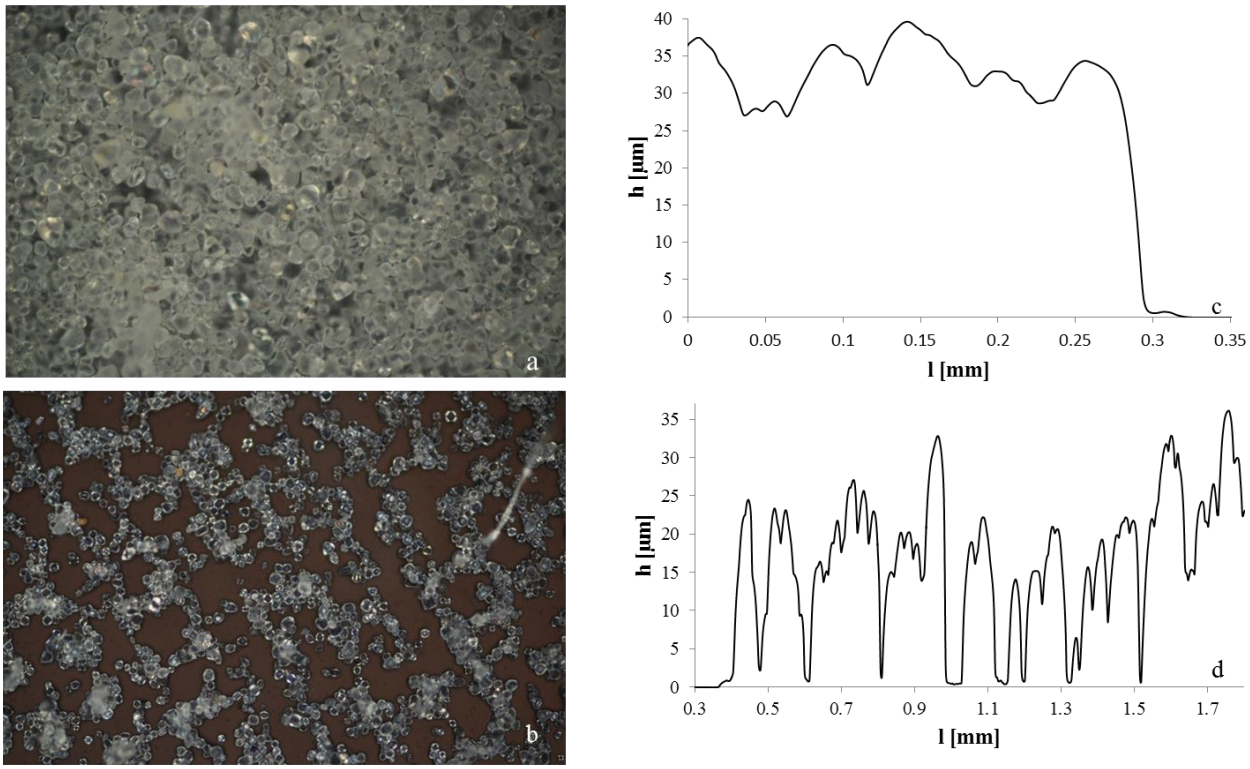

Fig. 29 *Comparison of phosphor layer printed under optimized (a, c) and not optimized (b, d) conditions.*

Typical thickness of printed optimized phosphor layer lies in the range of 25–30 microns but the size of grains cannot be reduced by mechanical milling as this treatment causes a decrease of the luminescent properties [78].

To determine the optimal thickness of a phosphor film multiple panels with varying amount of phosphor layers (1, 3 and 4) and thus varying total thickness of the film were prepared and their absolute spectral irradiance spectra were measured. The influence of thickness of the active layer was evaluated from their relative performance of the devices and from calculation of theoretical minimal driving voltage U_{ON} (volt).

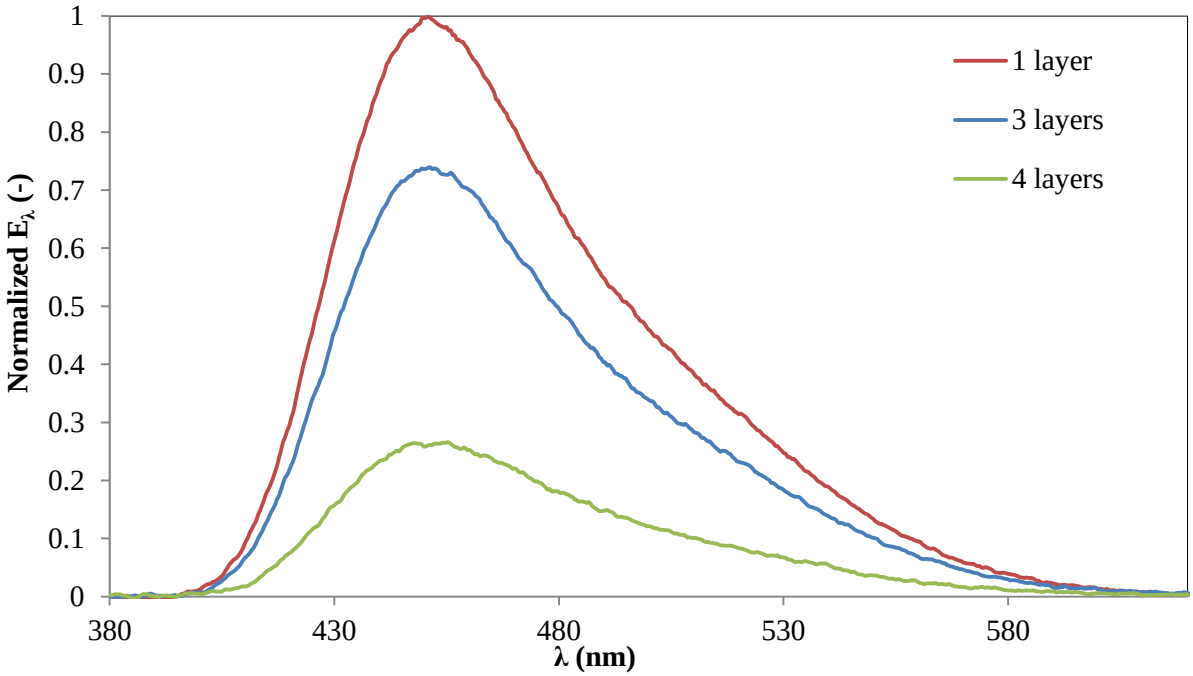

Fig. 30 *Normalized spectral irradiance of panels with varying thickness of the phosphor layer charged by alternating voltage with f = 1600 Hz and U = 200* V_{pp}.

Minimal driving voltages (**Tab. 8**) were calculated from quadratic dependencies of maximal spectral irradiance on the driving voltage at constant frequency (similar approach as with testing of optimal thickness of dielectric film – see **Fig. 26**)

Tab. 8 *The minimal driving voltage of samples needed for generation of light.*

Amount of phosphor layers	Driving voltage (V)
1	107
3	104
4	121

7.3.1 Conclusion

Fig. 29 clearly shows that the printing conditions of phosphor paste need to be well optimized or the phosphor will form individual clusters instead of a film. The key parameter positively influencing printing of a phosphor film is a preprinting. The printing formulation needs to be very well homogenized and preprinting needs to be introduced as is visible from both the analysis by mechanical profilometer and from the optical microscopy images.

Increasing of the total thickness of active layer is contra productive for the optoelectronic performance of the whole panel (see **Fig. 30**). The thickness of one layer printed under optimized conditions is in the range of approximately 25–30 μm. The sample consisting of 3 active layers shows around 75 % of performance of the panel with 1 layer and the sample with 4 phosphor layers shows only 30 % irradiance of the panel with 1 layer while the minimal driving voltage is roughly the same (see **Tab. 8**). It can be concluded that with decrease of a thickness of an active film the panel emits more light. This is caused by the fact that intensity of electric field increases linearly with decreasing distance of both electrodes (see **Eq. 1**). Unfortunately the decrease of

thickness of the active layer is limited by the size of phosphor grains which is difficult to modify since strong milling during the preparation of ZnS decreases radiative efficiency.

7.4 Optoelectronic properties of the developed ACPEL panels

The task of this chapter is to define and evaluate suitable parameters for characterization of large area light sources. Both luminance and power consumption – how much electrical energy will be wasted by operation of the panel – were found to be important parameters from the technological point of view. Another goal, directly resulting from the first one is to determine the optimal driving conditions leading to the radiation of panels based on different phosphors with a reasonable life time of panel.

A picture taken by optical microscopy of different phosphors (B – blue; O – orange; G – green and Mix) emitting light of different wavelengths is shown in **Fig. 31**. Figure *a* shows that the layer is formed by large individual grains where each grain acts as an individual point source of light. However the placing of grains is so dense that the whole panel exhibits properties of a plane source of light. Figure *c* shows a mixture which consists of blue green and orange phosphor mixed in the ratio 1:1:1. Figures *b*, *d* and *e* show phosphors emitting green, orange and blue light respectively.

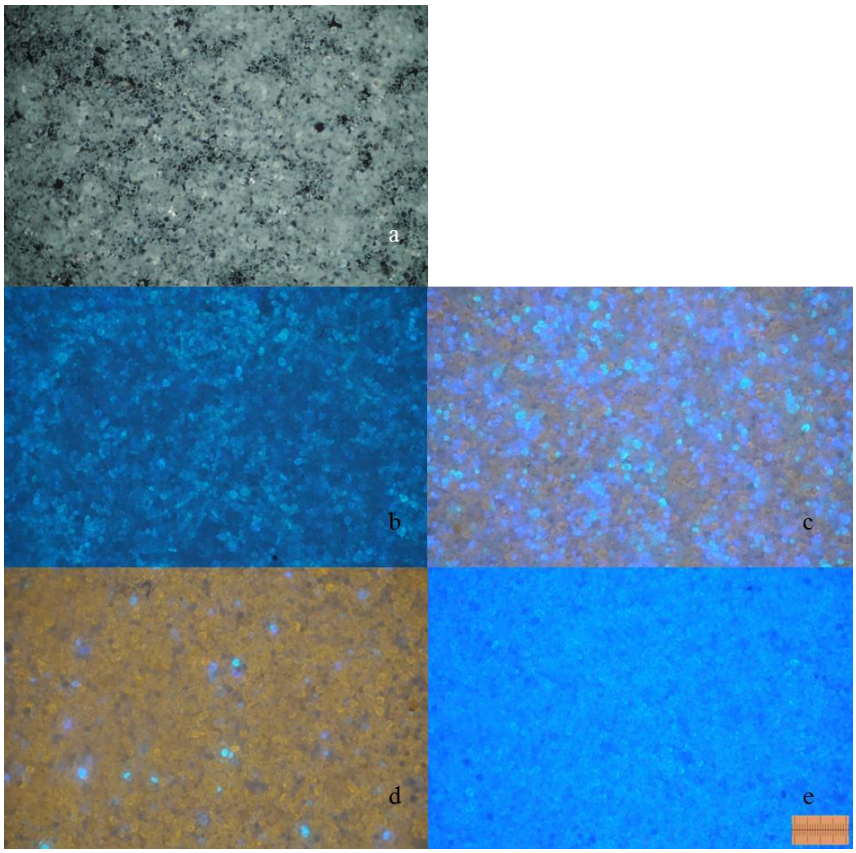

Fig. 31 *A microscopic photography of various emitting phosphor films with 1 micron scale.*

Absolute spectral irradiance of the emitting panels with various standard phosphors was measured with spectrophotometer with optical fiber at 3 different driving conditions for determination of the influence of both increasing voltage amplitude and frequency.

Driving conditions are following:

1 U_{pp} = 200 V; f = 1000 Hz
2 U_{pp} = 200 V; f = 450 Hz
3 U_{pp} = 400 V; f = 450 Hz

A sample B1 therefore means that the absolute spectral irradiance of the blue panel under driving voltage 200 V and frequency 1000 Hz was measured. Irradiance gives the amount of radiant flux that is incident on a surface in given distance and is a relevant quantity to characterize how much area will be irradiated. But the problem is that it is a radiometric quantity so it provides only a little information about how strongly the human eye will be sensitive to the light impulse. So the spectral illuminance as a photometric quantity was calculated and compared to the absolute spectral irradiance in **Fig. 32**.

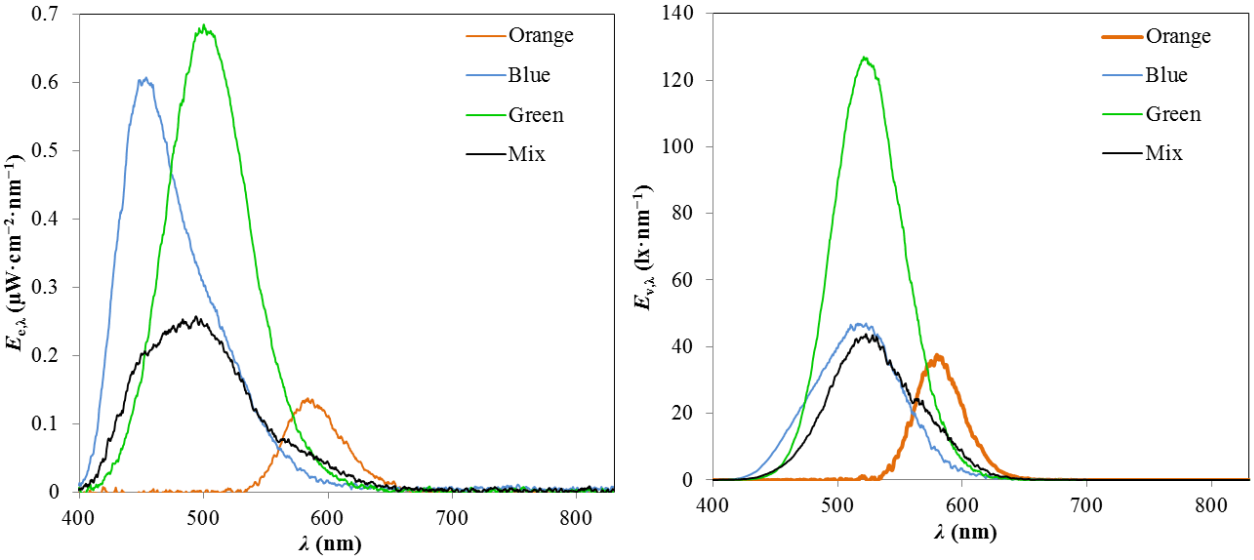

Fig. 32 *Spectral irradiance of panels (on the left) and spectral illuminance (on the right) taken under 250 V and 1000 Hz.*

It is clear that while the irradiance (the left spectrum in **Fig. 32**) of blue panel is much stronger than both orange and mixed phosphor panels the difference in perception of the emitted light is almost the same. The luminance of flat panels was calculated for determination of how bright the panels would appear to the observer. An illuminance E_v was calculated according to the **Eq. 13** and represents the luminous flux incident on an area in a fixed distance (d ~ 10 mm). A luminance L_v describes luminous flux emitted in a solid angle and characterizes a panel as a source of light. The active film of a panel itself is formed by homogenously spread crystals of phosphor – point sources of light that behave in a macroscopic scale as an extended source of light. In this case the calculation of luminance from the illuminance is given by **Eq. 21**

$$L_{e,\lambda} = \frac{E_{e,\lambda}}{\pi \cdot \sin^2\left(\frac{\vartheta}{2}\right)} \tag{21}$$

Where ϑ is the angle of view of the sampling optics. In the case of bare optical fiber the angle is $\vartheta \sim 25°$and $\vartheta \sim 180°$ with use of a cosine corrector. The values of irradiance E_e, illuminance E_v and luminance L_v of all the test subjects are summarized in the **Tab. 9**. Measurement of the irradiance shows that the orange panel emits only 20 % of radiation compared to blue and green panels and 30 % of radiation compared to mixed phosphor panel. The resulting photopic response of human eye is therefore very low and the orange panel is relatively a poor light source. Green panel is by far the most promising light source because of two facts. Firstly the light is generated with higher efficiency compared to the other panels and secondly the standard observer's eye is by definition most sensitive to green color. **Tab. 10** shows typical values of luminance given by various light sources for comparison with emitting ACPEL panels.

Tab. 9 *Radiometric and photometric properties characterizing the panels as extended sources of light. The first column "Conditions" describe which type of phosphor was subjected to which driving conditions.*

Conditions	**Irradiance, E_e (W·m^{-2})**	**Illuminance, E_v (lm·m^{-2})**	**Luminance, L_v (cd·m^{-2})**
O1	$9.50 \cdot 10^{-4}$	$4.39 \cdot 10^{-1}$	**2.98**
O2	$5.22 \cdot 10^{-4}$	$2.61 \cdot 10^{-1}$	**1.77**
O3	$2.97 \cdot 10^{-3}$	1.39	**9.48**
B1	$4.81 \cdot 10^{-3}$	$8.62 \cdot 10^{-1}$	**5.85**
B2	$2.69 \cdot 10^{-3}$	$5.81 \cdot 10^{-1}$	**3.95**
B3	$1.31 \cdot 10^{-2}$	2.85	**19.30**
G1	$6.07 \cdot 10^{-3}$	2.09	**14.20**
G2	$3.22 \cdot 10^{-3}$	1.14	**7.78**
G3	$1.45 \cdot 10^{-2}$	5.31	**36.10**
Mix1	$3.20 \cdot 10^{-3}$	$9.11 \cdot 10^{-1}$	**6.19**
Mix2	$2.06 \cdot 10^{-3}$	$6.05 \cdot 10^{-1}$	**4.11**
Mix3	$9.76 \cdot 10^{-3}$	3.04	**20.60**

Tab. 10 *A typical luminance of some light sources [79].*

Light source	**Luminance (cd·m^{-2})**
Nuclear flash	$2 \cdot 10^{12}$
Lightning	$8 \cdot 10^{10}$
Sun (as viewed from Earth)	$1.6 \cdot 10^{9}$
60 W opal bulb	$1.2 \cdot 10^{5}$
Clear blue sky	$4 \cdot 10^{3}$
Full moon (as viewed from Earth)	$3 \cdot 10^{3}$
Typical PC display	~ 50–300
Green panel (this work)	~ 40
Starlit sky	$5 \cdot 10^{-4}$

Another important parameter for characterization of a light source beside its luminance is the power consumption. It was estimated by a serial connection of a known resistor (R = 326 Ω) to the electroluminescent panel and a measurement of a voltage generated on the resistor (U_R – V); a

current flowing through both the panel and the resistor (I – A) and a phase shift (φ – rad) between the driving voltage and a flowing current since the ACPEL panel exhibits capacitive load. All the measurements were conducted by an oscilloscope Tektronix TBS 2000. The power consumption (P – watt) is calculated by **Eq. 22**

$$P = \frac{\left(U_{\mathrm{pp}} - U_{\mathrm{R}}\right)}{2\sqrt{2}} \cdot \frac{U_{\mathrm{R}}}{2R \cdot \sqrt{2}} \cdot \cos\varphi = \frac{\left(U_{\mathrm{pp}} - U_{\mathrm{R}}\right) \cdot U_{\mathrm{R}}}{8R} \cdot \cos\varphi \tag{22}$$

Tab. 11 shows estimated power consumption of printed panels with various active areas under different driving conditions together with calculated power consumption given per cm^2 of samples with various dimensions and the **Tab. 12** shows power consumption of some commonly used light sources.

Tab. 11 *An estimated power consumption of samples with an increasing active area A driven under different conditions.*

A (cm^2)	**U_{pp} (V)**	***f* (Hz)**	***P* (mW)**	***P*/*A* ($mW \cdot cm^{-2}$)**
78	200	370	103	1
78	200	1000	225	3
78	400	370	504	6
9	200	370	10	1
9	200	1000	23	3
9	400	370	44	5
1	200	370	1	1
1	200	1000	3	3
1	400	370	10	10

Tab. 12 *Comparison of some typical light sources from the point of view of their consumption of electric power. Taken from [80].*

Category	**Lamp type**	**Power (W)**
Incandescent and halogen bulbs	Halogen bulb	100
	Regular incandescent bulb	60
Fluorescent lamps	Hf fluorescent lamp	45
	Cool white fl. Lamp	36
	Bulb type fluorescent lamp	25
HID (high-intensity discharge) lamps	General HPS lamp	360
	Metal halide lamp	400
	Fluorescent mercury lamp	400
ACPEL panel (this work) under 400 V_{pp} and 370 Hz	78 cm^2	0.50
	9 cm^2	0.04
	1 cm^2	0.01

7.4.1 Conclusion

Parameter characterizing how bright the light of a light source will be perceived – luminance – was calculated from the measured spectra of absolute spectral irradiance. It was found that the

luminance is strongly dependent on both the driving voltage and frequency which is also responsible for decreasing of lifetime of panels. It is important to keep this fact in mind in order to set the driving conditions according to the desired luminance with reasonable life time.

It is clear by comparison of the brightest green panel with typical light sources shown in **Tab. 10** that ACPEL devices are not very efficient sources of light and their luminance is insufficient for illuminating objects in clear day light. On the other hand very low electrical consumption in comparison to traditional light sources (**Tab. 12**) cost and manufacturing simplicity are important factors speaking for the benefit of this type of devices. Another remarkable property enabling the panels to find application as various decorative features and/or warning signs is their inherent flexibility since they are printed on conductive PET substrate.

On the other hand **Tab. 11** shows that the power consumption of the ACPEL panel is 2–3 order lower than that of a regular incandescent opal bulb while still maintaining – at higher driving voltage and frequency – values of luminance comparable to PC displays. It was also found that the power consumption per area unit of larger panels (9 cm^2 and 78 cm^2) is the same but is somewhat lesser when compared to the sample 1 cm^2. Of course the total consumption increases with the area but the values are still several orders less than that of other light sources.

7.5 Effect of driving conditions on optoelectronic performance and stability of panels

From the theory of generating light by the APCEL panel (**Chapter 3**) is clear that both increasing driving voltage amplitude and frequency increase luminous performance of the panel. But the increasing values of driving conditions have a detrimental effect on the stability of panels which is a bottleneck for an application of electroluminescent devices. This chapter aims to investigate this effect and determine optimal driving conditions from both the optoelectronic and stability point of view. A test was conducted on a blue sample with increasing voltage at a fixed driving frequency and vice versa on increasing frequency at one fixed voltage. Absolute spectral irradiance of the blue panel was measured and plotted in **Fig. 33** and luminance was calculated for characterization of the panel.

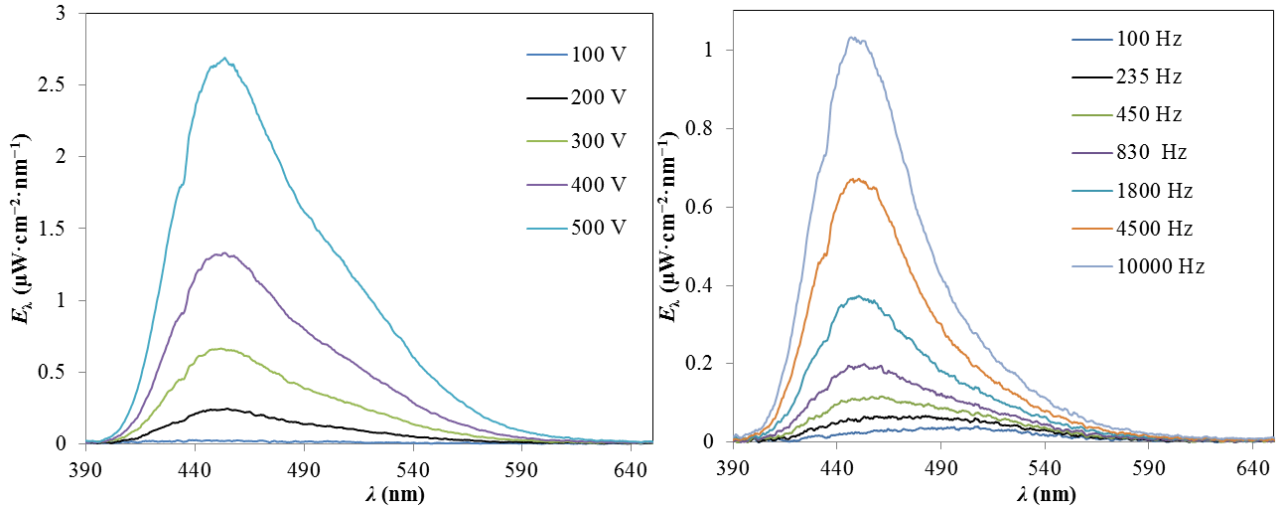

Fig. 33 *The left figure shows spectral irradiance of panel measured as a function of the driving frequency at a constant voltage 200* V_{pp} *with increasing driving frequency (*Hz*) and the right figure represents the effect of increasing the voltage (*V*) at a constant frequency 1000 Hz.*

Fig. 33 and **Tab. 13** clearly show that high voltage amplitude has higher impact on the overall optoelectronic properties than very high driving frequency. It was also found that the increasing frequency decreases the dominant wavelength λ_D of the emitted light (which shall be further discussed in **Chapter 7.6**).

Tab. 13 *Luminance of a panel with various driving conditions.*

Sample	Luminance (cd·m^{-2})
100 Hz	3.8
1800 Hz	14.6
10 kHz	30.6
100 V	2.6
300 V	32.4
500 V	133.0

Phosphor panels show several promising properties, namely the power consumption and flexibility, which makes them potentially interesting for market. However one of their most prominent red brick wall problems is their environmental and overall stability. Unfortunately the exact process of phosphor degradation is up to now not clarified, although Klassen et al [81] did a study on degradation of different phosphors with an aim to match ongoing physical processes in the phosphor with the drop of luminance. Detailed study was conducted by Swart et al [82] where the degradation of ZnS was conducted by electron bombardment in environment of residual gas (H_2O, H_2 and CH_4) with pressure $1.5 \cdot 10^{-6}$ Pa and oxygen $1.3 \cdot 10^{-4}$ Pa. A direct correlation between morphological changes of the phosphor and decrease of luminescence was found.

The possible degradation processes of ZnS can be summed up with the following **Eq**. **23–25**

$$2H_2O \rightleftharpoons 2H_2 + O_2 \tag{23}$$

$$ZnS + 2O_2 \rightleftharpoons ZnSO_4 \tag{24}$$

$$2ZnS + 3O_2 \rightleftharpoons 2ZnO + 2SO_2 \tag{25}$$

Molecules of water and residual gases are degraded by strong electron beam or strong electrical field to hydrogen and oxygen atoms (**Eq. 24**) which undergo further reactions to form non luminescent ZnO or $ZnSO_4$ (**Eq. 24** and **Eq. 25**). Both reactions are thermodynamically possible and preferred because their $\Delta H < 0$ kcal·mol^{-1}.

From the information given above results that setting of extremely high driving conditions will induce generation of light with increased brightness at the cost of decreased stability of a panel. The more intense electric field will create more non luminescent defects and the active luminescence centers in the bulk near the surface of the material will be depleted at higher speed. Furthermore humid environment has downright detrimental effect on the panels based on active phosphor film.

A test of stability was conducted on various panels under different conditions and different type of protection against the humid air. The parameters describing the stability L_{75} and L_{50} (the time

after which the luminance drops to 75 % respectively 50 % of the original value) were calculated from the fit and are summarized in **Tab. 14**.

Three different driving conditions (similar as in **Chapter 7.4**) were chosen to estimate an influence of voltage and frequency and encapsulation.

i U_{pp} = 200 V; f = 1000 Hz laminated

ii U_{pp} = 200 V; f = 370 Hz laminated

iii U_{pp} = 400 V; f = 370 Hz encapsulated between two glass plates with EVA foil

The drop of the luminance over time of sample *i* showed trend given by empirical **Eq. 26** [83].

$$\frac{E_e}{E_{e,0}} = (1 + \mathrm{K}t)^{-1} \tag{26}$$

Where E_e is absolute irradiance of sample in a given time t (hours), $E_{e,0}$ absolute irradiance at the beginning of the measurement and K is a time constant (h^{-1}).

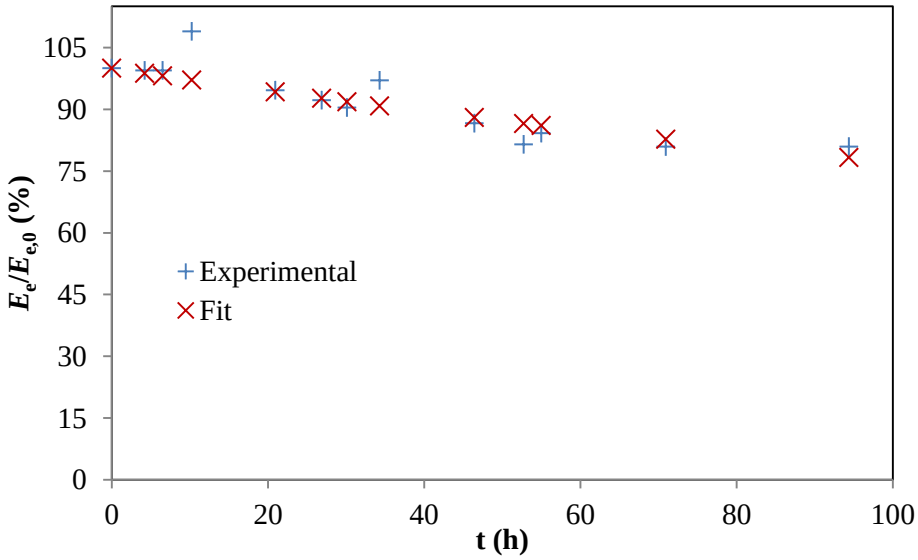

Fig. 34 *Drop of the luminance of panel* ***i*** *over 100 hours (blue crosses) and data fitted by* **Eq.26** *(red crosses).*

Fig. 34 shows very nice match between experimental and fitted data for the panel ***i***. The degradation of panel ***ii*** was measured over 80 hours and showed a very similar behavior as the sample ***i*** as can be seen in the **Fig. 35**. Parameters L_{50} and L_{75} show almost 3 times higher values than those of sample ***i***. It confirms that too high driving frequency has detrimental effect on the stability of the panel and should be set below 1000 Hz.

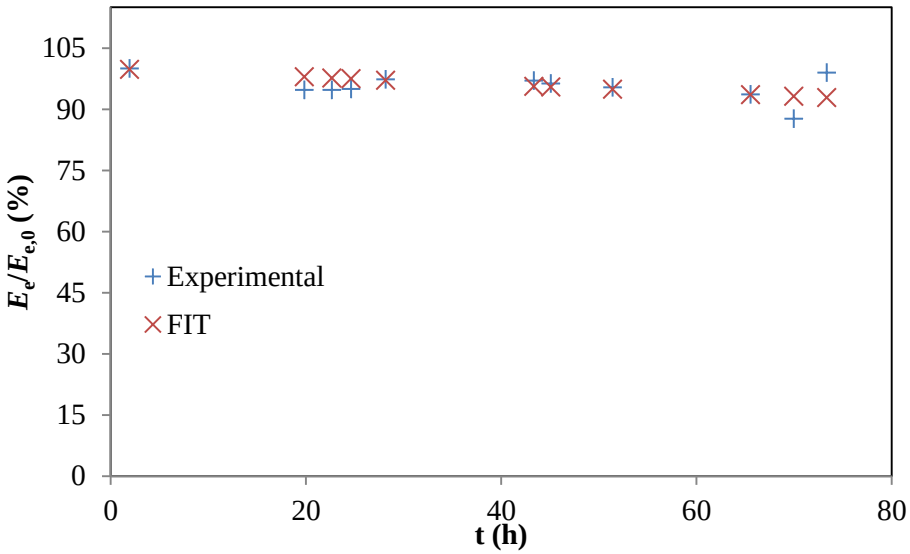

Fig. 35 *A panel* ***ii*** *shows slower degradation over time because of the reduced driving frequency. Red crosses show data fitted by* **Eq. 26** *and blue crosses are the measured data.*

The last tested sample ***iii*** was driven by the highest voltage of all the samples and was fully encapsulated by EVA foil between two flat glass panels. Its degradation over time and comparison of the experimental data with theoretical prediction given by **Eq. 26** is plotted as a **Fig. 36**.

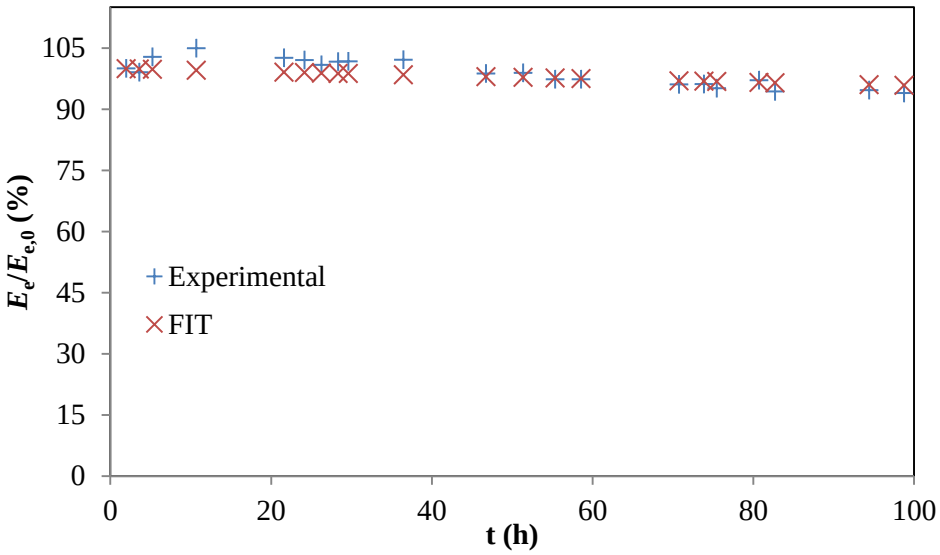

Fig. 36 *A panel* ***iii*** *with* U_{pp} *= 400 V with the best encapsulation showing enhanced stability and behavior according to* **Eq. 26**.

Tab. 14 *A summary of stability of all the tested devices with varying driving conditions and type of protection.*

Driving conditions	**Encapsulation**	**K·10^{-3} (h^{-1})**	**L_{75} (h)**	**L_{50} (h)**
i	Lamination	2.94	113	340
ii	Lamination	1.06	316	948
iii	Encapsulation	0.44	754	2261

7.5.1 Conclusion

It was clearly shown that increasing both the driving voltage and frequency has improving effect on the brightness of the panel. **Fig. 33** shows how much radiation will be emitted with increasing both frequency and voltage and how the human eye will perceive it. **Tab. 13** shows the values of luminance given by the extended source of light under given conditions. Although it might seem that the voltage of 500 V is quite high and an additional amplifier would be needed to achieve such a value it is important to note that the voltage applied on the panels this thesis deals with is peak-to-peak voltage while the voltage in power grid is an effective voltage (U_{RMS}). U_{pp} = 500 V equals U_{RMS} ~ 180 V while the effective voltage given by European power grid is 230 V. Therefore the maximal voltage under which the panels were tested in this work has actually lesser value than the voltage in socket and no special amplifier is needed to achieve luminance of printed panel above 100 $cd \cdot m^{-2}$ (under voltage 500 V peak-to-peak and higher). On the other hand a frequency of the AC voltage given by European power grid is 50/60 Hz which is too low for generation of bright light. A special type of frequency inverter needs to be included to enhance the frequency at least up to several hundred Hz but no more than 1000 Hz because of the dramatically decreased stability of the panel.

At the moment a stability of the electroluminescence panels is a major problem with respect to their broader use in industry. A stability study in this work (**Tab. 14**) showed that the panel ***iii*** encapsulated between robust glass panels with melted polymer foil showed highly improved stability compared to the laminated panels. This confirms the fact that the prevention of contamination of the phosphor by a gas containing water vapors increases the life time of a panel.

The stability of panel ***ii*** driven by alternating voltage with frequency 370 Hz also showed somewhat improved life time compared to the sample *i.* as can be seen from the **Tab. 14**. It confirms that with increasing driving frequency the stability of phosphor is decreased possibly due to the fact that more electrical energy is transferred to the bulk of phosphor, depleting the active luminescence centers as was proposed by Klassen et *al*.

The well encapsulated panel driven under 400 V_{pp} and 300 Hz showed parameter L_{50} around 2300 hours and L_{75} around 800 hours, which is comparable to classical 60 W 230 U_{RMS} opal bulbs.

7.6 Tuning of light emitted by an ACPEL panel

Phosphors showing emission from blue to red wavelengths are well known but the ability to tune the color of emitted light is limited. Therefore a study to broaden a palette of emitted light colors was conducted in this work. Extensive review of variously doped phosphors was given by [12]. Although the range of potential materials is large only a few of them turned out to be commercially suitable phosphors. For instance ZnS:Cu, Cl emits at 450 nm, ZnS:Cu, Al at 540 nm, ZnS:Cu,Mn,Al at 590 nm and ZnS:Cu at 690 nm.

There exist several ways how to change the color of emitted light. One is to change the driving frequency. Another approach is to prepare phosphor powders based on ZnS with various dopants based on rare earth metals (Eu^{+3}, Sm^{+3}, In^{+3}, Tb^{+3} etc.) [84, 85]. This way of modification is economically problematic because of the price of the above mentioned materials. Interesting approach is introduction of quantum dots with defined dimensions to modify the color of emission [86]. Quantum dots are however often based on very toxic elements such as lead or cadmium which renders them practically useless for large scale applications.

Very promising approach appears to be the modification of emitted color by addition of specific color conversion material (CCM). The light emitted by a phosphor is reabsorbed by the CCM and the light of different wavelength is obtained. Rhodamine dyes have been successfully used as a CCM material [87] since they show solid state fluorescence with solid quantum yields and good stability. The maximal absorbance of Rhodamine B is at ~550 nm and emission at 570 nm. This approach is somewhat problematic because not many materials absorb at the desired wavelengths where a specific phosphor emits and show good solid state fluorescence. Another issue is with the stability of the new mixture of phosphor and fluorophore since the latter materials tend to be easily photodegradable compared to the phosphor. Also the color of the phosphor under no voltage can be somewhat shifted from the default white which doesn't need to be desirable.

The last mentioned approach is topical for this dissertation thesis. Rhodamine B was used as a CCM for commercial orange paste because of the good compatibility between phosphor emission and Rhodamine absorption wavelengths. Potentially very interesting group of substances could be diketopyrrolopyrrole (DPP) derivatives because of their stability [88], solid state fluorescence [89] and a possibility to tune their fluorescence spectra by molecular tailoring [90].

7.6.1 Influence of driving frequency on the electroluminescence spectra

From the results in **Tab. 9** can be seen that both increasing voltage and frequency increase the total radiation given by ACPEL panels. The influence of higher voltage is quite clear (comparison of samples 2 and 3) and contributes to the increased luminance of the light source more significantly than the increase of frequency. The increase of driving frequency has effect both on increasing how bright the panel will be perceived (**Tab. 13**) and on the wavelength of emitted color. It was shown that the increasing values of driving frequency shift the emitted light toward shorter wavelengths

Tab. 15 summarizes the change of emitted dominant wavelength on the driving frequency of all tested phosphors. The dominant wavelength is determined from the CIE color coordinates space. A straight line connecting the measured point with white point is extrapolated and the intersection of the line with a closer boundary of the color space is called the dominant wavelength. It is defined as a monochromatic light that would evoke the same perception of a hue as is caused by the studied illuminant with a spectral light characteristic. It is a good parameter for characterization of a light mixture. The intersection on the opposite end is called the complementary wavelength. The orange phosphor emission is almost constant with the increasing frequency. The x and y coordinates were measured and plotted in the CIE 1931 chromaticity diagram as **Fig. 37** to visualize the change of emitted color.

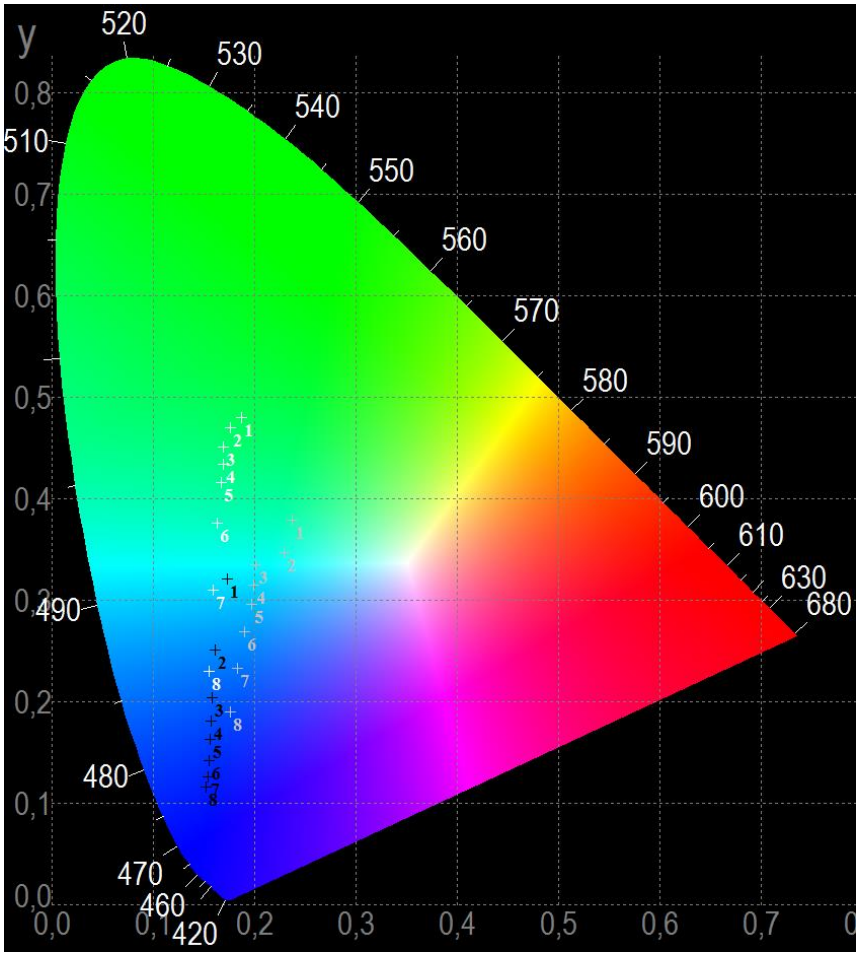

Fig. 37 *CIE 1931 color space. Black points represent the change of a blue panel, white points represent green panel and silver points represent mixed printing formulation under 250 V_{pp} and frequencies 100; 235;450; 680; 1000; 1800; 3700 and 10 000 Hz represent samples 1–8 respectively.*

Tab. 15 *Change of the dominant wavelength as a function of frequency taken at constant voltage of 250 V_{pp}.*

f **(Hz)**	$\lambda_{D,Blue}$ **(nm)**	$\lambda_{D,Green}$ **(nm)**	$\lambda_{D,Orange}$ **(nm)**	$\lambda_{D,Mix}$ **(nm)**
100	490	503	583	495
235	485	502	584	491
450	481	500	584	490
680	479	498	584	489
1000	477	497	584	487
1800	475	494	585	485
3700	473	489	586	482
10000	472	483	587	478

The mechanism of change of emitted light wavelength of blue and green phosphors by the change of frequency was described by Zalm [91]. Two different dopant energy levels (so-called blue and green centers) are present in the structure of ZnS. Upon excitation of electrons into the conduction band the electrons recombine radiatively with the vacant dopant centers. A position of the dopant activation center in a band gap determines the wavelength of emitted light. With

increasing frequency the dopant activation center with lower energy is preferred, giving rise to the shift of electroluminescent light toward blue region [91]. This process is shown in **Fig. 38**. For an orange phosphor no such a shift of activation center energies was observed and the color of emitted light is not changed.

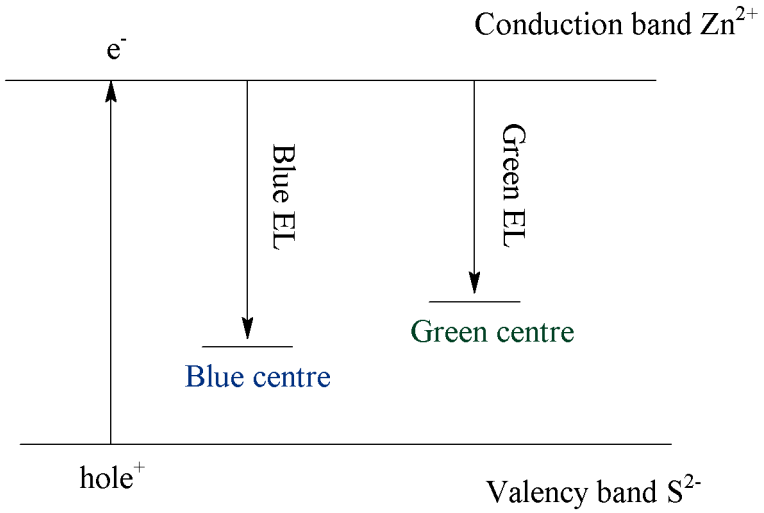

Fig. 38 *The electronic structure of ZnS crystal with dopant activation centers. Adapted from [91].*

7.6.2 DPP as a color conversion material

A novel DPP derivative used for modification of the blue phosphor was prepared by synthetic chemists at the Faculty of Chemical Technology at University of Pardubice. Its UV-Vis absorption spectra in water showed absorption in the region of wavelengths approximately from 450 to 520 nm and its fluorescence emission spectrum showed maximum emission at λ_{em} = 565 nm. Its emission in solid state showed shift to λ_{em} = 600 nm with a parameter full-width at half-maximum (FWHM) around 80 nm making this DPP an ideal CCM for studied standard blue phosphor. The measured absorption and fluorescence spectra are shown as **Fig. 39**.

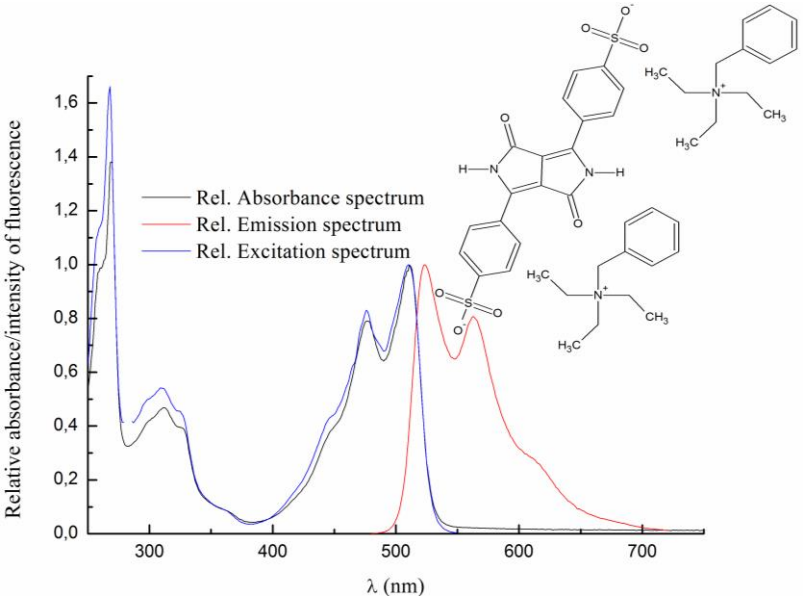

Fig. 39 *Absorption and excitation (black and blue curve respectively) and emission spectrum (red curve) with a structural formula of the studied DPP derivative.*

Two sets of samples were prepared (a) where fluorophore was added directly into the phosphor formulation with increasing concentration and printed via screen-printing: P1 – with mass fraction of fluorophore w = 0.8 %; P2 – with mass fraction of fluorophore 2.5 % and samples (b) where fluorophore was added in the form of thin layer between ITO substrate and phosphor layer: P3 – deposition by dip coating and P4 – deposition by spin coating with 2500 rpm. A reference blue phosphor with no added fluorophore was prepared as a sample P5. **Tab. 16** summarizes the conditions of preparation of individual samples.

Tab. 16 *Details on processing conditions of samples.*

Sample	Process
P1	Sample (a) with 0.8 $\%_W$ of DPP
P2	Sample (a) with 2.5 $\%_W$ of DPP
P3	Sample (b) with dip coated DPP layer
P4	Sample (b) with spin coated DPP layer
P5	Reference blue phosphor

The absolute spectral irradiance spectra of all the samples were taken at fixed voltage U_{pp} = 250 V_{pp} with increasing frequency in the range 100–25 000 Hz and the dominant wavelengths λ_D were plotted against the increasing frequency as **Fig. 40**.

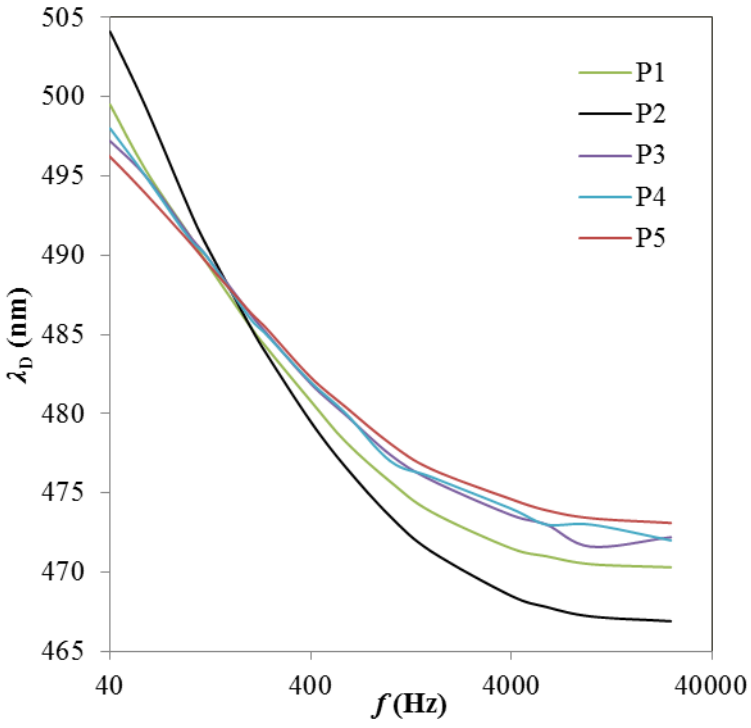

Fig. 40 *The dominant wavelength of emitted electroluminescence as a function of frequency.*

Samples P5 – reference, P4 and P3 with deposited thin layer of fluorophore show very similar light response and it can be concluded that CCM material deposited as a filter layer by coating technique does not show any effect on the conversion of emitted light in this experiment. This can be due to the fact that the spin-coated filter film was too thin to show any difference. Samples P1

and P2 with fluorophore incorporated directly into the printing formulation however show somewhat different behavior. Samples P3 and P4 were excluded from further characterization because of the minimal effect of a fluorophore as a very thin filter layer.

Normalized spectral irradiance of reference sample and both samples with color conversion material can be seen in **Fig. 41**. The presence of fluorophore changes the shape of spectrum in the region of maximal emission of fluorescence. The irradiance of samples P1 and P2 is slightly decreased in the region of wavelengths 480–530 nm (maximum of absorbance of the fluorophore) compared to the reference sample (red line) because the light was reabsorbed by the fluorophore. The rise of spectral irradiance in a region ~ 580–600 nm corresponds with region of emission of the DPP. It is worth noting that reference sample lacks this new peak [92].

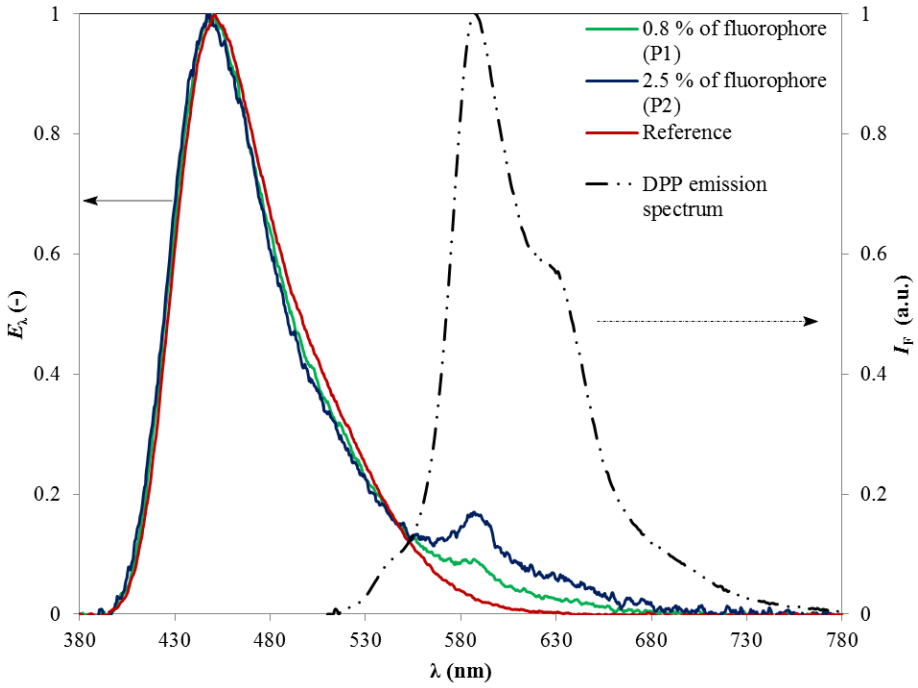

Fig. 41 *Normalized spectral irradiance of reference blue panel and panels with fluorophore. Emission spectrum of fluorophore (dotted line) is added for comparison.*

The change of color of the emitted light was further confirmed by plotting the *x* and *y* coordinates in the 1931 CIE chromaticity diagram as **Fig. 42**.

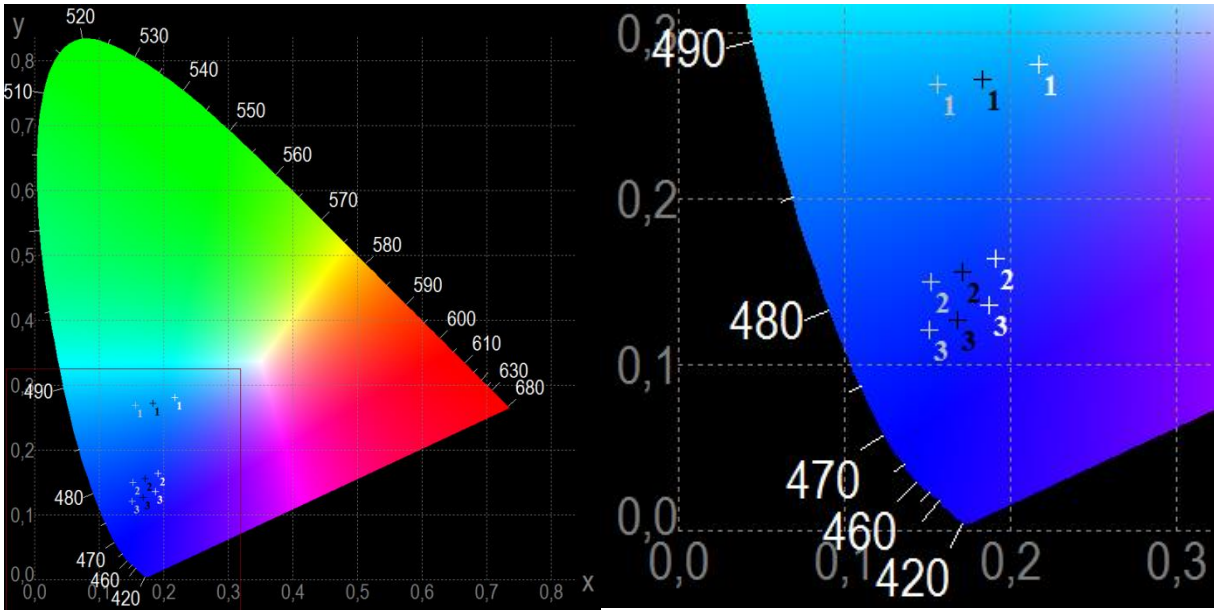

Fig. 42 *The change of lights color in 1931 CIE color space with cutout for better focus at varying frequencies (points 1 – 200 Hz; points 2 – 1600 Hz and points 3–10 kHz).*

The grey dots represent pure phosphor; black dots represent sample P1 and white dots represent sample P2 with higher concentration of fluorophore. All the measurements were conducted under the same voltage U_{pp} = 250 V. It can be seen that the samples show similar behavior but the coordinates of emitted light are shifted in the direction of longer wavelengths. It is also clear that the frequency of alternating voltage shifts the color of emitted light. While the difference between minimal frequency 200 Hz and 1600 Hz is notable further increasing of frequency does not change the color significantly and should be avoided because of the decreased stability of panel when exposed to the harmonic wave with high frequency.

7.6.3 Rhodamine B as a CCM

A similar test was conducted with standard fluorophore Rhodamine B showing maximal absorption at approximately 540 nm when dissolved in ethanol with maximal emission at approximately 565 nm [93]. These spectral properties could make Rhodamine B a promising material for modification of orange panel which emits light with small relative intensity compared to the other panels.

A series of 4 samples with varying concentration of Rhodamine B was prepared by addition of Rhodamine B solved in ethanol to the orange phosphor printing formulation. A reference sample (O) without presence of Rhodamine B; sample (R1) with 120 µL/g, sample (R2) with 500 µL/g and sample (R3) with concentration 600 µL/g. Absolute spectral irradiance of all the samples was measured at fixed U_{pp} = 200 V and f = 1000 Hz and absolute illuminance spectra were plotted as **Fig. 43**. Details of the prepared samples together with their optical properties are summarized in **Tab. 17**.

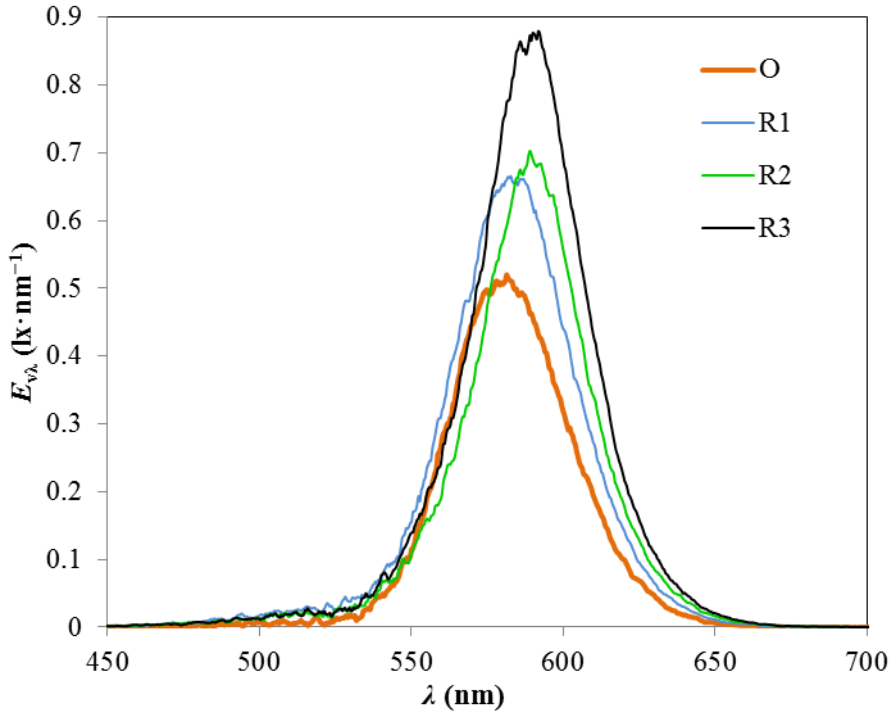

Fig. 43 *Absolute spectral illuminance of samples with increasing concentration of fluorophore.*

Tab. 17 *Concentration of Rhodamine B in tested samples.*

Sample	Conc. of fluorophore (μL·g^{-1})	E_v (lx)	L_v (cd·m^{-2})	Relative efficiency (%)
O	0	0.57	3.85	100
R1	120	0.76	5.18	134
R2	500	0.74	5.00	130
R3	600	0.92	6.26	163

The luminance increases with the higher concentration of fluorophore as can be seen in **Tab. 17**. The sample R1 and R2 show very similar behavior although the concentration of the fluorophore is more than 4 times higher. This fact might be given by the insufficient homogeneity of sample P3. The irradiance spectrum was taken by the bare fiber without the cosine corrector and so the angle of view, ϑ of the sampling optics was very narrow. It is 25° for the bare fiber compared to almost 180°for the cosine corrector. A very small area – statistically insufficient – of the shining surface was measured and the results are likely to be a subject to a large margin of error. Another explanation of the increasing luminance might be that addition of fluorophore in a solution is diluting the phosphor paste and the printed phosphor film is thinner. The thinner the film is the higher electric field is generated between the electrodes and the panel radiates more.

7.6.4 Conclusion

The strategy to change the emitted color by the change of frequency does not seem very effective. It was shown (**Fig. 37** and **Tab. 15)** that the emitted light wavelength can be changed only in phosphors with specific dopants and even then the shift of the dominant wavelength is only around 20 nm at 10 kHz. It is known that such a high frequency is harmful for the stability of the panel. On the other hand the frequency around 100 Hz and less induces emission of light with insufficient optic performance.

The use of fluorescent organic material as a CCM showed change of the absolute spectral irradiance as is shown in **Fig. 41.** The spectra of samples containing CCM with absorption in the range of 480–530 nm show slight decrease of irradiance in this region while a new peak occurs at the wavelengths of CCM emission.

The effect of Rhodamine B on the emission of orange phosphor is not so clear. The luminance of sample with the highest concentration was increased by 63 % compared to the reference spectrum. But it is difficult to distinguish if it is the effect of reabsorption of electroluminescence by Rhodamine B and emission of fluorescence or if it is caused by dilution of a phosphor paste resulting in printing a thinner active film. The effect of increasing thickness of phosphor film is described in the **Fig. 30**.

The change of the emitted light color is a serious challenge. Although several strategies were described in this thesis more investigation will be further needed. The increase of frequency is downright bad in the long run an addition of fluorescent CCM can drastically change the color of not operating panel with no information about the long time effect. It is not probable that both fluorophore and phosphor will show the same stability after long time exposure of either light or electric field. The color of light emitted by the conversion material thus could change after a period of time. The same applies for mixing of standard phosphors (orange, green and blue for this thesis) in various ratios to achieve some different shade of color. Preparation of quantum dots seems like a promising approach but is beyond the scope of this thesis.

8 CONCLUSIONS OF DISSERTATION THESIS

In order to fulfill the main aim of this thesis, development of ACPEL panels and overcoming red brick wall problems associated with this type of technology, the first step was to identify most suitable deposition techniques. The most relevant deposition and material printing techniques were introduced in **Chapter 4**. Several facts limit a broad portfolio of all the printing techniques suitable for this task. the panels are printed from inherently highly dense and viscous printing pastes, some films forming the whole panel need to be patterned, the height of active layers is typically in the order of tens of microns and of a printing technique should be R2R compatible for high output preparation. All these facts are making screen-printing technique an optimal mean for deposition of the ACPEL panels. Another advantage of the screen-printing is a fact that it is currently the most wide-spread technique in a field of printed electronics.

The main parameters that determine the quality of printed layers by the screen-printing are printing speed, viscosity and density of the printing paste, on-off ratio, and so-called preprinting. **Chapters 7.1–7.3** focused on optimizing the printing conditions to achieve homogenously printed films of (i) dielectrics, (ii) electrode material and (iii) the phosphor. Because of the fact that all three films fulfill very different roles, this topic was divided into three subchapters. Physical-chemical parameters of the printing pastes were not changed so only the parameters directly connected with screen-printing (printing speed, on-off ratio and preprinting) were investigated. It was found that thickness and homogeneity are crucial parameters determining a quality of the dielectric film (**Chapter 7.1**). A film thickness h and surface topology parameters roughness Ra and waviness Wa measured with contact profilometry were taken as a mean to determine the optimal printing conditions. It was shown that the optimal printing conditions include minimal achievable printing speed because of the high dynamic viscosity of the paste and preprinting. The dielectric films formed by two layers of dielectrics printed atop each other achieved a thickness $h = (19.10 \pm 0.3)$ μm with roughness $Ra = (0.67 \pm 0.10)$ μm and waviness $Wa = (0.48 \pm 0.09)$ μm. The dielectric film needs to be relatively bulky to ensure an electric stability of the panel and also homogeneous to achieve the same intensity of an electric field across the whole device. Therefore the printing conditions leading to relatively low roughness and waviness and a proper thickness of a dielectric film were found to be the most optimal. It was further determined that the optoelectronic performance is not decreased by increasing thickness of the dielectric film in the measured range of thicknesses. Because of the overall similar physical-chemical parameters of all the printing pastes the same printing conditions were evaluated to be the most suitable also for the other films.

Chapter 7.2 focused on investigating of the most suitable material as a top electrode. Measurement of sheet resistances of three suitable candidates, Ag paste, carbon paste and transparent organic PEDOT:PSS, were evaluated and absolute irradiance spectra of panels with different top electrodes were compared. Sheet resistance of the Ag paste is 4 orders of magnitude less than the other two materials which makes the silver paste more appropriate material as a top electrode. The carbon electrode panel exhibits around 80 % of optoelectronic performance of the silver electrode panel, while PEDOT:PSS electrode panel exhibits only 50 %. It was shown that the transparent PEDOT:PSS can be used to prepare an ACPEL device emitting light in both ways (top and bottom).

Optimization of processes leading to a homogenously printed phosphor layer is a subject of **Chapter 7.3**. A phosphor film was printed under the same screen-printing settings but a key factor influencing a quality of printed film is the so-called preprinting. It was concluded that without this step it is impossible to print a homogeneous layer but instead single well separated phosphor clusters are printed. An impact of film thickness of phosphor on optoelectronic performance of various panels was tested and a drop of absolute spectral irradiance with increasing amount of layers (with typical thickness 30 μm) forming the film was observed. It was therefore concluded that the printed phosphor film should be as thin as possible. However a typical size of ZnS grains is in the order of tens of microns and cannot be reduced by mechanical milling without decreasing the radiative properties of the grains. It was concluded from the above mentioned facts that the ideal composition of the panels is therefore one layer of a phosphor, two layers forming a dielectric film and one layer of Ag forming a top electrode.

Determination of influence of driving conditions on the optoelectronic performance of the ACPEL panels together with their electric power consumption is one of the main goals of the whole thesis and was covered in **Chapter 7.4**. Absolute spectral irradiance spectra of panels with different phosphors driven by varying driving conditions were measured and the values of luminance and electric power consumption were evaluated. It was shown that the highest value of luminance was achieved when a panel containing green phosphor was subjected to higher tested amplitude of alternating voltage. It was shown that both increasing the voltage and frequency increase the optoelectronic performance of panels but the effect of the increasing voltage amplitude is more profound. The highest achieved luminance was $L_V = 130\ \mathrm{cd \cdot m^{-2}}$ on the panels driven at $f = 1000$ Hz and $U_{pp} = 500$ V. A power consumption of panels increases with increasing voltage, frequency and an area of the phosphor film. A typical power consumption per unit area (P/A) of panels driven by 400 V_{pp} and 370 Hz was estimated to be $P/A = (7 \pm 3)\ \mathrm{mW \cdot cm^{-2}}$ and panel with 78 cm^2 showed the total power consumption $P = 0.5$ W, which is several order less than other typical light sources. These values make panels based on this technology interesting for practical applications.

Increasing both amplitude of alternating voltage and frequency has negative effect on the lifetime of the panel. The aim of **Chapter 7.5** was to investigate how a lifetime of panels changes under different driving conditions. Parameters L_{75} and L_{50}, describing time after which luminance drops to 75 % respectively 50 % were evaluated for samples differing with driving frequency, driving voltage amplitude and type of encapsulation. It was proved that increasing the values of driving conditions has negative effect on the stability of panels. The best stability with $L_{50} = 2260$ hours was obtained on a panel that was driven by frequency 370 Hz and was encapsulated by polymer foil between two glass panels. Values of both the stability parameters were almost 7 times higher compared to the not encapsulated panel driven by $f = 1000$ Hz. To ensure the highest possible stability of panels one must take into consideration both driving conditions and the type of encapsulation. The frequency of applied voltage needs to be less than 1000 Hz to ensure high stability but higher than 200 Hz to ensure reasonable optoelectronic performance suitable for the given application of the large area light sources.

Chapter 7.6 addresses possibilities to modify color of light emitted by an electroluminescent panel. One way is a change of a driving frequency. It was shown that the color coordinates of light emitted by a blue phosphor driven with increasing frequency are changed therefore a light of different hue is emitted. This effect was measured on the panels formed by blue, green, orange and

mix phosphors for the frequencies in a range f = (100–10 000) Hz and a dominant wavelength of light was measured. It was found that the change of wavelength between 100 Hz and 10 000 Hz is approximately 20 nm for blue, green and mix phosphors and orange phosphor does not change color of emitted light at all. It was concluded that this effect cannot lead to efficient change of color because human eye cannot distinguish colors with so close values of wavelength. Another problem is that frequencies higher than 1000 Hz are destructive for a long time stability of panels as was concluded in **Chapter 7.5**. A more promising way was an addition of color conversion material directly into the phosphor printing formulation and/or deposition of a CCM as a filter covering the phosphor film. A DPP derivative with suitable absorption and emission spectra was chosen as a CCM to change color of light emitted by a blue phosphor panel. An addition of the CCM achieved a 7 times increase of irradiance at wavelengths around 680 nm corresponding to a maximum emission of the CCM.

A similar test was conducted for orange phosphor with Rhodamine B as a CCM leading to increase of illumination up to 63 %. It was, however, difficult to associate it with the effect of reabsorption of light by the CCM as with the blue CCM. Both inhomogeneity of orange panels or the effect of dilution the printing formulation, thus decreasing a thickness of the film and increasing the intensity of electric field between the electrodes are possible explanation of the measured of increased optoelectronic performance.

This thesis concludes that the red brick walls defined in the introduction can be overcome with careful setting of both the parameters leading to preparation of the panels and driving conditions. Reasonable luminance above 130 $cd \cdot m^{-2}$, power consumption per unit area 0.5 $mW \cdot cm^{-2}$ with L_{50} in order of thousands of hours can be obtained. Typical values of the achieved luminance make panels based on the ACPEL technology excellent candidates for various indoor decorative light sources and large area background sources of light. ACPEL panels have already found partial application in automotive and commercial industry and in future it might be expected that they will find more applications.

9 LIST OF SYMBOLS

AFM	Atomic force microscopy
AC/DC	Alternating/direct current
ACTFEL	Alternating-current thin film electroluminescence
ACPEL	Alternating-current powder electroluminescence
CCD	Charge-coupled device
CCM	Color conversion material
c	Concentration of solid material in solution
CIJ	Continuous inkjet
cP	Centipois
D	Characteristic length
d	Thickness of wet layer
DOD	Drop on demand
DPP	Diketopyrrolopyrrole
E_e	Irradiance
E_V	Iluminance
EGBE	Ethylene glycol monobutyl ether
FWHM	Full width at half maximum
HID	High-intensity discharge
HPS	High pressure sodium vapors
$\dot{V}$	Flow rate
f	Frequency
g	Gap distance
h	Film thickness
IR	Infrared radiation/region
ITO	Indium tin oxide
I	Electric current
I_D	Displacement current
K	Time constant representing stability of a panel
k_p	Paste volume of screen

$k_{spin,\alpha}$	Empirical constants for spin coating
L_V	Luminance
L_e	Radiance
L_{50}	Time after which luminance drops on 50 % of initial value
L_{75}	Time after which luminance drops on 75 % of initial value
LEC	Light-emitting cells
MDMOPPV	Poly[2-methoxy-5-(3′,7′-dimethyloctyloxy)-1,4-phenylenevinylene]
MEHPPV	Poly(p-phenylene vinylene)
MOX	metal oxide
mW	Miliwatt
n	Refractive index
N_D	Number of droplets deposited per area
NIR	Near infra-red region
NMR	Nuclear magnetic resonance
NP	Nanoparticle
Oh	Ohnesorge number
(O)LED	(Organic) light-emitting diode
(O)PV	(Organic) photovoltaics
(O)SC	(Organic) solar cell
(O)TFT	(Organic) thin-film transistor
P/A	Power consumption per unit area
P3HT	Poly(3-hexyl)thiophene
pBTTT	Poly(2,5-bis(3-hexadecylthiophen-2-yl)thieno[3,2-b]thiophene)
$PC_{60}BM$	[6,6]-phenyl C61 butyric acid methyl ester
PCE	Power conversion efficiency
PEDOT:PSS	Poly(3,4-ethylenedioxythiophene) polystyrene sulfonate
PEN	Poly(ethylene 2,6-naphtalate)
PET	Polyethylene terephthalate
PSC	Polymer solar cell
PVs	Photovoltaics

R	Electrical resistivity
Ra	Roughness of a layer
RPM	Rotations per minute
R2R	Roll to roll
Re	Reynolds number
S/D	Source drain channel
SEM	Scanning electron microscopy
TFE	Thin Film Electronics AB
TFT	Thin film transistor
T_T	Transition temperature
v_c	Coating (web) speed
v	Velocity of droplets
U	Voltage
U_{pp}	Peak-to-peak voltage
U_{RMS}	Effective voltage
UV	Ultraviolet radiation/region
V_D	Volume of droplet
Vis	Region of visible light
V_{screen}	Volume of screen
Wa	Waviness of a layer
w	Coating width
We	Weber number
Z	Inverse value of Ohnesorge number
ZnS	Zinc sulfide
Φ_e	Radiant flux
Φ_V	Luminous flux
λ	Wavelength
λ_D	Dominant wavelength
λ_{em}	Maximum fluorescence wavelength
φ	Phase shift

φ_V	Volume fraction of ZnS grains
η	Dynamic viscosity
ρ	Density
σ	Surface tension
ϑ	Angle of view
ω	Rotational speed

10 REFERENCES

[1] Flexible, Printed and Organic Electronics 2019 - 2029: Forecast, Players & Opportunities, 2018. *www.idtechex.com* [online]. USA: IDTechEx [cit. 2018-10-25]. Dostupné z: https://www.idtechex.com/research/reports/flexible-printed-and-organic-electronics-2019-2029-forecasts-players-and-opportunities-000639.asp.

[2] HECKER, K, BREITUNG, S, CLEMEN,S W, LUPO, D. *OE-A roadmap for organic and printed electronics: 6th edition*. Frankfurt am Main: OE-A, 2015. ISBN 978-3-8163-0673-3.

[3] DESTRIAU, G. AC electroluminescence in ZnS, J.Chim.Phys. 34 (1937), 117 – 124.

[4] HOWARD, B T, Ivey, H F, LEHMANN, W. Voltage Dependence of Electroluminescent Brightness. *Physical Review*.1954, **96**: 799-800. doi:10.1103/PhysRev.96.799.

[5] PIPER, W W, WILLIAMS, F E. Theory of electroluminescence. *Physical Review*. 1955, **98**:1809-1813. doi:10.1103/PhysRev.98.1809.

[6] BREDOL, M, DIECKHOFF, H S. Materials for Powder-Based AC-Electroluminescence. *Materials*. 2010, **3**:1353-1374. doi:10.3390/ma3021353.

[7] WITHNALL, R, HARRIS, P, SILVER, J, JONES, S. Invited Paper: Novel, Bright, Inorganic Electroluminescent Flexible Displays Comprising Ink Jet Printed Silver Back Electrodes. *SID Symposium Digest of Technical Papers*. 2010, **41**:397-400. doi: 10.1889/1.3500470.

[8] WEN, L, LIU, N, WANG, S, ZHANG, H, ZHAO W, YANG Z, WANG Y, SU J, LI L, LONG F, et al. Enhancing light emission in flexible AC electroluminescent devices by tetrapod-like zinc oxide whiskers. *Optics Express*. 2016, **24**(23419-23428). doi: 10.1364/OE.24.023419.

[9] FISCHER, A G. Electroluminescent Lines in ZnS Powder Particles. *Journal of The Electrochemical Society*. 1963, **110**:1043-1049. doi: 10.1149/1.2425863.

[10] SMET, P F, MOREELS, I, HENS, Z, POLEMAN D. Luminescence in Sulfides: A Rich History and a Bright Future. Materials. 2010. **3**(2834-2883). doi: 10.3390/ma3042834.

[11] WINSCOM, C J, WITHNALL, R, SILVER, J,. Thick Film AC Electroluminescence. *Handbook of Digital Imaging*. 2015. Chichester, UK, 2015-03-02, 1-18. DOI: 10.1002/9781118798706.hdi065. ISBN 9781118798706

[12] HARRIS, P, DEN ENGELSEN, D, FERN, G, SILVER, J,. . AC electroluminescent lamps: shedding some light on their mysteries. *Journal of Materials Science: Materials in Electronics.* 2017. **28,** 7006-7012. doi: 10.1007/s10854-016-5965-4

[13] CHADHA S S. *Powder Electroluminscence*. In: KITAI AH *Solid State Luminescence Theory, materials and devices*. 1993, Springer, Dordrecht Netherlands, pp 195-229.

[14] KREBS, F C, GHANBARI-SIAHKALI, A, LARSEN, N B. Fabrication and processing of polymer solar cells: A review of printing and coating techniques. *Solar Energy Materials and Solar Cells*. 2009, **93**(4), 394-412. DOI: 10.1016/j.solmat.2008.10.004. ISSN 09270248.

[15] NORRMAN, K., A. GHANBARI-SIAHKALI a N. B. LARSEN. 6 Studies of spin-coated polymer films. Annual Reports Section "C" (Physical Chemistry). 2005, **101**(1), 174-. DOI: 10.1039/b408857n.

[16] SPIN COATER MODELS. *POLOS*™ [online]. 1998. Dostupné z: https://www.spincoating.com/en/spin-processor-models/substrate-size-550/102/https://www.spincoating.com/en/spin-processor-models/substrate-size-550/102/

[17] LI, G, SHROTRIYA, V, HUANG, J, YAO, Y, MORIARTY, T, EMERY, K, YANG, Y. High- efficiency solution processable polymer photovoltaic cells by self-organization of polymer blends. *Nat. Mater*. 2005, 4, 864–868.

[18] MA, W., YANG, C, GONG, X, LEE, K, HEEGER, A J. Thermally Stable, Efficient Polymer Solar Cells with Nanoscale Control of the Interpenetrating Network Morphology: Knife-over-edge coating, slot-die coating and screen-printing. *Advanced Functional Materials* [online]. 2005, **15**(10), 1617-1622 [cit. 2016-01-11]. DOI: 10.1002/adfm.200500211.

[19] KERDCHAROEN, T., WONGCHOOSUK, C. Carbon nanotube and metal oxide hybrid materials for gas sensing. *Semiconductor Gas Sensors*. Elsevier, 2013, 386-407. DOI: 10.1533/9780857098665.3.386. ISBN 9780857092366.

[20] ECKER, M, PRETSCH T. Novel design approaches for multifunctional information carriers. *RSC Adv*. 2014, **4**(87), 46680-46688. DOI: 10.1039/C4RA08977D. ISSN 2046-2069.

[21] SØNDERGAARD, R, HÖSEL M, KREBS, F C. Roll-to-Roll fabrication of large area functional organic materials. *Journal of Polymer Science Part B: Polymer Physics*. 2013, **51**(1), 16-34. DOI: 10.1002/polb.23192. ISSN 08876266.

[22] MENS, R, ADRIAENSENS P., LUTSEN, L, SWINNEN, A, BRETHO, S, RUTTENS, B, D'HAEN, J, MANCA, CLEIJ, T, et al. NMR study of the nanomorphology in thin films of polymer blends used in organic PV devices: MDMO-PPV/PCBM. *Journal of Polymer Science Part A: Polymer Chemistry*. 2008, **46**(1), 138-145. DOI: 10.1002/pola.22365. ISSN 0887624

[23] KIM, J H., Spencer T W, CHO N, CHUEH, C, JEN, K Y A.. Enhanced Environmental Stability of Planar Heterojunction Perovskite Solar Cells Based on Blade-Coating. Advanced Energy Materials. 2015. **5**(4). DOI: 10.1002/aenm.201401229.

[24] PIERRE, A, SADEGHI, M, M M PAYNE, FACCHETTI, A, ANTHONY, J E, ARIAS, AC.. All-Printed Flexible Organic Transistors Enabled by Surface Tension-Guided Blade Coating. Advanced Materials. 2014. **26**(32), 5722-5727. DOI: 10.1002/adma.201401520.

[25] KREBS, F C. Polymer solar cell modules prepared using roll-to-roll methods: Knife-over-edge coating, slot-die coating and screen-printing. Solar Energy Materials and Solar Cells. 2009, **93**(4), 465-475. DOI: 10.1016/j.solmat.2008.12.012. ISSN 09270248.

[26] HAN, G H, LEE, S H a JUNG, H W. Effect of shim configuration on flow dynamics and operability windows in stripe slot coating process. J. Coat. Technol. Res. 2014, **2014**(11), 19-29. DOI: 0.1007/s11998-013-9485-3.

[27] Slot die coating. *Plasticphotovoltaics.org: a hub for OPVs research* [online]. Lastupdate:Wed,27Jan2016 [cit. 2016-01-27]. Dostupné z: http://plasticphotovoltaics.org/lc/lc-fabrication/lc-coating/lc-slotdie.html#fn3

[28] YAMAGUCHI, M. a FARA, M. *Advanced Solar Cell Materials, Technology, Modeling, and Simulation*. 1. Hershey PA 17033: IGI Global, 2012. ISBN 9781466619272.

[29] KREBS, F C. All solution roll-to-roll processed polymer solar cells free from indium-tin-oxide and vacuum coating steps. *Organic Electronics* [online]. 2009, **10**(5), 761-768 [cit. 2016-01-11]. DOI: 10.1016/j.orgel.2009.03.009. ISSN 15661199.

[30] SHIN, S, YANG, M, GUO, L J, YOUN, H. Roll-to-Roll Cohesive, Coated, Flexible, High-Efficiency Polymer Light-Emitting Diodes Utilizing ITO-Free Polymer Anodes. *Small*. 2013, **9**(23), 4036-4044. DOI: 10.1002/smll.201300382. ISSN 16136810.

[31] SANDSTRÖM, A, DAM H F, KREBS, F C, EDMAN, L. Ambient fabrication of flexible and large-area organic light-emitting devices using slot-die coating. *Nature Communications*. 2012, **3**, 1002-. DOI: 10.1038/ncomms2002. ISSN 2041-1723

[32] BELLINGHAM, A, BROMHEAD, N, FONTECCHIO, A. Rapid Prototyping of Slot Die Devices for Roll to Roll Production of EL Fibers. *Materials*. 2017. **10**(6). DOI: 10.3390/ma10060594. ISSN 1996-1944.

[33] RIEMER, D E. The Theoretical Fundamentals of the Screen-Printing Process. *Microelectronics International*. 1989, **6**(1), 8-17. DOI: 10.1108/eb044350. ISSN 1356-5362.

[34] HÖSEL, M; KREBS, F C. *Large-scale Roll-to-Roll Fabrication of Organic Solar Cells for Energy Production*. Roskilde, 2013. PhD Thesis. Technical University of Denmark, Denmark. Department of Energy Conversion and Storage Solar Energy.

[35] BAO, Z, FENG, Y, DODABALAPUR, A, RAJU, V R, J. LOVINGER, A. *High-Performance Plastic Transistors Fabricated by Printing Techniques* [online]. DOI: 10.1021/cm9701163. ISBN 0897-4756.

[36] PARDO, D A., JABBOUR, G E, PEYGHAMBARIAN, N. Application of Screen Printing in the Fabrication of Organic Light-Emitting Devices. *Advanced Materials*. 2000, **12**(17), 1249-1252. DOI: 10.1002/1521-4095(200009)12:17<1249::AID-ADMA1249>3.0.CO;2-Y.

[37] BERGGREN, M, RICHTER-DAHLFORS, A. Organic Bioelectronics. *Advanced Materials* [online]. 2007, **19**(20): 3201-3213. DOI: 10.1002/adma.200700419. ISSN 09359648.

[38] MANNERBRO, Richard a Martin RANLÖF. *Inkjet and Screen Printed Electrochemical Organic Electronics*. Linköping, 2007. LITH-ISY-EX--07/3876--SE. Master Thesis. Linköping Institute of Technology.

[39] BENDONI, R, SANGIORGI, N, SANGIORGI, A, SANSON, A. Role of water in TiO2 screen-printing inks for dye-sensitized solar cells. *Solar Energy*. 2015, **122**, 497-507. DOI: 10.1016/j.solener.2015.09.025.

[40] KREBS, F C, JOERGENSEN, M. *Decomposable vehicles in printing or coating compositions*. Denmark. US 8,257,786 B2 Foreign patent document. Granted 4.9.2012.

[41] KREBS, F C., SØNDERGAARD, R, JØRGENSEN, M. Printed metal back electrodes for R2R fabricated polymer solar cells studied using the LBIC technique. *Solar Energy Materials and Solar Cells*. 2011, **95**(5), 1348-1353. DOI: 10.1016/j.solmat.2010.11.007.

[42] GSI technologies - Inteligent Printing, 2017. Http://www.gsitech.com/ [online]. Illionois: GSI Technologies - All Rights reserved [cit. 2018-10-30]. Dostupné z: http://www.gsitech.com/electroluminescent-light-manufacturer/

[43] Eye-catching, paper thin Electroluminescent displays, 2017. Display-innovations [online]. London: Display innovations [cit. 2018-10-30]. Dostupné z: http://display-innovations.com/displays/electroluminescent-technology

[44] Elumin8 - innovations, 2018. Elumin8 - the art of light engineering [online]. Romsey: Elumin8 [cit. 2018-10-30]. Dostupné z: http://www.elumin8.com/innovation-2/

[45] Printing Technologies find their Place in Printed Electronics, 2018. *Www.idtechex.com* [online]. USA: IDTechEx [cit. 2018-10-30]. Dostupné z: https://www.idtechex.com/research/reports/flexible-printed-and-organic-electronics-2019-2029-forecasts-players-and-opportunities-000639.asp.

[46] POWELL, C, SAVAGE, A, GUTHRIE, J T. Computational simulation of the printing of Newtonian liquid from a trapezoidal cavity. International Journal of Numerical Methods *for Heat*. 2002, **12**(4), 338-355. DOI: 10.1108/09615530210433251.

[47] LEE, A J, ROTHSTEIN, J P, PASQUALI, M. Computational study of viscoelastic effects on liquid transfer during gravure-printing. *Journal of Non-Newtonian Fluid Mechanics*. 2013, **199**, 1-11. DOI: 10.1016/j.jnnfm.2013.05.005.

[48] DE LA FUENTE VORNBROCK, A, SUNG, D, KANG, H, KITSOMBOONLOHA, R, SUBRAMANIAN, V. Fully gravure and ink-jet printed high speed pBTTT organic thin film transistors. *Organic Electronics*. 2010, **11**(12), 2037-2044. DOI: 10.1016/j.orgel.2010.09.003.

[49] SUN, J, PARK, H, JUNG, Y, et al., 2017. Proving Scalability of an Organic Semiconductor To Print a TFT-Active Matrix Using a Roll-to-Roll Gravure. *ACS Omega*. **2**(9), 5766-5774. DOI: 10.1021/acsomega.7b00873.

[50] Gravure-printing. *Siemens: Ingenuity for Life* [online]. 2016 [cit. 2016-01-26]. Dostupné z: http://w3.siemens.com/mcms/mc-solutions/en/mechanical-engineering/printing-machines/gravure-printing-machine/pages/gravure-printing-machine.aspx

[51] KOPOLA, P, AERNOUTS, T, SLIZ, R et al. Gravure printed flexible organic photovoltaic modules. *Solar Energy Materials and Solar Cells*. 2011, **95**(5), 1344-1347. DOI: 10.1016/j.solmat.2010.12.020.

[52] KOPOLA, P, AERNOUTS, T *et al*. High efficient plastic solar cells fabricated with a high-throughput gravure-printing method. *Solar Energy Materials and Solar Cells*. 2010, **94**(10), 1673-1680. DOI: 10.1016/j.solmat.2010.05.027.

[53] Flexography. *Printing Methods* [online]. 0201n. l. [cit. 2016-01-29]. Dostupné z: https://printingmethods.wordpress.com/printing-techniques/flexography/

[54] KREBS, F C, HÖSEL, M, CORAZZA, M, *et al*. Freely available OPV-The fast way to progress. *Energy Technology*. 2013, **1**(7), 378-381. DOI: 10.1002/ente.201300057.

[55] JO, J, YU, J, LEE, T, KIM, D. Fabrication of Printed Organic Thin-Film Transistors Using Roll Printing. *Japanese Journal of Applied Physics*. 2009, **48**(4), 04C181-. DOI: 10.1143/JJAP.48.04C181.

[56] SCHMIDT, G C, BELLMANN, M, MEIER, B, HAMBSCH, M, REUTER, K, KEMPA, H HÜBLER, A C. Modified mass printing technique for the realization of source/drain electrodes with high resolution. *Organic Electronics*. 2010, **11**(10), 1683-1687. DOI: 10.1016/j.orgel.2010.07.018.

[57] HUEBNER, C F, CARROLL, J B, EVANOFF, D D *et al*. Electroluminescent colloidal inks for flexographic roll-to-roll printing. *Journal of Materials Chemistry*. 2008, **18**(41), 4942-. DOI: 10.1039/b809450k.

[58] MARTIN, G D, HOATH, S D, HUTCHINGS, I M. Inkjet printing - the physics of manipulating liquid jets and drops. *Journal of Physics: Conference Series*. 2008, **105**, 012001-. DOI: 10.1088/1742-6596/105/1/012001.

[59] *Annual Review of Materials Research*. 2010, **40**(1). ISSN 1531-7331.

[60] DE GANS, B J, DUINEVELD, P C, SCHUBERT, U S. Inkjet Printing of Polymers: State of the Art and Future Developments. *Advanced Materials*. 2004, **16**(3), 203-213. DOI: 10.1002/adma.200300385.

[61] JANG, D, KIM, D, MOON, J. Influence of Fluid Physical Properties on Ink-Jet Printability. *Langmuir*. 2009, **25**(5), 2629-2635. DOI: 10.1021/la900059m.

[62] LANGE, A, SCHINDLER, W, WEGENER, M, FOSTIROPOULOS, K, JANIETZ, S. Inkjet printed solar cell active layers prepared from chlorine-free solvent systems. *Solar Energy Materials and Solar Cells*. 2013, **109**, 104-110. DOI: 10.1016/j.solmat.2012.10.011.

[63] EOM, S H, PARK, H, MUJAWAR, S H, *et al*. High efficiency polymer solar cells via sequential inkjet-printing of PEDOT: PSS and P3HT. *Organic Electronics*. 2010, **11**(9), 1516-1522. DOI: 10.1016/j.orgel.2010.06.007.

[64] SOWADE, E, RAMON, E, MITRA, K Y, *et al*. All-inkjet-printed thin-film transistors: manufacturing process reliability by root cause analysis. *Scientific Reports*. 2016. **6**(1). DOI: 10.1038/srep33490.

[65] SHAHEEN, S E, RADSPINNER, R, PEYGHAMBARIAN, JABBOUR G E. Fabrication of bulk heterojunction plastic solar cells by screen-printing. *Applied Physics Letters*. 2001, **79**(18), 2996-. DOI: 10.1063/1.1413501.

[66] SALYK, O, VÍTEČEK, J, OMASTA, L, ŠAFAŘÍKOVÁ, E, STŘÍTESKÝ, S, VALA, M, WEITER, M. Organic Electrochemical Transistor Microplate for Real-Time Cell Culture Monitoring. *Applied Sciences* [online]. 2017, **7**(10). DOI: 10.3390/app7100998. ISSN 2076-3417.

[67] Nature. *WeWantToLearn.net* [online]. October16,2004 [cit. 2016-02-22]. Dostupné z: https://wewanttolearn.wordpress.com/tag/nature/

[68] BHUSHAN B. *Surface Roughness Analysis and Measurement Techniques. In:BHUSHAN B Modern tribology handbook:* 2001. Boca Raton, FL: CRC Press, s. 1-71.

[69] OHRING, M. Material science of thin films: Second edition. San Diego: Academic Press, 2001. ISBN 978-0125249751.

[70] GREZSKOWIAK, N E, WINKEL, J F. Structure and Location of Electroluminescent Light Emission within ZnS⁄Cu ACEL Powder Phosphor Particles. *Journal of The Electrochemical Society*. 2007, **154**(10).DOI: 10.1149/1.2761781. ISSN 00134651.

[71] Rods and Cones of the Human Eye, 2018. In: *Arizona state university* [online]. Tempe AZ 85281: Arizona state university [cit. 2018-11-07]. Dostupné z: https://askabiologist.asu.edu/rods-and-cones

[72] ARLT, G, HENNINGS, D, DE WITH, G. Dielectric properties of fine-grained barium titanate ceramics. *Journal of Applied Physics.* 1985, **58**, 1619-1625. doi: 10.1063/1.336051.

[73] HARTNER, S, MOAZZAM, A, SCHULZ, C, WINTERER, M, WIGGERS, H. Electrical properties of aluminum-doped zinc oxide (AZO) nanoparticles synthesized by chemical vapor synthesis. *Nanotechnology*. 2009, **20**(44), 445701-. DOI: 10.1088/0957-4484/20/44/445701.

[74] CRANTON, W M., WILSON, S L, RANSON, R et al. Excimer laser processing of inkjet-printed and sputter-deposited transparent conducting SnO2: Sb for flexible electronics. *Thin Solid Films*. 2007, **515**(24), 8534-8538. DOI: 10.1016/j.tsf.2007.03.118.

[75] RIVNAY, J, INAL, S, SALLEO A, OWENS M R., BERGGREN, M, a MALLIARAS G G. Organic electrochemical transistors. *Nature Reviews Materials*. 2018. **3**(2), 17086-. DOI: 10.1038/natrevmats.2017.86

[76] WU, J, PISULA, W, MÜLLEN, K. Graphenes as Potential Material for Electronics. *Chemical Reviews*. 2007 **107**(3), 718-747. DOI: 10.1021/cr068010r.

[77] HRABAL, Michal, Petr DZIK, Lukáš OMASTA, Martin VALA, Michal KALINA, Pavel FLORIÁN a Martin WEITER, Improvement of Performance of Electroluminescent Panel by Reducing the Thickness of Dielectric Layer. *Material science forum*. ISSN 1662-9752. accepted.

[78] YEN, W. M., Shigeo SHIONOYA a Hajime YAMAMOTO, c2007. *Phosphor handbook*. 2nd ed. Boca Raton, FL: CRC Press/Taylor and Francis. ISBN 08-493-3564-7.

[79] Light, 2018. *National Physical Laboratory* [online]. Teddington: National Physical Laboratory [cit. 2018-12-12]. Dostupné z: http://www.npl.co.uk/upload/pdf/light-poster.pdf

[80] Y, TAKEI, 2009. Energy Saving Lighting Efficiency Technologies. *Science and Technology Trends*. **32**(59), 59-71.

[81] D. B. M. KLAASEN, de LEEUW, D M and WELKER, J. Degradation of phosphors under cathode-ray excitation. *Journal of Luminescence*. 1987. **37**, 21 – 28. DOI: 10.1016/0022-2313(87)90178-5.

[82] SWART, H. C., J. S. SEBASTIAN, T. A. TROTTIER, S. L. JONES and P. H. HOLLOWAY. Degradation of zinc sulfide phosphors under electron bombardment. *Journal of Vacuum science & Technology A.* 1996. **14**(3), 1697-1703. DOI: 10.1116/1.580322. ISSN 0734-2101.

[83] LEHMANN, W. Investigations of long-living Destriau-type electroluminescent phosphors. *Journal of Electron Materials*. 1982. **11** (2). 341 – 354. DOI: https://doi.org/10.1007/BF02654677.

[84] HU, H, ZHANG W. Synthesis and properties of transition metals and rare-earth metals doped ZnS nanoparticles. *Optical Materials*. 2006. **28**:536-550. doi: 10.1016/j.optmat.2005.03.015

[85] VAN HAECKE, J E, SMET, P F, POELMAN, D. The Formation of Eu2+ Clusters in Saturated Red Ca0.5 Sr0.5S:Eu Electroluminescent Devices. *Journal of The Electrochemical Society*. 2005. 15: H225-H228. doi: 10.1149/1.2118207

[86] STECKEL, J S, COE-SULLIVAN, S, BULOVIC, V, BAWENDI, M G. 1.3 μm to 1.5 μm Tunable Electroluminescence from PbSe Quantum Dots Embedded within an Organic Device. *Advanced Materials*. 2003. **15**:1862-1866. doi: 10.1002/adma. 200305449

[87] WITHNALL, R, SILVER, J, HARRIS, P G, IRELAND, T G, MARSH, P J. AC powder electroluminescent displays. *Journal of the Society for Information Display*. 2011. **19**(11), 798-. DOI: 10.1889/JSID19.11.798.

[88] KUČEŘÍK, J, DAVID, J, WEITER, M *et al*. Stability and physical structure tests of piperidyl and morpholinyl derivatives of diphenyl-diketo-pyrrolopyrroles (DPP). *Journal of Thermal Analysis and Calorimetry*. 2012. 108: 467–473. doi: 10.1007/s10973-011-1896-8

[89] VALA, M, KRAJČOVIČ, J, LUŇÁK, S, OUZANNE, I, BOUILLON, J P, WEITER, M. HOMO and LUMO energy levels of N,N′-dinitrophenyl-substituted polar diketopyrrolopyrroles (DPPs). *Dyes and Pigments*. 2014. 106:136–142. doi: 10.1016/j.dyepig.2014.03.005.

[90] LUŇÁK, S, VALA, M, VYŇUCHAL, J *et al*. Absorption and fluorescence of soluble polar diketo-pyrrolo-pyrroles. *Dyes and Pigment* 2011. 91:269-278. doi:10.1016/j.dyepig.2011.05.004

[91] ZALM, P. *The Electroluminescence of ZnS Type Phosphors*. In. Philips *Research Reports*. 1956 11, 353-451.

[92] HRABAL, M., ZHIVKOV, I., OMASTA, L. *et al*. Solid-state fluorescence organic materials as a tool for spectral modification of ZnS-based screen-printed thick layer electroluminescence devices. Chemical. Papers. (2018) 72: 1677. https://doi.org/10.1007/s11696-018-0404-z

[93] Rhodamine B, c2018. *Laser Photomedicine and Biomedical Optics at the Oregon Medical Laser Centre* [online]. Oregon Medical Laser Center: Scott Prahl & Steve Jacques [cit. 2018-12-04]. Dostupné z: https://omlc.org/spectra/PhotochemCAD/html/009.html